



The Hashemite Kingdom of Jordan Scientific Research Support Fund The Hashemite University

JJEES

Jordan Journal of Earth
and Environmental Sciences

Volume (10) Number (2)

Cover photo © Prof. Issa Makhoul



JJEES is an International Peer-Reviewed Research Journal

Jordan Journal of Earth and Environmental Sciences (JJEES)

JJEES is an International Peer-Reviewed Research Journal, Issued by Deanship of Scientific Research, The Hashemite University, in corporation with, the Jordanian Scientific Research Support Fund, the Ministry of Higher Education and Scientific Research.

EDITORIAL BOARD:

Editor –in-Chief:

- **Prof. Fayez Ahmad**
The Hashemite University, Jordan

Assistant Editor:

- **Dr. Mohammed Al-Qinna**
The Hashemite University, Jordan

Editorial Board:

- **Prof. Najib Abou Karaki**
University of Jordan
- **Prof. Nizar Abu-Jaber**
German-Jordan University
- **Prof. Anwar Jiries**
Mu'tah University
- **Prof. Atef Al-Kharabsheh**
Al Balqa Applied University

- **Prof. Khaled Al Tarawneh**
Al-Hussein Bin Talal University
- **Prof. Abdullah Al-Diabat**
Al al-Bayt University
- **Prof. Nezar Al-Hammouri**
The Hashemite University
- **Prof. Muheeb Awawdeh**
Yarmouk University

ASSOCIATE EDITORIAL BOARD: (ARRANGED ALPHABETICALLY)

- **Professor Ali Al-Juboury**
Mosul University, Iraq
- **Dr. Bernhard Lucke**
Friedrich-Alexander University, Germany
- **Professor Dhirendra Pandey**
University of Rajasthan, India
- **Professor Eduardo García-Meléndez**
University of León, Spain
- **Professor Franz Fürsich**
Universität Erlangen-Nürnberg, Germany
- **Professor Olaf Elicki**
TU Bergakademie Freiberg, Germany

INTERNATIONAL ADVISORY BOARD:

- **Prof. Sayed Abdul Rahman,**
Cairo University, Egypt
- **Prof. Abdullah Al-Amri,**
King Saud University, Saudi Arabia
- **Prof. Waleed Al-Zubair,**
Arabian Gulf University, Bahrain
- **Prof. Ute Austermann-Haun,**
Fachhochschule und Lipp, Germany
- **Prof. Ibrahim Banat,**
University of Ulster, UK
- **Prof. Matthias Barjenbruch,**
Technisch Universität Berlin, Germany
- **Prof. Mohamed Boukhary,**
Ain Shams University, Egypt
- **Prof. Mohammad El-Sharkawy,**
Cairo University, Egypt
- **Prof. Venugopalan Ittekkot,**
Center for Tropical Marine Ecology, Bremen, Germany
- **Prof. Christopher Kendall,**
University of North Carolina, U.S.A.
- **Prof. Elias Salameh,**
University of Jordan, Jordan.
- **Prof. V. Subramanian,**
Jawaharlal Nehru University, India.
- **Prof. Omar Rimawy,**
University of Jordan, Jordan.
- **Prof. Hakam Mustafa,**
Yarmouk University, Jordan.
- **Dr. Michael Crosby,**
The National Science Board, National Science Foundation, Virginia, U.S.A.
- **Dr. Brian Turner,**
Durham University, U.K..
- **Dr. Friedhelm Krupp,**
Senckenberg Research Institute and Natural History Museum, Germany.
- **Dr. Richard Lim,**
University of Technology, Australia.

EDITORIAL BOARD SUPPORT TEAM:

- Language Editor
- **Dr. Halla Shureteh**
- Publishing Layout
- **Obada Al-Smadi**

SUBMISSION ADDRESS:

Manuscripts should be submitted electronically to the following e-mail:

jjees@hu.edu.jo

For more information and previous issues:

www.jjees.hu.edu.jo



Hashemite Kingdom of Jordan



Scientific Research Support Fund



Hashemite University

Jordan Journal of Earth and Environmental Sciences

JJEES

An International Peer-Reviewed Scientific Journal

Financed by the Scientific Research Support Fund

Volume 10 Number (2)

<http://jjees.hu.edu.jo/>

ISSN 1995-6681

المجلة الأردنية لعلوم الأرض والبيئة
Jordan Journal of Earth and Environmental
Sciences (JJEES)

<http://jjees.hu.edu.jo>

Hashemite University
Deanship of Scientific Research
TRANSFER OF COPYRIGHT AGREEMENT

Journal publishers and authors share a common interest in the protection of copyright: authors principally because they want their creative works to be protected from plagiarism and other unlawful uses, publishers because they need to protect their work and investment in the production, marketing and distribution of the published version of the article. In order to do so effectively, publishers request a formal written transfer of copyright from the author(s) for each article published. Publishers and authors are also concerned that the integrity of the official record of publication of an article (once refereed and published) be maintained, and in order to protect that reference value and validation process, we ask that authors recognize that distribution (including through the Internet/WWW or other on-line means) of the authoritative version of the article as published is best administered by the Publisher.

To avoid any delay in the publication of your article, please read the terms of this agreement, sign in the space provided and return the complete form to us at the address below as quickly as possible.

Article entitled:-----

Corresponding author: -----

To be published in the journal: Jordan Journal of Earth & Environmental Sciences (JJEES)

I hereby assign to the Hashemite University the copyright in the manuscript identified above and any supplemental tables, illustrations or other information submitted therewith (the "article") in all forms and media (whether now known or hereafter developed), throughout the world, in all languages, for the full term of copyright and all extensions and renewals thereof, effective when and if the article is accepted for publication. This transfer includes the right to adapt the presentation of the article for use in conjunction with computer systems and programs, including reproduction or publication in machine-readable form and incorporation in electronic retrieval systems.

Authors retain or are hereby granted (without the need to obtain further permission) rights to use the article for traditional scholarship communications, for teaching, and for distribution within their institution.

☐ I am the sole author of the manuscript

☐ I am signing on behalf of all co-authors of the manuscript

☐ The article is a 'work made for hire' and I am signing as an authorized representative of the employing company/institution

Please mark one or more of the above boxes (as appropriate) and then sign and date the document in black ink.

Signed: _____ Name printed: _____

Title and Company (if employer representative) : _____

Date: _____

Data Protection: By submitting this form you are consenting that the personal information provided herein may be used by the Hashemite University and its affiliated institutions worldwide to contact you concerning the publishing of your article.

Please return the completed and signed original of this form by mail or fax, or a scanned copy of the signed original by e-mail, retaining a copy for your files, to:

Deanship of Scientific Research

The Hashemite University P.O. Box 150458, P.C.13115, Zarqa, Jordan

Tel.: 00962 53903333/ Ext. 4235

Fax: 00962 53826823

E-mail: jjees@hu.edu.jo



Name:	الاسم:
Specialty:	التخصص:
Address:	العنوان:
P.O. Box:	صندوق البريد:
City & Postal Code:	المدينة: الرمز البريدي:
Country:	الدولة:
Phone:	رقم الهاتف:
Fax No:	رقم الفاكس:
E-mail:	البريد الإلكتروني:
Method of payment:	طريقة الدفع:
Amount Enclosed:	المبلغ المرفق:
Signature:	التوقيع:

Cheques should be paid to Deanship of Research - The Hashemite University

I would like to subscribe to the Journal:

For

- ☐ One year
☐ Two years
☐ Three years

One year Subscription Rates

	Inside Jordan	Outside Jordan
Individuals	10JD	70\$
Students	5JD	35\$
Institutions	20JD	90\$

Correspondence

Subscriptions and sales:

Professor Fayez Ahmad
 Deanship of Scientific Research
 The Hashemite University P.O. Box 150458, P.C.13115, Zarqa, Jordan
 Tel.: 00962 53903333/ Ext. 4235
 Fax: 00962 53826823
 E-mail: jjees@hu.edu.jo

PAGES	PAPERS
64 - 74	Mineralogical and Geochemical Studies on Some Early Miocene Sediments of Southwestern Sinai, Egypt <i>Nabil Abd El-Hafez, Ahmed Mousa, Tarek El-Hariri, Mohamed Abd El-Moghny, Hossam Sharaka</i>
75 - 84	Assessment of Metal Pollution of the Surface Sediments along the Wadi Al Rayyan area, Jordan <i>Ibrahim Bany Yaseen and Zayed Al-Hawari</i>
85 - 91	Status and Prediction of Nitrogen Oxides in the Air of Shiraz City, Iran <i>Masoud Masoudi, Fatemeh Ordibeheshti, Neda Poor</i>
92 - 96	Morphometric Analysis of Lake Ruma, Song, Adamawa State in Northeastern Nigeria <i>Yonnana Ezekiel, Apollos Thandime, James Thomas</i>
97 - 103	Estimation of Global Solar Radiation, Sunshine Hour Distribution and Clearness Index in Three Geopolitical Regions of Southern Nigeria <i>Adeniji Nathaniel, Akinpelu Jacob, Adeniji Joshua, Adeola Solomom</i>
104 - 112	Assessment of Heavy Metal Pollution in the Sediments of the Lower Litani River Basin, Lebanon <i>Nada Nehme, Chaden Haidar, Walaa Diab, Khaled Tarawneh, Frédéric Villieras</i>
113 - 117	Road Rehabilitation Using Mobile Mapping System and Building Information Model <i>Omar Al-Bayari</i>
118 - 126	Development of Irrigation Water Quality Index for Wadi Araba Basin, Southern Jordan <i>Ali El-Naqa and Amani Abu Al Adas</i>

Mineralogical and Geochemical Studies on Some Early Miocene Sediments of Southwestern Sinai, Egypt

Nabil Abd El-Hafez¹, Ahmed Mousa²,
Tarek El-Hariri², Mohamed Abd El-Moghny¹, Hossam Sharaka³

¹Al-Azhar University, Faculty of Science, Geology Department, Cairo, Egypt.

²Egyptian Petroleum Research Institute, Exploration Department, Nasr City, Egypt.

³Egyptian Mineral Resources Authority, Abbassiya, Cairo, Egypt.

Received 8 November 2018, Accepted 12 January 2019

Abstract

The present work provides a comparison and a contrast of the lithostratigraphy, mineralogy, and geochemistry of the early Miocene rocks exposed in El-Markha and Wadi Gharandal sections (Nukhul and Rudeis formations) at Southwest Sinai. Miocene succession of Southwest Sinai is classified from base to top into: Nukhul and Rudies formations. Rudies Formation unconformably overlies Nukhul Formation and unconformably underlies Kareem Formation. The Early Miocene sequence revealed the presence of calcite as the dominate minerals in the nonclastic rocks. Quartz is the main mineral in the clastic rocks, while goethite is most important minerals in the iron-rich sand, whereas halite is foremost minerals in evaporate samples. Hematite, kaolinite, halite and gypsum are the secondary minerals constituting the studied rock units with varying amount. The foremost clay minerals present in Nukhul Formation are montmorillonite and kaolinite. In Rudeis Formation, the main clay minerals is montmorillonite. Geochemically, the studied sections are characterized by higher percentage of SiO₂ and Fe₂O₃ in iron-rich sand. SiO₂, Fe₂O₃ and Al₂O₃ gathering to form the ferruginous and glauconitic sandstone. The high content of SiO₂, Na₂O, Cl, CaO and SO₃ as main elements of compound together and forming gypsum and evaporitic sandstone. On the other hand, the high content of CaO and MgO gathering to give limestone, dolomitic limestone and dolomite. So, through the light on the geochemical conditions the two different formations are deposited.

© 2019 Jordan Journal of Earth and Environmental Sciences. All rights reserved

Keywords: Mineralogy, Geochemical Studies, Early Miocene, Sinai and Egypt.

1. Introduction

The Miocene rocks in the Gulf of Suez areas have been studied by several authors (Said and El Heiny, 1967; El-Bakry et al., 2010; Hewaidy et al., 2012; Al-Husseiny, 2012; Abd El-Hafez et al., 2015). The Miocene sediments in the study areas are located between latitudes 29° 14' and 29° 18' N and longitudes 32° 55' and 33° 00' in Wadi Gharandal section. El Markha section is located between latitudes 29° 00' and 29° 03' N and longitudes 33° 10' and 33° 16' (Fig. 1).

The Miocene sediments developed on both rifts and in the central sub-basins display two markedly contrast sedimentary facies, a marginal and a deeper marine. The deeper marine facies is subdivided into two major groups namely Gharandal and Ras Malaab. On the other hand, the marginal (costal) marine facies is divided into four formations from base to top, namely Abu Gerfan, Gharamul, Gemsa and Sarbut El- Gamal respectively (El-Azabi, 1997). The Early Miocene is started with the deposition of algal limestone that changed later into fan-conglomeritic facies under the effect of the clysmic tectonic events (Abul-Nasr and Salma, 1999). The Nukhul Formation is Last Oligocene – Early Miocene age implying the Suez rift system started in the Oligocene. This study is based on the results of a biostratigraphic study of the Nukhul Formation at Wadi Babaa (Hewaidy et al., 2012). The Lower Miocene rocks can be classified into clastic (sandstones and argillaceous) and non-clastic (carbonate rocks with thin

evaporitic intercalations). The microscopic examination revealed different sandstone microfacies types such as: quartz arenite, calcareous quartz arenite, ferruginous quartz arenite, evaporitic quartz arenite, glauconitic quartz arenite and ferruginous evaporitic quartz arenite. The carbonate microfacies types in the studied formations include sandy micrite, biosparite, foraminiferal biomicrite, dolo-biomicrite, dolosparite, dolostone, pelsparite, oo-biosparite and evaporitic dolomicrite (Abd El-Hafez et al., 2015). The present work aims to shed more light at the lithostratigraphical, mineralogical and geochemical properties to evaluate the influence of geochemical conditions on the mineralogical composition.

2. Materials and Methods

To achieve this target, samples were collected to represent the different mineralogical and geochemical conditions. These samples were studied as follows:

2.1 X-ray diffraction (XRD)

Sixty-seven samples were selected and analyzed by XRD to identify the mineralogical composition. The analysis was carried out at the Egyptian Geological Survey and Mining Authority (central laboratories sector), using automated powder diffractometer system of Philips type Pan Alytica X-pert-pro with Ni-filter, Cu-radiation ($\lambda=1.542 \text{ \AA}$) at 40kV, 30mA and a normal scanning speed 0.02°/S. The reflection peaks between $2\theta = 2^\circ$ and 60° were obtained for the un-oriented analysis and between (2° - 35°) 2θ for the

* Corresponding author e-mail: el_hariri@yahoo.com

oriented analysis. The identification of the powder samples is determined by qualitative and semi-quantitative analysis. On the other hand, the clay size ($< 2\mu\text{m}$) fraction (eighteen samples) of clay minerals (three mounted slides for each sample) were prepared. The corresponding d-spacing and

relative intensities (I/I°) were obtained and compared with the standard data of the ICDD/2010 files by using APD program. The interpretation takes place by using APD and PDF programs which contain Powder Diffraction and PDF-2 Database Sets 1-45.

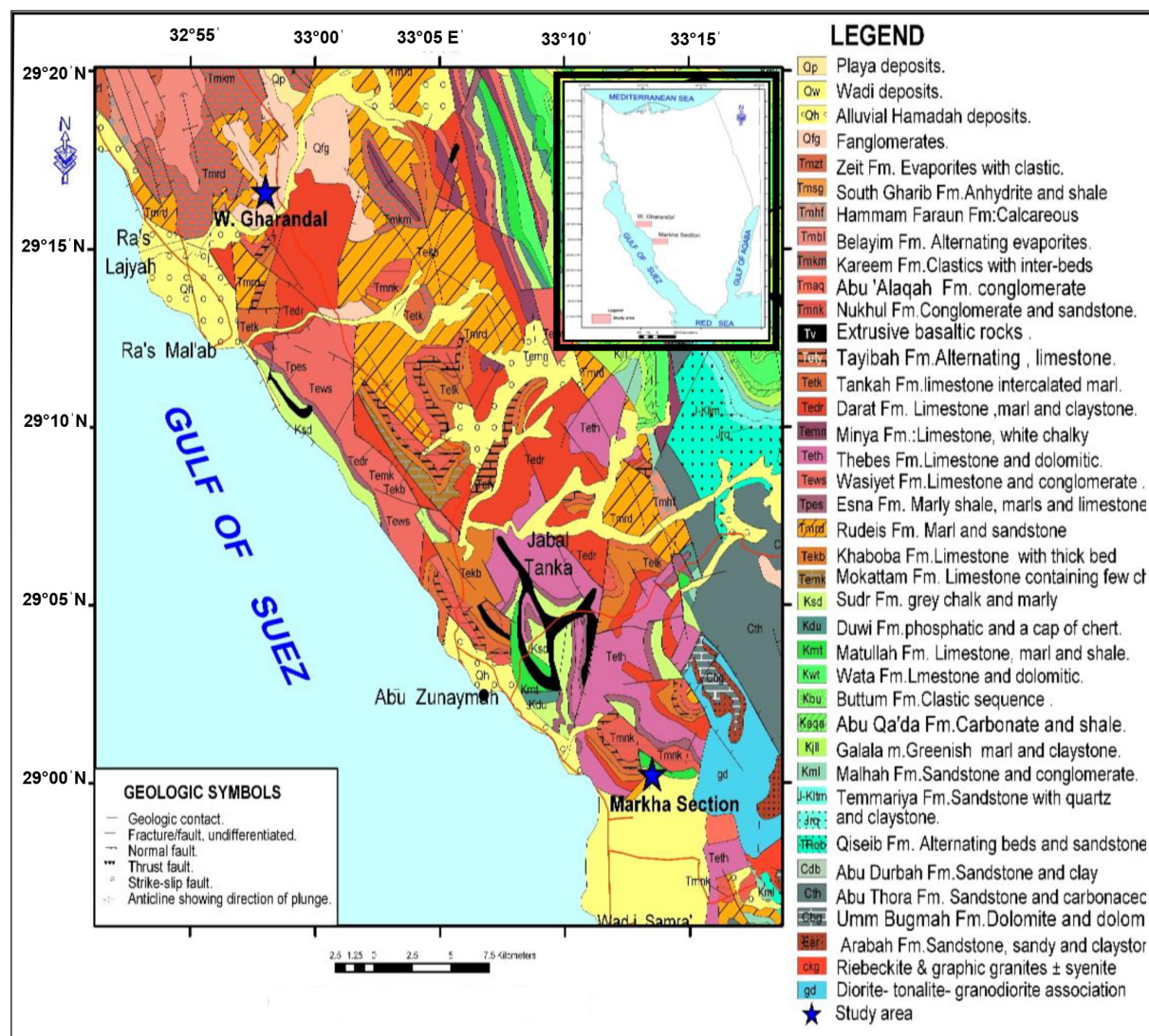


Figure 1. Location and geological map of the studied sections (After Conoco, 1986).

2.2 Scanning Electron Microscope (SEM)

Scanning electron microscopy (SEM) for four samples of different lithofacies was performed in order to understand the microstructure and diagenetic relationships among the pore spaces, main constituents and matrix of the studied sediments. Identification of the different minerals through SEM was facilitated by comparing their morphologic characteristics with those shown in the SEM petrology Atlas (Welton, 1984). SEM was carried out at the Egyptian Geological Survey and Mining Authority (central laboratory sector), using a SEM Model Philips XL30 attached with EDX units, with an accelerating voltage of 30 KV., magnification 10x up to 400,000x and resolution for W. (3.5nm). The samples were coated with gold.

2.3 X-Ray Fluorescence (XRF)

Forty-two samples representing clastic and non-clastic rock units were chemically analyzed after grinding at the Egyptian Geological Survey and Mining Authority (central

laboratory sector) using X-Ray fluorescence apparatus Technique. Philips X-Ray fluorescence equipment, model Philips PW/2404 and six analyzing crystals were used for determining major and trace elements. The maximum power of the equipment was 30 K.wt., Crystals (LIF-200), (LIF-220).

2.4 Statistical Analysis

The statistical studies were carried out using principally the SPSS (statistical Package for Social Science) program. The geochemical data were interpreted, and the factor analysis has been used by several investigators (Tamish, 1988) among other authors.

3. Lithostratigraphy

The lower Miocene in the Gulf of Suez and West Central Sinai is generally represented by two distinct facies, the marine facies and the non-marine or coastal facies. The variation of the environment is attributed to sea level changes that have

been overprinted twice by two major tectonic movements: the mid-Rudies and post-Kareem event (Abul-Nasr et al., 1999). The Nukhal Formation in the studied section is represented by limestone, sandstone and shales. Limestones are grayish white to yellow in color, massive, siliceous, hard, compact, dolomitic and fossiliferous lithofacies. Sandstones are yellow to reddish brown, compact, ferruginous, argillaceous with some salt intercalation. Shales are yellow brown to grayish in color, compact with veinlets of evaporites (Abd El-Hafez, 1986). The Rudeis Formation is formed of shale, sandstone and limestones. Shale are varicolored (greenish brown, grey, yellowish grey, yellowish brown and light grey) silty, semi-compact, ferruginous, calcareous, laminated high fossiliferous

lithofacies, (El-Bakry et al. 2010).

To achieve objectives of the present work, two early Miocene stratigraphic sections are represented; one in El-Markha and the second at Wadi Gharandal as follows:

3.1 El-Markha Section

The sedimentary succession of El-Markha section is represented by the Nukhul and Rudeis formations, which is about 170m thick together; Nukhul Formation is about 100m thick. It is unconformably capped by the Rudeis Formation which is 70m thick, and unconformably overlies Tayiba Formation of the Upper Oligocene. The Rudeis Formation is unconformably overlain by Kareem Formation of the Middle Miocene age (Fig. 2).

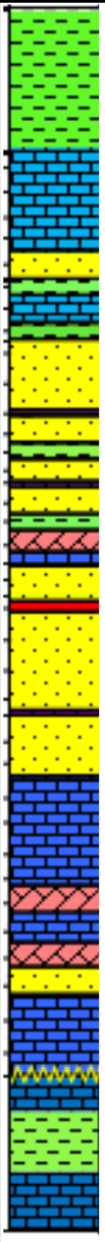
Tertiary		Neogene		Rock units		Thickness m.	Sample No.	Lithology	Description														
Period	Epoch	Age	Group	Formation	Member																		
Paleogene	Upper Oligocene	Chattian	Agaitantian	Burdigalian	Langhian	M. Miocene	Ras Maalat	Kareem	Rhumi	Mreir	24	34-38		Shale: Brown grey to brown compact, gypsum veinlets fissile , ferruginous and siliceous.									
															Gharandal	Rudies	Asl	11	31-33	Limestone: Yellowish white hard, compact, fossiliferous, evaporitic patch, brownish yellow sandstone in lower part.			
																					Mheiherratt	35	Shale: multi-colored (brown grey, brown, greenish grey), silty, semi compact, ferrugineou, intercalation of yellow compacted limestone.
Nukhul	100	1-30	Limestone: Yellowish white, hard, compact, fossiliferous, reddish yellow ferruginous dolomite in the upper part.																				
				Tayiba	Sandstone: Yellowish to reddish brown, very dense, compact ferruginous rust-colored (bearing iron), argillaceous, intercalation of yellowish brown of salt bed.																		
								Limestone: Yellowish to white, massive, hard, compact fossiliferous, intercalation of reddish brown, to brownish yellow dolomite with brownish yellow, evaporitic sandstone with conglomerate bed at the base not exposure.															
													Limestone: Yellowish to grayish white, massive, hard, compact, grayish brown to brownish yellow, evaporitic shale intercalation.										

Figure 2. Lithostratigraphic columnar section of Early Miocene sequence in El-Markha section, Southwest Sinai, Egypt.

3.2 Wadi Gharandal Section

In Wadi Gharandal section, the sedimentary units are about 325m thick. Nukhul Formation (ca. 90m thick) is unconformable and overlined by the Rudeis Formation (Mheiherratt Member) which is 235m thick and unconformable

overlying the Tanka Formation of Upper Eocene. Rudeis Formation is unconformably capped by the Kareem Formation which is related to the Middle Miocene age (Fig. 3). The studied areas can be subdivided into two formations from base to top as shown in Figure 3.

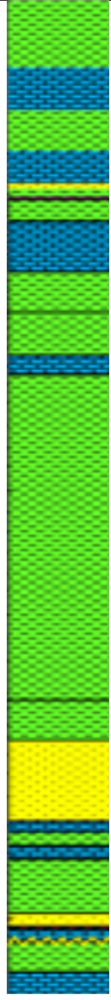
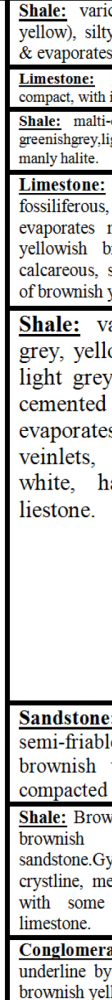
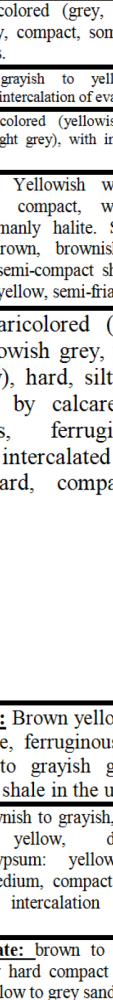
Period	Epoch	Age	Rock units			Thickness m.	Sample No.	Lithology	Description
			Group	Formation	Member				
Tertiary	Neogene	Early Miocene	Burdigalian	Gharandal	Rudies	31 m.	38-65		<p>Shale: varicolored (grey, brown and greenish yellow), silty, compact, some patches of gypsum & evaporates.</p> <p>Limestone: grayish to yellowish, hard, massive, compact, with intercalation of evaporates mainly halite.</p> <p>Shale: multi-colored (yellowish brown, brownish to greenish grey, light grey), with intercalation of evaporates mainly halite.</p> <p>Limestone: Yellowish white, hard, massive, fossiliferous, compact, with intercalation of evaporates mainly halite. Some of varicolored, yellowish brown, brownish to greenish grey, calcareous, semi-compact shale, with intercalated of brownish yellow, semi-friable sandstone</p> <p>Shale: varicolored (greenish brown, grey, yellowish grey, yellowish brown, light grey), hard, silty, semi-compact, cemented by calcareous clay, some evaporates, ferruginous, gypsum veinlets, intercalated with yellowish white, hard, compact, fossiliferous liestone.</p>
	Paleogene	Upper Oligocene	Agaitantian	Nukhul	Mheiherratt	144 m.	18-38		<p>Sandstone: Brown yellow, fine to medium, semi-friable, ferruginous, calcareous, with brownish to grayish green, silty, semi-compact shale in the upper part</p> <p>Shale: Brownish to grayish, semi-compact, some brownish yellow, dense, ferruginous sandstone. Gypsum: yellowish white, coarsal crystalline, medium, compact trace of argillaceous with some intercalation of yellow compact limestone.</p> <p>Conglomerate: brown to grey, hard, compact, underlined by hard compact yellow limestone and brownish yellow to grey sandy shale bed.</p>
	Paleogene	Upper Oligocene	Agaitantian	Nukhul	Mheiherratt	90 m.	1-17		<p>Sandstone: Brown yellow, fine to medium, semi-friable, ferruginous, calcareous, with brownish to grayish green, silty, semi-compact shale in the upper part</p> <p>Shale: Brownish to grayish, semi-compact, some brownish yellow, dense, ferruginous sandstone. Gypsum: yellowish white, coarsal crystalline, medium, compact trace of argillaceous with some intercalation of yellow compact limestone.</p> <p>Conglomerate: brown to grey, hard, compact, underlined by hard compact yellow limestone and brownish yellow to grey sandy shale bed.</p>

Figure 3. Lithostratigraphic columnar section of Early Miocene sequence in Wadi Gharandal section, Southwest Sinai, Egypt.

4. Results and Discussion

4.1 Mineralogy

4.1.1 Mineralogical Composition of the Bulk Samples

Minerals identified from the bulk samples of the studied clastic sediments are illustrated in (Fig. 4). The obtained X-ray data were interpreted using American Society for Testing Materials (ASTM, 1960) data Cards together with data published by Brown (1961) and Deer et al., (1963). From this figure, it can be seen that quartz is the main mineral in the sandstone. Iron oxides mainly goethite and hematite represent the dominant mineral in the iron-rich sand and ferruginous

sandstone. Calcite is considered the main mineral in the calcareous sandstone, while montmorillonite and kaolinite were the main minerals in the argillaceous sandstone. The main constituting minerals in the evaporitic sandstone are represented by halite and gypsum. On the other hand, the non-clastic sediments represent calcite as a major mineral in carbonate (limestone) minerals, while dolomite is a secondary mineral in the dolomitic limestone and a major mineral in the dolomite samples (Fig. 4). Halite and gypsum are the major minerals in the evaporite minerals. Kaolinite, montmorillonite, quartz, iron oxides and some evaporite minerals are present as accessory minerals.

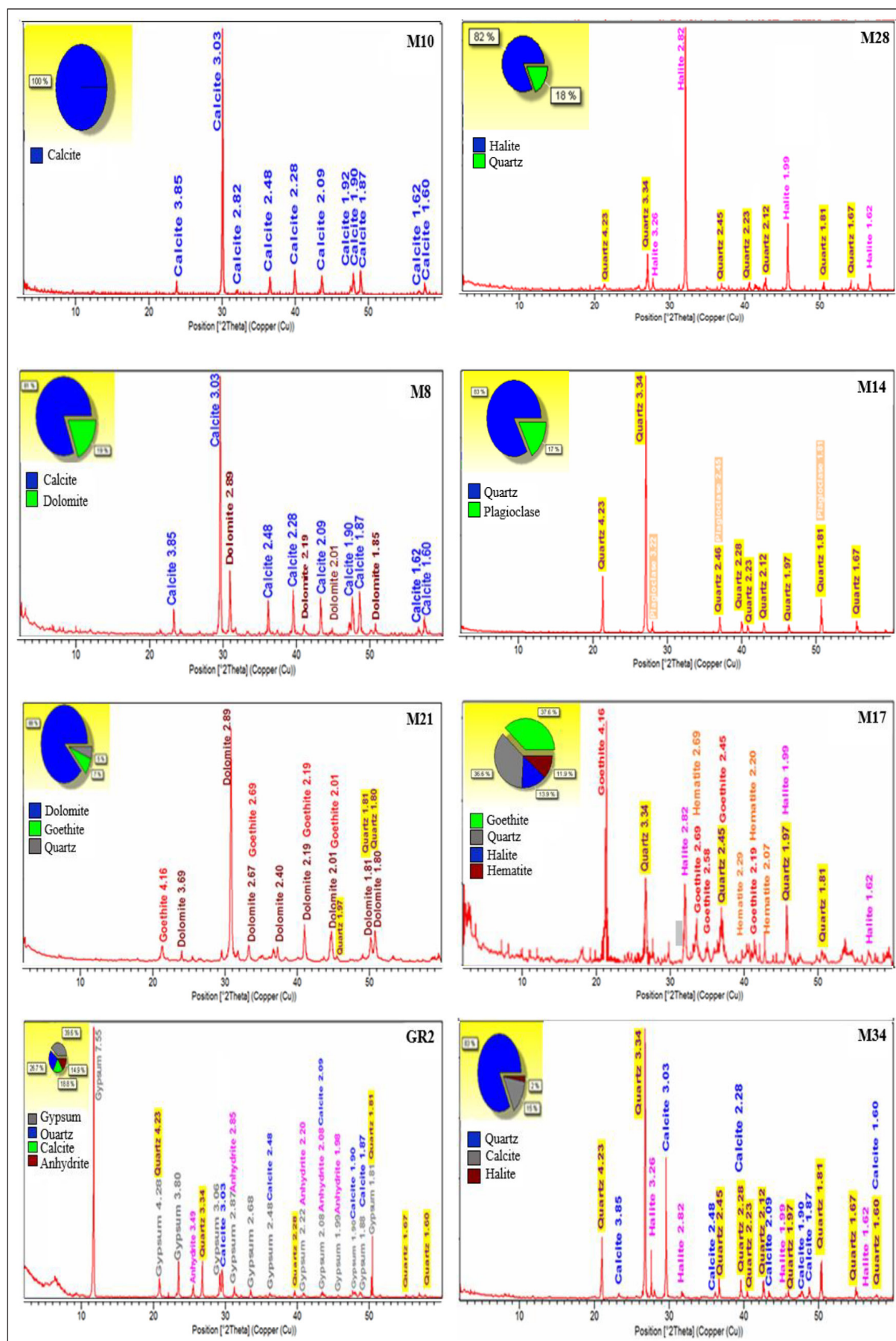


Figure 4. X-Ray Diffraction chart of the studied bulk samples of the studied sections.

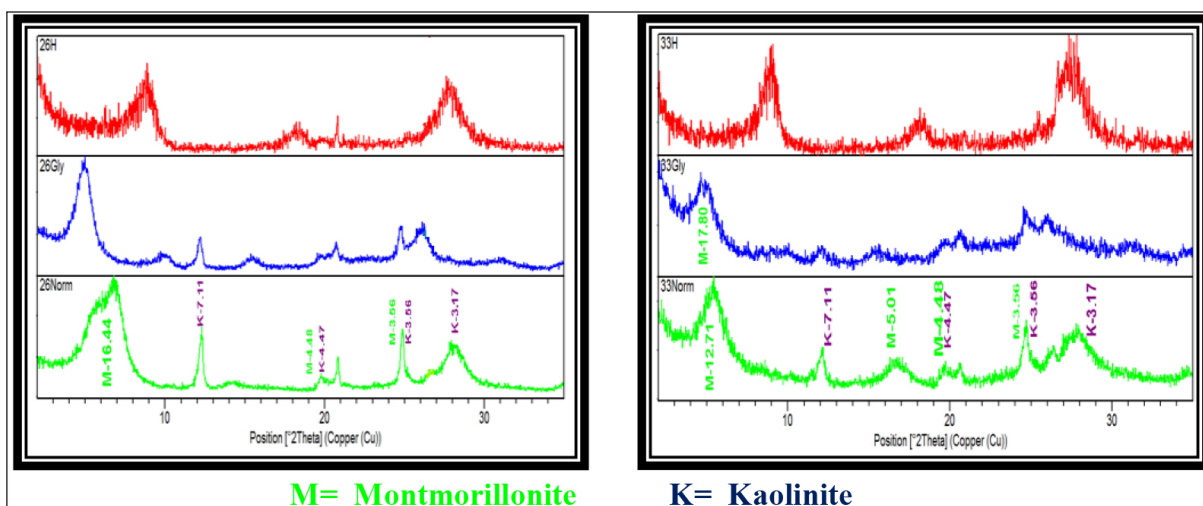


Figure 5. X-Ray Diffraction pattern of the studied clay rich samples in El-Markha section (Samples No. 26 and 33).

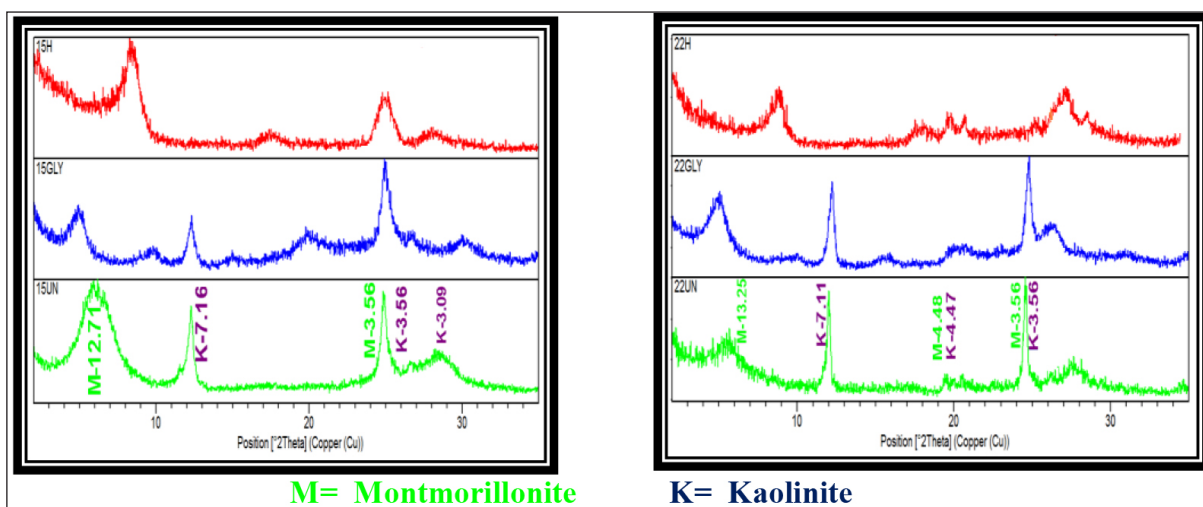


Figure 6. X-Ray Diffraction pattern of the studied clay rich samples in Wadi Gharandal section (Samples No. 15 and 22).

Montmorillonite is the most common mineral in shale of all rock units. Nukhul Formation samples contain montmorillonite about (52.63-72.03 %) with an average 60.91 %, while the samples of the Rudeis Formation are composed of (31.27-85.26 %) with an average 60.95 % of this mineral, (Figs. 5, 6, and 11).

Kaolinite is the most minor mineral in shale of all rock units excluding two samples (19 and 44) of the Rudeis Formation at Wadi Gharandal section where it is the main component. Nukhul Formation contains 27.97-47.37% with an average of 39.09% while Rudeis Formation contains of 14.74-68.73% kaolinite with an average of 39.05% (Figures 5, 6 and 10).

4.1.2 Semi-quantitative determination of clay minerals

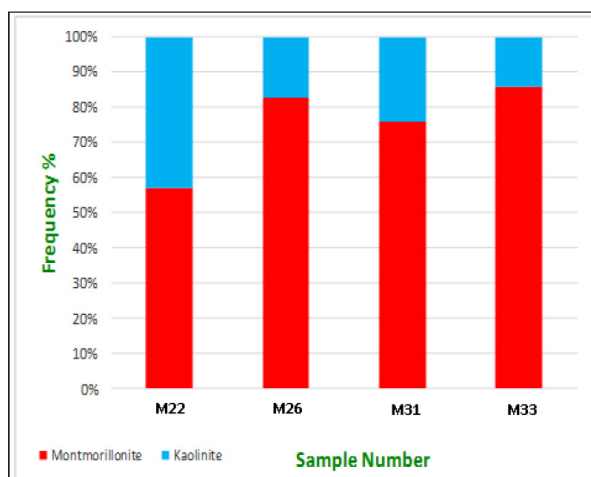
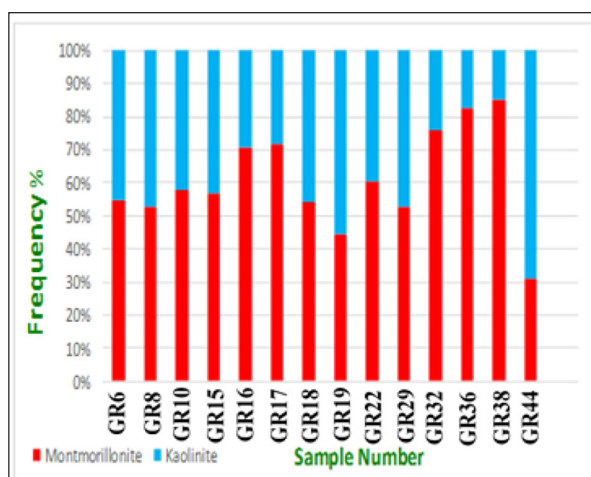
The semi-quantitative analysis of the studied samples is shown in Tables (1 and 2) and Figures (7 and 8). This method is mentioned by Pierce and Siegel (1969) and Siegel et al., (1981) to detect the clay minerals by using the peak height of the strongest reflections of the individual clay minerals.

Table 1. Relative frequency distribution of the detected clay minerals (wt. %) in the studied samples (El-Markha section).

Age	For.	Mem.	S.No	Montmorillonite	Kaolinite
Early Miocene	Rudeis	Asl	33	85.71	14.29
			31	75.68	24.32
	Hawara		26	82.76	17.24
			22	57.14	42.86

Table 2. Relative frequency distribution of the detected clay minerals (wt. %) in the studied samples (Wadi Gharandal section).

Age	For.	Mem.	S.No.	Montmorillonite	Kaolinite
Early Miocene	Rudeis	Asl	44	31.27	68.73
		Hawara	38	85.26	14.74
			36	82.76	17.24
			32	76.1	23.9
			29	52.94	47.06
			22	60.53	39.47
			19	44.37	55.63
			18	54.4	45.6
	Nukhul		17	72.03	27.97
			16	70.92	29.08
			15	56.9	43.1
			10	57.98	42.02
			8	52.63	47.37
			6	55	45

**Figure 7.** Frequency distribution of the detected clay minerals in the studied samples (El-Markha section).**Figure 8.** Frequency distribution of the detected clay minerals in the studied samples (Wadi Gharandal section).

4.1.3 Mineralogical Composition by Scanning Electron Microscopy

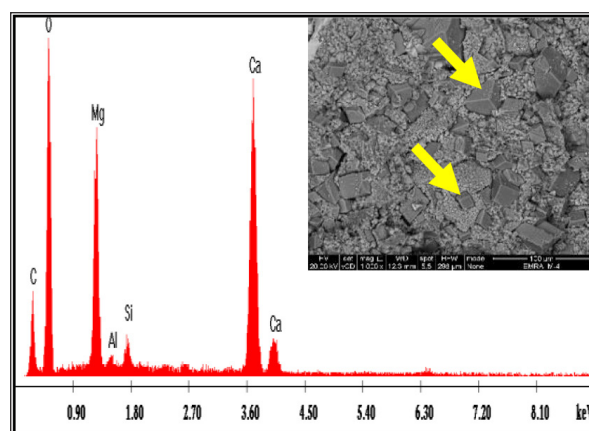
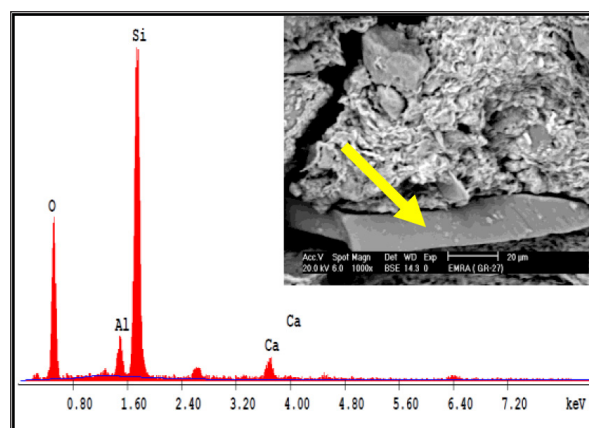
A petrographical study when combined with scanning electron microscope (SEM) investigations (Figs. 9, 10, 11, and 12) provides a good mean in identifying the mineralogical characteristics and the diagenetic process affecting the rock forming minerals. (El-Hariri, 2008 and Mousa et al., 2009).

The following SEM study is used to illustrate and identify the authigenic minerals, pore geometry and diagenetic events produced by different environments for examining sandstone, limestone, and clay minerals (Nukhul and Rudeis formations):

- 1- Dolomite crystal is shown in Figure 9, sample No. 4, Nukhul Formation at Markha section.
- 2- Kolinit is shown in Figure 10, sample No. 27, Rudeis Formation at Wadi Gharandal section.
- 3- Montmorillonite is shown in Figure 11, sample No. 27, Rudeis Formation at Wadi Gharandal section.
- 4- Iron oxides (Hematite and goethite in Figure 12, Sample No. 16, Nukhul Formation (El-Markha section).

5. Geochemical Composition

The main objective of the geochemical studies is to investigate the compositional variations of the studied samples and the vertical and lateral changes of the major and trace constituents and its mutual relationship. The following discussion is focused on the major and trace element response to the physicochemical conditions and deals with the abundance and distribution of these elements.

**Figure 9.** EDX and SEM photomicrograph showing dolomite crystals (arrows). Sample No. 4, Nukhul Formation (El-Markha section).**Figure 10.** EDX and SEM photomicrograph showing kaolinite (arrow). Sample No. 27, Rudeis Formation (Wadi Gharandal section).

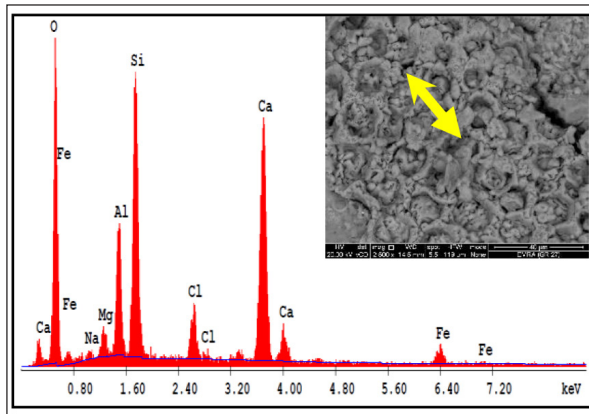


Figure 11. EDX and SEM photomicrograph showing montmorillonite mineral (arrow). Sample No. 27, Rudeis Formation (Wadi Gharandal section).

Forty-two samples representing El-Markha and Wadi Gharandal sections were chemically analyzed for their major and trace elements.

The obtained data of both major and trace element constituents in the studied Early Miocene rocks with the average composition of each rock unit is given in Tables 3

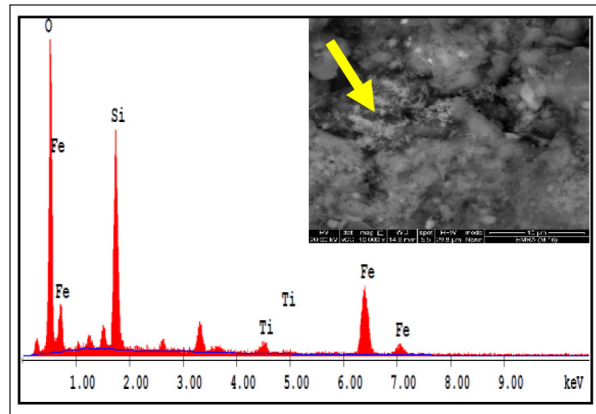


Figure 12. EDX and SEM photomicrograph showing iron oxides (goethite & hematite) (arrow). Sample No. 16, Nukhul Formation (El-Markha section).

and 4. The average composition of each studied rock unit is compared with those reported by other workers as shown in Table 5. The vertical distributions of the elements in the studied Lower Miocene successions are shown in Figures 13 and 14. The cluster analysis from the studied two sections are shown in Figure 15.

Table 3. Major oxides in wt. % and Trace elements in ppm of the Early Miocene rocks (El-Markha section).

Age	Rock units		S.No.	Major element oxides %																
	Form.	Mem.		SiO ₂	TiO ₂	Al ₂ O ₃	Fe ₂ O ₃	MnO	MgO	CaO	K ₂ O	Na ₂ O	P ₂ O ₅	SO ₃	Cl	L.O.I	Ba	Sr	Cr	
Early Miocene	Burdigalian	Rudeis	Mreir	M38	17.02	0.18	2.79	1.64	0.02	5.22	32.8	0.23	3.01	0.13	0.4	2.12	34.16	430.9	257.9	64.8
			M35	16.22	0.38	4.35	5.04	0.13	7.8	27.42	0.45	4.5	0.21	0.3	3.13	30.07	452.6	184.9	148.1	
			M34	55.01	0.65	2.9	2.26	0.06	1.47	17.41	0.78	2.81	0.15	0.4	1.9	14.03	464.3	270.1	66.6	
			M33	44.2	0.81	17.25	4.05	0.01	6.01	1.04	0.84	7.72	0.05	0.7	6.92	10.15	502.4	235.2	110.9	
			M32	2.49	0.04	0.26	1.27	0.12	0.69	53.2	0.02	0.32	0.14	0.2	0.08	40.9	348.3	152.5	28.5	
			M31	47.32	0.89	18.65	2.93	0.01	2.66	1.26	0.41	9.15	0.09	0	8.21	8.07	530.4	209.5	117	
		Hawara		M30	39.91	0.58	4.1	8.66	0.01	3.23	0.79	0.5	15.2	0.12	0.3	13.9	12.68	504.7	175.5	285
				M29	34.84	0.15	2.63	8.13	0.34	3.14	2.4	0.4	10.52	0.24	0.3	12	24.55	372	118.8	11.2
				M28	16.24	0.17	4.72	2.69	0.03	2.31	0.97	0.42	19.03	0.09	0.4	17.7	35.28	425.1	118.7	106.1
				M26	45.75	0.86	16.2	3.67	0.01	5.65	0.32	0.54	5.57	0.05	0.3	7.04	13.98	558.3	132.9	108.7
				M24	22.46	0.36	7.48	2.65	0.02	0.81	0.22	0.25	18.33	0.05	1.2	17.5	28.54	444.4	106.6	77.1
				M23	73.28	0.71	12.75	2.94	0.03	1.47	0.65	1.46	1.9	0.1	0.1	1.1	3.42	619.8	117.6	103.4
				M22	49.85	1.18	19.35	3.99	0.01	4.15	3.85	0.83	1.48	0.01	0.1	2.33	12.8	583.9	277.1	116.9
				Aver.	35.74	0.535	8.73	3.84	0.062	3.435	10.95	0.548	7.656	0.11	0.3	7.21	20.66	479.8	181.3	103.4
	Aquitanian	Nukhul		M21	4.7	0.04	0.42	7.12	0.37	22.15	23.8	0.07	0.4	0.07	0.5	0.8	39.3	317.9	113	57
				M20	6.7	0.06	0.83	14.6	0.36	3.86	35.79	0.27	2.25	0.35	0.3	3.53	31.02	245.7	95.5	87.6
				M19	42.7	0.31	6.32	8.64	0.09	2.46	1.07	0.39	11.1	0.14	0.8	10.2	15.49	376.7	105.3	74.2
				M17	16.16	0.11	0.99	47.65	0.74	1.71	2.25	0.05	3.87	1.17	0.7	5.82	21.48	196.2	57	125.9
				M16	48.83	0.69	0.46	10.39	0.3	1.59	0.82	0.68	11.41	0.07	0.1	12.9	11.5	432.9	96.2	103.6
				M13	21.1	0.26	0.26	3.35	0.08	0.86	5.69	0.59	21.15	0.12	1.3	24	20.96	418.2	88.9	57.3
				M10	0.26	0.01	0.08	0.46	0.05	0.23	54.57	0.06	0.23	0.14	0.6	0.26	42.75	329.9	166.2	31.11
				M8	0.54	0.01	0.04	1.33	0.05	3.85	52.4	0.01	0.02	0.12	0.8	0.01	40.54	337.6	175.2	32.1
				M4	4.21	0.12	0.34	0.5	0.07	22.01	26.75	0.55	2.8	0.08	0.4	2.1	40.01	376.6	178.3	43.2
				M3	44.43	0.71	4.13	2.46	0.02	1.86	2.7	1.38	12.8	0.21	1.7	15.1	12.23	547.8	439.7	71
				M2	2.23	0.01	0.08	0.44	0.02	0.52	53.93	0.04	0.01	0.1	0.6	0.01	41.78	340.2	236.4	28.4
				M1	12.4	0.05	1.2	3.01	0.12	4.27	39.2	0.01	2.03	0.34	0.5	2.4	34.3	330.8	152.9	39.1
				Aver.	17.022	0.198	1.26	8.33	0.19	5.44	24.9	0.34	5.67	0.24	0.69	6.43	29.3	354.21	158.7	62.54

The mineralogical and chemical composition of clastic sedimentary rocks is controlled by various factors, including:

- (1) The composition of their source rocks.
- (2) Environmental parameters influencing the weathering of source rocks (e.g., atmospheric chemistry, temperature, rainfall and topography).

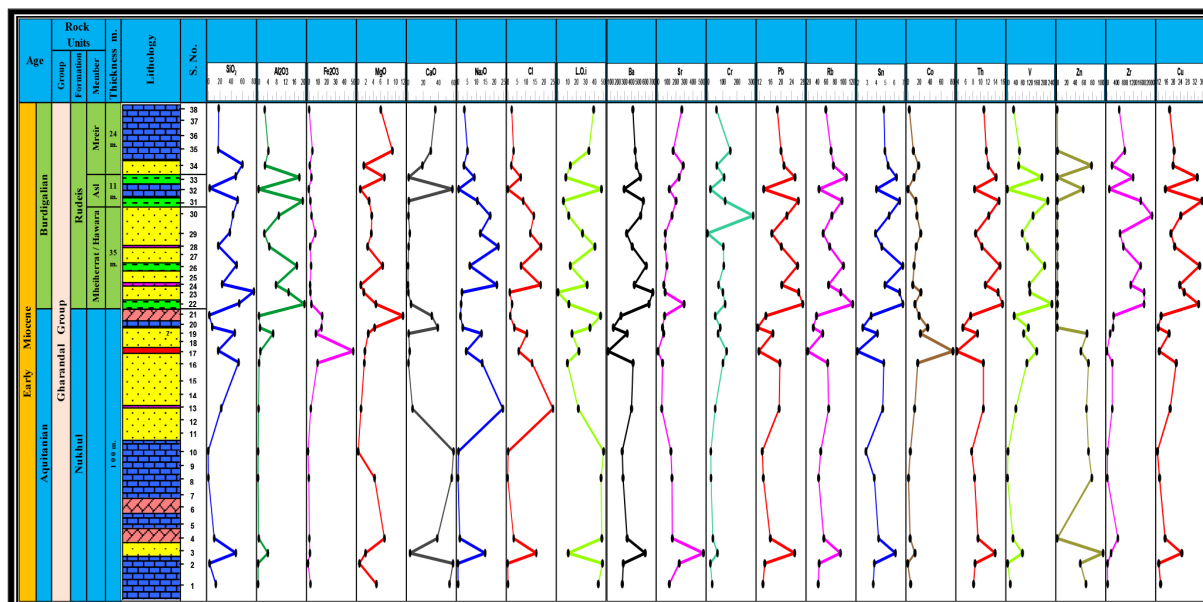
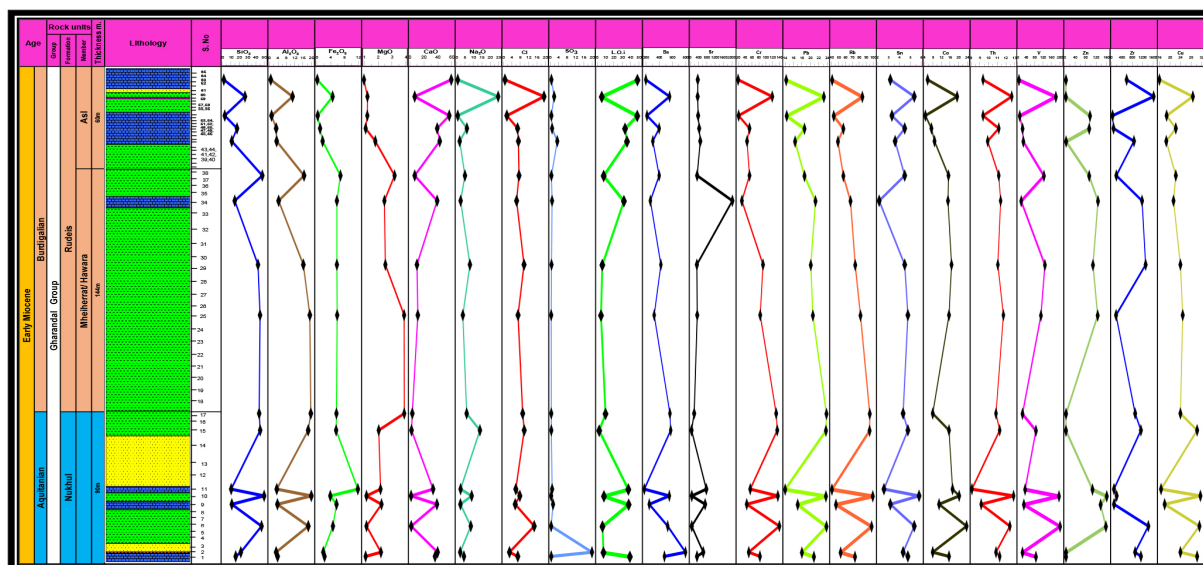
Table 4. Major oxides in wt. % and Trace elements in ppm of the Early Miocene rocks (Wadi Gharandal).

Age		Rock units		S.No.	Major element oxides %														Trace				
		Form.	Mem.		SiO ₂	TiO ₂	Al ₂ O ₃	Fe ₂ O ₃	MnO	MgO	CaO	K ₂ O	Na ₂ O	P ₂ O ₅	SO ₃	Cl	L.O.I	Ba	Sr	Cr	Pb	Rb	
Early Miocene	Burdigalian	Rudeis	Asl	GR63	1.01	0.02	0.21	0.24	0.01	1.03	53.1	0.01	0.52	0.06	0.2	0.53	42.7	337.8	394.5	36.3	15.5	48.4	
				GR59	24.6	0.82	9.44	4.51	0.03	1.28	5.68	0.42	23.42	0.07	1.5	16	11.88	492.3	390.4	116.8	22.7	83.5	
				GR53	2.05	0.04	0.56	0.36	0.01	1.27	50.5	0.06	0.51	0.17	0.2	1.29	42.56	345.1	407.9	37.4	15.6	50.2	
				GR49	15.7	0.12	2.5	1.01	0.02	1.15	34.9	0.14	5.69	0.42	0.5	5.54	32.01	424.5	446	63.1	19	61.4	
				GR45	9.83	0.17	2.7	1.72	0.05	1.85	38.2	0.2	1.61	1.07	3	5.87	33.7	383.4	486	57.3	17.2	55.1	
				GR38	43.9	0.79	14.31	6.69	0.02	3.25	5.7	0.51	4.59	0.09	0.2	6.1	13.52	424.5	371.2	63.1	19	61.4	
	Hawara		GR34	13.1	0.13	3.54	5.7	0.23	2.51	34.8	0.1	2.15	0.61	0.5	5.15	31.04	367.3	1660	45.1	21.1	69.7		
			GR29	39.1	0.82	14.02	5.7	0.05	2.58	8.58	0.56	7.41	0.1	0.2	8.1	12.38	435.8	361.3	95	20.2	75.2		
			GR25	41.4	0.89	16.76	5.78	0.02	3.94	9.7	0.61	3.4	0.11	0.1	5.72	11.24	392.2	374.7	88.4	20.6	81.3		
			Aver.	21.2	0.42	7.11	3.52	0.05	2.1	26.8	0.29	5.477	0.3	0.7	6.03	25.67	400.3	543.6	66.9	18.99	65.13		
	Aquitanian	Nukhul	GR17	40.4	0.97	17.18	5.58	0.03	3.95	2.5	0.59	5.56	0.06	0.1	7.56	15.15	494.6	263.1	126.1	23.2	92.1		
			GR15	41.5	1.08	16.07	5.49	0.02	2.1	1.5	0.67	13.08	0.05	0.1	8.17	9.7	499.7	167.3	128.6	23.1	91.9		
			GR11	9.18	0.17	2.75	11.6	0.39	2.23	29.5	0.16	2.11	1.3	0.5	4.83	34.87	328	706.9	64.8	15.3	48.1		
			GR10	45.9	0.71	17.39	3.86	0.01	1.21	0.96	0.46	8.4	0.04	0	6.43	13.8	490.7	176.2	130	23.1	95.6		
			GR9	9.89	0.19	3.05	5.6	0.16	2.3	34.5	0.15	2.01	0.94	1	4.6	35.15	360.1	663.5	56.6	17.7	52.8		
			GR6	43	0.65	16.12	4.6	0.04	1.21	1.13	0.38	7.9	0.05	0	12.1	12.53	480.1	174.6	133.6	23.2	94.2		
			GR2	20	0.16	2.5	1.9	0.04	2.26	35.4	0.14	1.9	0.14	20	2.33	13.35	596	594.4	61.4	18.5	58.2		
			GR1	14.2	0.25	3.11	2.26	0.33	1.15	32.1	0.28	4.01	0.09	0.1	5.63	36.18	458.9	366.1	87.7	20.8	74.9		
			Aver.	28	0.52	9.77	5.11	0.128	2.05	17.2	0.35	5.62	0.333	2.71	6.46	21.34	463.51	389.01	98.6	20.61	75.98		

- (3) Duration of weathering.
- (4) Transportation mechanisms of clastic material from source region to depocentre.
- (5) Depositional environment (e.g., marine versus fresh water).
- (6) Post-depositional processes (e.g., diagenesis, metamorphism) Hayashi et al., (1997).

Table 5. Average major and trace element contents in the studied different rock types compared with other works.

Rock type	Author	Major oxides (%)										
		SiO ₂	TiO ₂	Al ₂ O ₃	Fe ₂ O ₃	MnO	MgO	CaO	K ₂ O	Na ₂ O	P ₂ O ₅	SO ₃
Carbonate	Turekian and Wedepohl (1961)	5.1	0.1	0.8	0.5	0.1	7.8	42.3	0.7	0.1	0.2	ND
	Ronov and Migdisov (1971)	6.1	ND	1.5	1.4	ND	6.3	43.2	ND	0.2	ND	ND
	Wedepohl (1978)	8.3	ND	1.7	1.3	ND	7.4	39.7	ND	0.3	ND	ND
	Wedepohl (1978)	ND	0.0	0.4	0.5	0.1	<6.0	38.9	0.3	0.1	0.1	ND
	Wedepohl (1978)	ND	0.0	0.4	0.5	0.1	<6.0	35.6	0.3	0.1	0.1	ND
	Present work	7.9	0.1	1.6	3.5	0.1	4.7	39.3	0.2	1.9	0.4	0.6
Sandstone	Turekian and Wedepohl (1961)	78.8	0.3	4.8	1.3	ND	1.2	5.5	1.3	0.5	0.0	ND
	Wedepohl (1978)	ND	0.2	2.5	1.5	1.1	ND	3.4	1.5	1.2	0.7	ND
	Present work	44.4	0.5	4.9	10.8	0.2	2.1	3.5	0.1	8.7	0.3	0.5
Shale	Turekian and Wedepohl (1961)	15.6	0.8	15.1	6.7	0.1	2.5	3.1	3.1	1.2	0.3	ND
	Wedepohl (1978)	ND	0.9	8.2	2.5	6.6	ND	4.8	2.5	0.6	0.2	ND
	Present work	43.8	0.9	16.7	4.8	0.0	3.3	3.3	0.6	6.8	0.1	0.2

**Figure 13.** Chemo-stratigraphy of the different major and trace element constituents in Early Miocene rocks, El-Markha section.**Figure 14.** Chemo-stratigraphy of the different major and trace element constituents in Early Miocene rocks, Wadi Gharandal section.

6. Cluster Analysis

The cluster analysis of data obtained from X-ray fluorescence analysis is shown in Figure 15. These data represented the different various microfacies which indicate the presence of clastic sediments (Abd El-Hafez et al., 2015) such as quartz arenite, ferruginous quartz arenite, calcareous quartz arenite, iron-rich sand and shale and non-clastic rock units such as limestone, dolostone and gypsum. This type of analysis was performed by using cluster (SPSS) program.

Only two super-clusters, namely A and B were extracted representing all the different microfacies. The first super cluster (A) is Calcium oxides which are divided into two clusters (A₁ and A₂). The first one (A₁) consists of CaO, Zr, Sr and Br which are the main components of dolo-biomicroite, foraminiferal biomicroite, and biosparite microfacies (pure limestone). It is divided into four factors. The first factor includes CaO, MgO, Fe₂O₃, Zr, and Br which are all common components of (Dolostone) microfacies. The second factor consists of CaO, SO₃, SiO₂, Ba, Sr and Zr which are all common components of the (Gypsum) factor. Factor number three includes CaO and Fe₂O₃, Sr, Br and Zr which are the main components of Pelsparite and evaporitic dolomicroite microfacies (limestone). The last factor include CaO, SiO₂, Al₂O₃, Sr and Zr and Br which are all common components of Sandy micrite, foraminiferal biomicroite, and dolosparite microfacies (Sandy limestone).

The second super-cluster (B) is silicon dioxides which are divided into two clusters B₁ and B₂. The first cluster (B₁) is divided into two sub-clusters.

The first one (A₁) consists of CaO, Zr, Sr and Br which is the main components of dolo-biomicroite, foraminiferal biomicroite, and biosparite microfacies (pure limestone). The last one (A₁) is divided into four factors. The first factor involves CaO, MgO, Fe₂O₃, Zr and Br which are all common components of (Dolostone) microfacies. The second factor consists of CaO, SO₃, SiO₂, Ba, Sr and Zr which are all common components of the (Gypsum) factor. Factor number three includes CaO and Fe₂O₃, Sr, Br and Zr which are the main components of Pelsparite and evaporitic dolomicroite microfacies (limestone). The last factor consists of CaO, SiO₂, Al₂O₃, Sr and Zr, and Br which are all common components of Sandy micrite, foraminiferal biomicroite, and dolosparite microfacies (Sandy limestone).

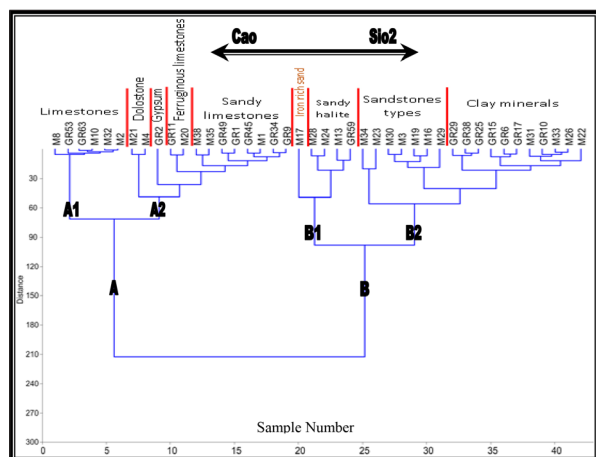


Figure 15. Cluster analysis of the Early Miocene rock units in studied areas, Southwest Sinai, Egypt.

The first one represented by SiO₂, Fe₂O₃, V, and Cr which include the main components of iron-rich sand. The second one includes SiO₂, Na₂O, Cl, Zr, Sr, and Ba which are the main common components of sandy halite bed. The second cluster (B₂) is divided into three factors. The first one includes the main components of calcareous quartz arenite and glauconitic quartz arenite such as SiO₂, Al₂O₃, CaO, Zr, and Br. The second factor is represented by SiO₂, Fe₂O₃, Na₂O, Cl, Zr, Br, Cr and, Sr of all common components of ferruginous evaporitic quartz arenite, Ferruginous quartz arenite and evaporitic quartz arenite microfacies. The last one is represented by SiO₂, Al₂O₃, Fe₂O₃, MgO, Zr, Br, Sr, V, Rb and Cr of all common components of clay minerals factors. The Montmorillonite is a main mineral while kaolinite is a minor mineral.

7. Conclusions

The present study is concerned primarily with exposed Early Miocene rocks in Southwestern Sinai along the Eastern side of the Gulf of Suez, at Wadi Gharandal and El-Markha sections. Both areas represented by the Nukhul and Rudeis formations. The Miocene succession variety in thickness ranges from 170 meters at El-Markha section to 325 meters at Wadi Gharandal section and is characterized by the presence of different rock types such as: sandstone, ferruginous sandstone, evaporitic sandstone, calcareous sandstone, iron-rich sand, evaporites, highly fossiliferous limestone, evaporitic limestone, dolostone, sandy limestone, dolomitic limestone and shale.

Mineralogically, the X-ray diffraction analysis of the Early Miocene sequence revealed the presence of calcite as the dominant minerals in the nonclastic rocks. Quartz was the dominant mineral in the clastic rocks, while goethite was the dominant mineral in the iron-rich sand, halite was the dominant mineral in the evaporite samples. Hematite, kaolinite, halite and gypsum are secondary minerals constituting the studied rock units with varying amounts.

The clay minerals in the studied samples of different formations were analyzed by the application of a semi-quantitative analysis which shows that the main clay minerals present in the Nukhul Formation are montmorillonite and kaolinite. In the Rudeis Formation, the main clay mineral is montmorillonite excluding two samples in which kaolinite is the main mineral.

From the data obtained by chemical analysis and the use of SPSS program it became clear that only two super-clusters namely (A and B) were extracted representing all the different microfacies. The first-super cluster (A) is Calcium oxides which are divided into two clusters (A₁ and A₂). The first one (A₁) consists of CaO, Zr, Sr, and Br which are the main components of dolo-biomicroite, foraminiferal biomicroite, and biosparite microfacies (pure limestone). The last one (A₁) is divided into four factors. The first factor involves CaO, MgO, Fe₂O₃, Zr, and Br which are all common components of (Dolostone) microfacies. The second factor consists of CaO, SO₃, SiO₂, Ba, Sr and Zr which are all common components of the (Gypsum) factor. Factor number three includes CaO and Fe₂O₃, Sr, Br, and Zr which are the main components of Pelsparite and evaporitic dolomicroite microfacies (limestone).

The last factor includes CaO, SiO₂, Al₂O₃, Sr and Zr,

and Br which are all common components of Sandy micrite, foraminiferal biomicrite and dolosparite microfacies (Sandy limestone).

The second super cluster (B) is Silicon dioxides which are divided into two clusters (B₁ and B₂). The first cluster (B₁) divided into two sub-cluster. The first one which are represented by SiO₂, Fe₂O₃, V, and Cr which include the main components of (Iron-rich sand). The last one includes SiO₂, Na₂O, Cl, Zr, Sr, and Ba which are the main common components of (Sandy halite) bed. The second cluster (B₂) is divided into three factors. The first one includes the main components of (Calcareous quartz arenite and glauconitic quartz arenite) such as SiO₂, Al₂O₃, CaO, Zr and Br.

The second factor is represented by SiO₂, Fe₂O₃, Na₂O, Cl, Zr, Br, Cr, and Sr of all common components of (Ferruginous evaporitic quartz arenite, Ferruginous quartz arenite and evaporitic quartz arenite) microfacies.

The last one is represented by SiO₂, Al₂O₃, Fe₂O₃, MgO, Zr, Br, Sr, V, Rb and Cr of all common components of (Clay minerals) factors. Montmorillonite is a main mineral, while kaolinite is a minor mineral.

References

- Abd El-Hafez, N.A.M. (1986). Evaluation of petroleum prospect of some areas in the Gulf of Suez region. Ph. D., Al Azhar Univ. A. R. E., Cairo, p. 384.
- Abd El-Hafez, N.A.M., Abd El-Moghny, M.W., Ahmed Mousa, S.T., El-Hariri, Y. M., El-Din, H., Sharaka, K. (2015). Effect of diagenetic processes on storage capacity of Lower Miocene rocks at Southwestern Sinai, Egypt, *Intr. Jour. of Sci Eng. & App. Sci.*, 1(9): 2395-3470.
- Abul-Nasr, R.A., and Salama, G.R. (1999). Paleecology and depositional environments of the Miocene rocks in WESTERN Sinai, Egypt. M.E.R.C., Ain Shams Univ., Earth Sci. Ser., 13: 92-134.
- Al-Husseiny, M.I. (2012). Late Oligocene-Early Miocene Nukhul Sequence, Gulf of Suez and Red Sea. *Geo Arabia*, V. (17), pp. 17 - 44.
- American Society of Testing Material (1960). A.S.T.M., of X-Ray diffraction data, Amer. Soc. of Testing Materials, Phil., U.S.A., pp. 1119 - 1129.
- Brown, C. (1961). The X-Ray identification and crystal structure of clay minerals. A symposium, the Mineralogical Soc., London, p. 544.
- Conoco (1986). Geological map of Egypt, Scale 1:500,000, 6 Sheets, with cooperation of Egyptian General Petroleum Corporation, Klitzsch, E., List, F.K. and Pohlmann, G. (Editors), Berlin, Cairo, Egypt.
- Deer, W.A. Howie, R.A. Zssman, J. (1963). "Rock forming minerals". non-silicates, V. (5), p. 1788. John Wiley and Sons, New York.
- El-Azabi, M.H. (1997). The Miocene marginal marine facies and their equivalent deeper marine sediments in the Gulf of Suez, Egypt: A revised stratigraphic setting. *Egypt. J. Geol.*, 41(2A): 273-308.
- El-Bakry, H.M., Zahra, H.A., Khater, T.M., Fawwaz, S.E., Almoazamy, A.A. (2010). Geology of West Central Sinai, Egypt. *Geol. Surv. (Unpublished)*. Report No. 53, p. 61.
- El-Hariri, T.Y. (2008). Depositional environment and petrophysical studies on subsurface Devonian sediment from Faghur-I well at Northwestern Desert. *Jour. App. Sci. Res.*, 4 (1): 65-75.
- Garnder, J.V., Deab, W.E., Alonso, B. (1990). Inorganic of surface sediments of the Ebro shelf and slop northwestern Mediterranean. *Mar. Geol.*, Amsterdam, (95): 225-245.
- Hayashi, M., Komiya, T., Nakamura, Y., Maruyama, S. (1997). Archean regional metamorphism of the Isua supracrustal belt, Southern West Greenland: Implication for a driving force for Archean plate tectonics. *International Geology Review*, 42: 1055-1115.
- Hewaidy, A.A., Farouk, S., Ayyad, H.M. (2012). Nukhul Formation in Wadi Baba, Southwest Sinai Peninsula, Egypt. *Gulf Petro Link, Bahrain, Geo Arabia*, 17(1): 103-120.
- Mousa, A.S., El-Hariri, T.Y., El-Meligy, W.M. (2009). Assessing the Influence of diagenetic processes at El-Gedida Mines, El-Bahariya Oasis, Egypt, *Australian Journal of Basic and Applied Sciences*, 3(3): 1749-1762.
- Pierce, J.W., and Siegel, F.R. (1969). Quantification in clay mineral studies to sediments and sedimentary rocks. *J. Sed. Petrol. Tulsa.*, (39): 187-193.
- Said, R., and El Heiny, I. (1967). "Planktonic foraminifera from the Miocene rocks of the Gulf of Suez region, Egypt", Cushman contribution from the Cushman foundation. Part (I), V. (XVIII), pp. 14-26.
- Siegel, F. R., Pierce, J. W. and Kostick, D. S. (1981). Suspensates and bottom sediments in the Chilean Archipelago. *Modern Geology.*, (7): 217-299.
- Tamish, M., (1988). "Geomathematical and geochemical studies on Egyptian phosphorite deposits". *Berliner Geowiss. Abh. (A)*, Berliner, pp 98- 97.
- Welton, J.E. (1984). "SEM Petrology Atlas". A.A.P.G., Chevron oil field research company, U.S.A., Methods in exploration series no. (4), p. 237.

Assessment of Metal Pollution of the Surface Sediments along the Wadi Al Rayyan area, Jordan

Ibrahim Bany Yaseen¹ and Zayed Al-Hawari²

¹Al-al-Bayt University, Institute of Earth and Environmental Sciences, Department of Earth and Environmental Sciences, Al-Mafraq, Jordan.

²University of Jordan, Faculty of Science, Department of Environmental and Applied Geology, Amman, Jordan.

Received 15 November 2018, Accepted 20 January 2019

Abstract

Seventy surface sediment samples were collected from Wadi Al Rayyan area. These samples were extracted by Ammonium-Acetate-EDTA, and analyzed by Atomic Absorption Spectrometer to determine their metal concentrations of Cu, Zn, Fe, Mn, Pb, Cd, Cr and Ni. XRF was used to analyze CaO wt%, and XRD was used to determine the mineral composition. The chemical analyses of the samples show an enrichment of Cu, Mn, Pb, Cd, Cr and Ni along the Wadi Rayyan from upstream to downstream, but valuable concentrations of Zn and Fe were found along the Wadi. To evaluate the level of contamination for the surface sediments of Wadi Al Rayyan in this study, the Enrichment Factor (EF), Geoaccumulation index (I_{geo}), Pollution Index (PI) and Pollution Load Index (PLI) have been used. EF shows the surface sediments to be moderately-to-strongly polluted and strongly-to-extremely polluted with Cu, Zn, Mn, Pb, Cd, Cr and Ni. In regard to Zn, the sediments are moderately polluted, and significantly polluted with Mn and Cr. I_{geo} values for Zn, Fe, and Mn reveal the sediments to be unpolluted ($0 < I_{geo} \leq 1$), while they are moderately polluted ($1 < I_{geo} \leq 2$) with Cu, Cd, and Cr, and strongly polluted ($2 < I_{geo} \leq 3$) with Ni and Pb. PI for Zn, Fe, and Cd shows a low level of pollution ($PI < 1$), a high level of pollution ($PI \geq 3$) with Cu, Pb, Cr and Ni, and a middle level pollution ($PI \leq 1$) with Mn. The PLI values for Wadi Al Rayyan sediments were found to be less than 1 ($PLI < 1$), thus, revealing that the surface sediments are unpolluted with respect to Cu, Zn, Fe, Mn, Pb, Cd, Cr, and Ni. These metals can be derived from anthropogenic sources, such as fertilizers and pesticides used in agricultural activities.

© 2019 Jordan Journal of Earth and Environmental Sciences. All rights reserved

Keywords: Heavy Metals, Pollution, Assessment, Surface Sediments, Wadi Al Rayyan, Jordan.

1. Introduction

The various kinds of heavy metal pollution constitute a problem in modern societies. Toxic heavy metals are a major concern, since these elements are not biodegradable, but their elevated uptake by crops may affect food quality and safety. Heavy metals at high concentrations have toxic effects on living organisms (Schuurmann and Market, 1998; MacFarlane and Burchett, 2000; Habes and Nigem, 2006). Heavy metals are very important in the ecological system, because they are not removed from water by self-purification processes, but they tend to be bio-accumulated during the food chain (Loska and Wiechula, 2003; Al-Khashman, 2004). Heavy metals enter into aquatic systems mainly through natural inputs, such as chemical weathering of rocks, volcanic activities, industrial processes and mining activities. The anthropogenic and manufacturing sources include industrial processes, energy production, industry, vehicle exhausts, waste disposal, coal combustion, and agricultural activities as well as the use of synthetic products (e.g. pesticides, paints, batteries, industrial waste, and land applications of industrial, terrestrial runoff and sewage disposal or domestic sludge (Martin et al., 1998; Li et al., 2001; Gray et al., 2003; Bin Chen et al., 2005; Biasoli et al., 2006). These activities can increase the levels of the metals in various parts of the ecosystems (Auburn, 2000; Bilos et al., 2001; El-Hasan and Jiries, 2001; Komarek and Zeman, 2004; Moller et al., 2005; Çevik et al., 2009; Lu et al., 2009;

Yang et al., 2011).

Stream sediments and soil are generally mixtures of several components, including different mineral species and organic constituents and debris. The sediments accumulate through complex physical and chemical adsorption mechanisms, depending on the nature of the sediment matrix and the properties of the adsorbed compounds (Maher and Aislabie, 1992; Ankley et al., 1992; Leivouri, 1998; Al-Khashman and Shawabkeh, 2006). Heavy metals discharged into the aquatic systems have been immobilized within the stream sediments by main processes such as adsorption, flocculation, precipitation and co-precipitation. Therefore, sediments in aquatic environments serve as a pool that can retain metals or release metals to the water column by various processes of remobilization (Caccia et al., 2003; Pekey, 2006; Marchand et al., 2006). The main processes lead to the association of heavy metals with solid phases, such as direct absorption by fine-grained, clay particles, adsorption of hydrous ferric and manganese oxides. This may in turn be associated with clays; adsorption on or complication with natural organic substances, and direct precipitation as new solid phases (Habes and Nigem, 2006; Cao et al., 2011).

Numerous studies have demonstrated that the concentrations of heavy metals in sediments can be sensitive indicators of contaminants in the aquatic systems (Bellucci et al., 2002; Bloundi et al., 2009; Suthar et al., 2009; Al-Khashman and Shawabkeh, 2009; Mhamdi et al., 2010, Al-

* Corresponding author e-mail: ibanyyaseen@yahoo.com

Khashman, 2013). Several approaches have been applied in order to assess the severity of sediment contamination and to understand the natural and anthropogenic inputs in the river system. The metal assessment indices include the Enrichment Factor (EF), Geo Accumulation Index (I_{geo}), pollution Index (PI) and Pollution Load Index (PLI). The sediment quality guidelines were often used to screen the potentiality of contaminants within sediments. The aims of this study focus on the concentrations of heavy metals (Cu, Zn, Fe, Mn, Pb, Cd, Cr and Ni) and their distribution in the sediments of Wadi Al Rayyan area in Jordan. This study provides an assessment of heavy metal pollution in the sediments using the Enrichment Factor (EF), Geoaccumulation Index (I_{geo}), Contamination Factor (CF), Pollution Index (PI) and Pollution Load index (PLI).

2. Geological Setting

The study area is covered by Late Cretaceous carbonate rocks. The dominant outcropped rocks belong to Ajlun and Belqa Groups (Table 1). The oldest rocks cropped out in the area belong to the Mesozoic – Cenozoic (Cenomanian, Turonian, Campanian and Maastrichtian) periods, as limestone Formation within Ajlun and Belqa Group (Fig. 1a). Quaternary recent sediments as wadi deposits and soils overlie the Late Cretaceous rocks (Abu Qudaria, 2005).

The study area of Wadi Al Rayyan was affected by different environmental activities such as agriculture in addition to the road networks along the Wadi. Agriculture activities in Wadi Al Rayyan area depend on rainfall throughout the winter season and irrigation processes utilizing the effluents of Arjan springs in other seasons.

Table 1. Geological Classification of Rock Units in the Study Area (Abu Qudaria, 2005).

Era	Period	Epoch	Stage	Group	Formation	Description
Cenozoic	Quaternary	Recent	Holocene -Recent		Soil (S) Calcrete (Cl)	Soil, Calcrete and Gravel
Mesozoic	Late Cretaceous	Upper	Maastrichtian/ Paleocene	Belqa	Muwaqqar Marl (B3)	The formation consists of massive marl and chalk, with bitumen lenses in the lower part, and limestone embedded within clay marl at the top.
			Campanian/ Maastrichtian		Amman Silicified Limestone / Al Hisa Phosphorite (B2) (ASL/AHP)	The formations consists of chert, limestone, phosphates, coquina limestone and marl
		Middle	Turonian	Ajlun	Wadi As-Sir (A7) (WSL)	Hard crystalline limestone, yellowish dolomitic limestone and dolomite, over lained by marly limestone well bedded massive micrite and chert nodules.
					Shuayb (Sh)	Light grey limestone interbedded with marls alternating with chalky limestone.
			Cenomanian		Hummar (H)	Hard dense limestone and micritic limestone with bedded clay, overlain by dolomite limestone, the formation highly fractured and cavernous

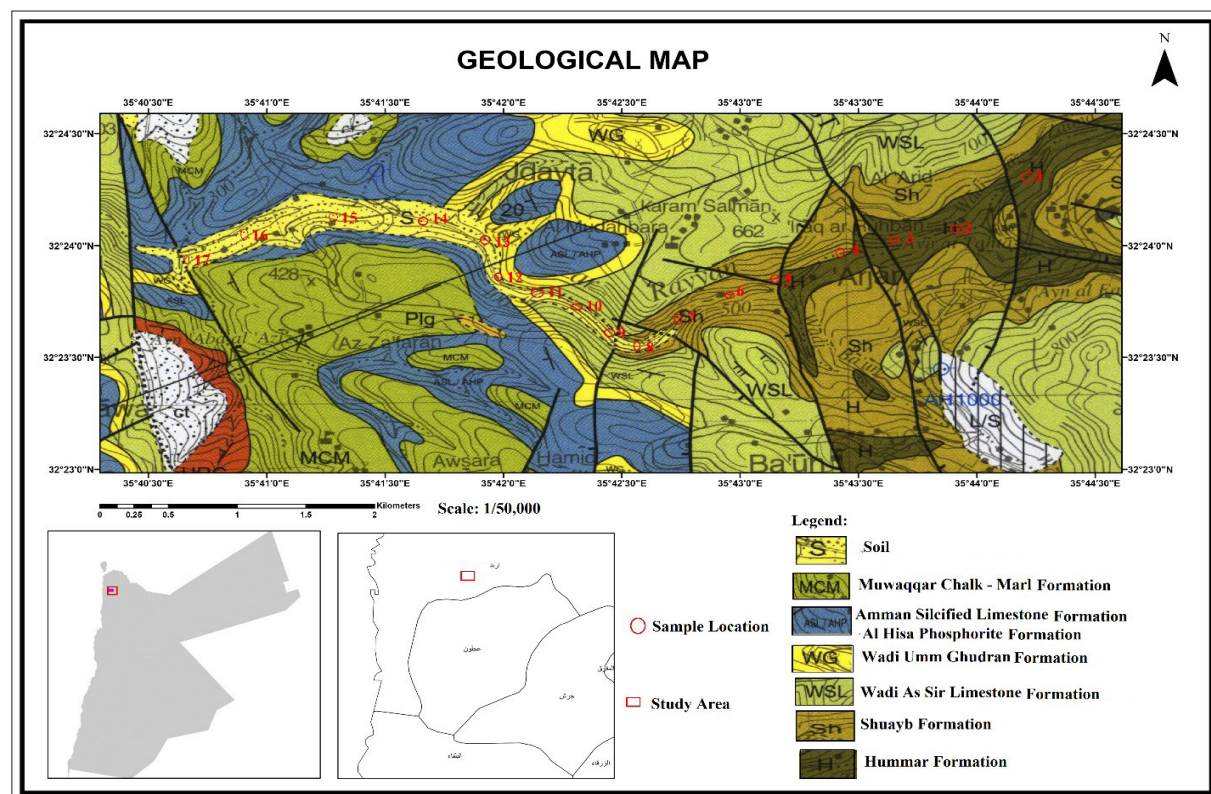


Figure 1. A geological map showing the area under study, and sample location (Modified After Abu Qudaria, 2005)

3. Sampling and Analytical Techniques

Seventy composite stream sediment samples were collected along the main valley of Wadi Al Rayyan area (Fig. 1b). The samples were taken from depths of 5–20 cm depending on the sediment condition. The samples were collected in May, 2016 and were, then, transported to the laboratory of Al-Al-Bayt University using polyethylene bags. The samples were dried in the oven at 50°C for twenty-four hours. All the samples were sieved (1/256 mm) and particles <63 µm (0.05-mm) in size. This size has been provided to be the best size for analysis for arid and semi-arid regions (Saffarini and Lahwani, 1992; Singh et al., 1999).

The extraction method was used to assess the heavy metal pollution contents of Cu, Zn, Fe, Mn, Pb, Cd, Cr and Ni. The best extraction results were obtained with Ammonium-Acetate-EDTA. The extraction solution was prepared by adding 0.5M NH₄Ac 0.5M+ HAc + 0.02M EDTA (pH 4.65). Then, 38.5gm of NH₄Ac was dissolved in 500 ml H₂O+ 25ml Acetic Acid and 5.8gm EDTA was added, then the volume was increased to one liter with distilled water. Thereafter, 20 gm of the air-dried sediment samples (<63 µm) were placed in a 300 ml Erlenmeyer flask and 100 ml of the extracting solution was added. Then, it was shaken mechanically for thirty minutes. After shaking, suspension materials were filtered through 0.45-µm filters, and the clear solution was collected in polyethylene bottles (Albanese, 2008). Heavy metals were determined using Atomic Absorption Spectrophotometer (AAS) (2280 Model; Perkin Elmer) at the University of Jordan. The quality control was performed for Cu, Zn, Fe, Mn, Pb, Cd, Cr, and Ni using Merck ICP4 standard solutions. A 95 % confidence level was used. The results of the studied samples are shown in Table 1.

The organic matter (OM %) in each sample was determined

using loss on ignition (LOI) at 550°C for two hours at the Institute of Earth and Environmental Sciences Lab, Al-al-Bayt University (Dean 1974). The pH measurements were performed using 2gm of dry sediment samples (< 63 µm), with the beaker kept undisturbed for about five minutes, and the solution was stirred with a glass rod (Dean 1974). After that, the pH was measured by pH electrode (Table 1). The chemical analysis of the CaO wt % for the samples was carried out using Phillips X-ray Florescence (XRF) Majex PW-2424 model. In addition, the mineralogical compositions of all the samples were evaluated by X-ray Diffraction (XRD) using a Phillips diffractometer with Cu Ka radiation at Water Environment and Arid Regions Research Center labs, at AL al-Bayt University.

4. Assessment of Contamination Level

To quantify the level of metal contamination in the surface sediments for the present study, many calculation methods have been proposed. In this study, the Enrichment Factor (EF), Geoaccumulation index (Igeo), Contamination Factor (CF), Pollution Index (PI) and Pollution load index (PLI) have been used to assess the metal contamination level in the surface sediments collected in the investigated area (Shi et al., 2008; Yang et al., 2011).

The Enrichment factor (EF) was used to compare the metals originating from anthropogenic activities to those of natural origins, and to determine the degree of contamination and the possible anthropogenic impact on the sediments of Wadi Al Rayyan area. The EF analysis was first presented by Mason, (1966) and Simex and Helz (1981) to evaluate trace element concentration as follows: $EF = (M/Fe)_{sample} / (M/Fe)_{background}$. Where, M/Fe sample is the ratio of metal and Fe concentration in the sample, M/Fe background is the ratio of metal and Fe

Table 2. Chemical analyses of the surface sediment samples collected from Wadi Al Rayyan area.

S. No.	OM %	CaO wt%	Ppm								PH	EC
			Cu	Zn	Fe	Mn	Pb	Cd	Cr	Ni		
1	1.10	14.2	244	20.5	30.5	2475	1650	61.5	299	415	8.36	240
2	0.28	25.3	278	45.5	35.5	6300	1800	84.5	331	426.5	8.47	310
3	0.57	21.1	182	35	32	1618.5	1400	63	207.5	445.5	8.14	280
4	0.20	23.2	212	32	26.75	4870	1350	64.5	250.5	500	8.54	340
5	0.34	27.3	214.5	69.5	26.05	1458.5	850	57.5	250.5	453	8.45	425
6	0.11	23.5	193	26	25	2094.5	1300	55.5	248	518	8.32	335
7	0.84	24.8	248.5	23.5	25.5	1832	1150	60.5	257	560.5	8.32	310
8	0.10	38.2	261	34	65	1772	1846	60.5	265.5	571	8.33	860
9	0.39	24.1	279.5	156	20	2749	1538	81	262	704	8.50	450
10	0.40	23.2	237	42	29.5	2790.5	1692	62	257.5	648	8.47	361
11	0.30	26.3	211.5	14.5	25	2374.5	1615	64	254.5	590	8.46	610
12	0.36	25.2	208	25	29.55	3242	1625	57	269	503	8.54	540
13	0.25	18.3	209	18	23.5	1283.5	1618	53.5	251.5	473	8.73	280
14	0.55	23.3	198	23	120	1213.5	1628	50	250.5	435.5	8.41	300
15	0.33	22.8	251.5	25.5	30	3419.5	1769	68.5	252	413	8.17	290
16	0.41	24.8	194	44.5	25	2243	1355	50.5	188.5	261	8.37	400
17	0.17	20.2	234	21.5	30	2926	1700	58.5	304	401	8.45	310
Max	1.10	38.2	279.5	280	156	120	6300	1846	84.5	331	8.73	860
Min	0.10	14.2	182	14.5	20	120	850	50	84.5	261	8.14	240
Average	0.42	24.1	227.21	50.0	40.78	2363.3	1739	155.2	240.39	468.9	8.42	407

concentration of a background (Ergin et al., 1991; Chakravarty and Patgiri, 2009; Seshan et al., 2010; Bentum et al., 2011). The geochemical normalization of heavy metal data was employed for conservative elements such as Fe, Al and Si. According to Schiff and Weisberg, (1999) and Mucha et al. (2003), Fe was used to normalize heavy metal contaminants. In this study, Fe was used as a conservative tracer to differentiate natural components from anthropogenic ones. The background concentrations of the heavy metal study are taken from Turekian and Wedepohl (1961). The classification of pollution degree based on the enrichment ratio methodology was divided into a five-category system (Sutherland et al., 2000); If ($EF < 2$), this implies a depletion to minimal enrichment suggestive of no or minimal pollution. If EF is within the range of 2–5, this indicates a moderate enrichment, suggestive of a moderate pollution. If EF is within the range of 5–20, it means a significant enrichment, suggestive of a significant pollution. If EF is within the range of 20–40, it means a very high enrichment, indicative of a very strong pollution, and if ($EF > 40$), it means an extreme enrichment, indicative of an extreme pollution signal.

The Geoaccumulation index (I_{geo}) was used by Muller, (1981) and Wei et al. (2009) to assess heavy metal pollution. The I_{geo} was used to assess metal contamination in urban soils by comparing current and pre-industrial values (Wei et al. 2009; Al-Khashman, 2013). In this study, the geoaccumulation index (I_{geo}) was used to determine the extent of heavy metal pollution in Wadi Al Rayyan surface sediments. The following equations are used in the calculation: $I_{geo} = \log_2 (C_n / 1.5B_n)$, (Rath et al., 2005). Where C_n is the concentration of the element 'n', and B_n is the geochemical background value of the element n, and 1.5 is the background matrix correction factor due to lithogenic effects. The geochemical background value in average shale is used to calculate I_{geo} (Turekian and Wedepohl, 1961). The geo-accumulation index (I_{geo}) scale consists of seven grades from 0 to 6, ranging from unpolluted to highly polluted (Rath et al., 2005, Faiz et al., 2009). The Geoaccumulation index value class designation of sediment quality is as follows:

- $I_{geo} < 0$ unpolluted environments
- $0 < I_{geo} \leq 1$ unpolluted-to-moderately polluted
- $1 < I_{geo} \leq 2$ moderately polluted
- $2 < I_{geo} \leq 3$ moderately-to-strongly polluted
- $3 < I_{geo} \leq 4$ strongly polluted
- $4 < I_{geo} \leq 5$ strongly to- extremely- polluted, and
- $I_{geo} > 5$ extremely polluted

The pollution index (PI) and Pollution load index (PLI) were used to assess heavy metal pollution in the soil, sediments, and dust. The pollution index (PI) was defined by the following equation: $PI = C_n / B_n$ where C_n and B_n are the measured and background concentrations of metal n, respectively, in the surface sediment samples. PI is classified by (Faiz et al., 2009) as follows: $PI \leq 1$ indicates a low level of pollution; $1 < PI \leq 3$ indicates a middle level of pollution, and $PI > 3$ a high level of pollution. The pollution Load Index (PLI) for each sample was calculated following the method by Tomilson et al., (1980) and Soares et al., (1999). It was defined by the following equation:

$$PLI = \sqrt[n]{CF1 + CF2 + CF3 + \dots + CFn} \dots\dots\dots (1)$$

where n is the number of metals and CF is the contamination factor. Contamination Factor (CF) is calculated from the following relationship:

$$CF = \frac{(C_n) \text{Concentration of the heavy metal in the soil sample}}{(B_n) \text{Background concentration of the same metal}} \dots\dots\dots (2)$$

where C_n is the measured concentration of a heavy metal in the surface sediments, and B_n is the background value. According to Harikumar et al., (2009), Faiz et al., (2009), and Seshan et al., (2010), the PLI value ($PLI \leq 1$) indicates a low level of pollution, while $1 < PLI \leq 2$ indicates a middle level of pollution and $PLI > 2$ a high level pollution.

5. Results and Discussion

5.1. Physicochemical Properties of the Surface Sediments

The concentrations of different metals in the surface sediments along Wadi Al Rayyan area were studied according to the strength of anthropogenic, natural sources and PH values. The pH values show a relatively equal distribution in the investigated area. The pH-values range between 8.14 and 8.73 (Table 2), suggesting alkaline-prevailing conditions for all the sediment samples. The concentrations of metals in the sediments can vary greatly depending on the organic matter content and pH-values. Usually, pH-values influence the sediment composition, which in turn affects the heavy metal mobility and distribution in the sediment samples (Odat and Alshammari, 2011).

The high pH value of the samples was attributed to the high percentage of carbonate materials in the surface sediments (Murray and Hendershot 2000). Kim et al. (2003) explain that the changes of soil acidity can influence neutral compositions in the soils by removing the bivalent base such as Ca^{+2} and Mg^{+2} from soil distribution in the investigated area. The electrical conductivity (EC) values range between 240 and 860 $\mu S.cm^{-1}$. A high electrical conductivity (EC) value was found at the human activity site, while the lowest value of electrical conductivity was found at the low human activity site (240 $\mu S.cm^{-1}$). The percentage of organic matter (OM%) in the surface sediments of Wadi Al Rayyan range between 0.1 and 1.1 %, with an average of 0.42 % (Table 2). The content of organic matter in Wadi Al Rayyan sediments is related to the organic content of plant remains located adjacent to the Wadi site at various stages of decomposition. Cells and tissues of plant organisms and substances from plant roots, and soil microbes are considered as additional sources.

The value of the CaO wt% contents of the surface sediments range from 14.2 to 38.2 wt%, with an average of 24.12 wt% (Table 1). The percentage of CaO content in the sediments is mainly derived from the carbonate rocks exposed along the Wadi site and in the catchment area. These rocks mainly include limestone, chalky marl and caliches. These results are documented for the XRD analysis for all the surface sediment samples. The main mineral composition analysis for all the samples reveals that calcite, dolomite, quartz gypsum and clay minerals are dominant minerals. The carbonate mineral is important for the co-precipitation of heavy metals such as Cd and Zn (Alloway and Ayres, 1997).

5.2. Heavy Metal Distribution

The chemical concentrations of the heavy metals determined for the study sample are listed in Table 2. The variable concentration of heavy metal distributions along

Wadi Al Rayyan area are shown in Fig. 2. The high level of Cu, Mn, Pb, Cd, Cr and Ni was found along the Wadi Rayyan surface sediments from upstream to downstream, but valuable concentrations of Zn and Fe were found along the Wadi. The enrichment concentration for these elements are located near the roads across the stream and in areas of human activity along the Wadi, as shown in samples 2, 4, 9, 15 and 17 (Fig. 2). The average concentrations of Cu, Zn, Fe, Mn, Pb, Cd, Cr, and Ni in Wadi Al Rayyan sediments are (227.21, 43.5, 38.9, 2746, 1504, 62.47, 258.84 and 488.58) respectively and have been compared with uncontaminated sediments and soils. Zn and Cd levels in uncontaminated sediments and soils contain 0.09 and 0.0003 mg g⁻¹ dry wt., respectively (Bowen, 1979). The elevated concentrations of heavy metals in the sediments of Wadi Al Rayyan were probably due to the anthropogenic sources as well as human and agricultural activities near the wadi surface sediments' site (Calace et al., 2005). The sources include fertilizers and pesticides used in agricultural activities and sewage wastewater discharges and seepage for running of the surface water near areas of human activities along the Wadi Al Rayyan. According to Zarei et al., (2014), the elevated values of Pb and Cd might be related to human activities such as wastewater discharges in the surface water along the Wadi, which mixes with the surface running water discharge from the Arjan spring.

The Pearson's correlation coefficients for the contents of Cu, Zn, Fe, Mn, Pb, Cd, Cr and Ni in the surface sediments of Wadi Al Rayyan are presented in Table 3. A positive correlation was found for Cu with Cd ($R^2 = 0.75$) and Cr ($R^2 = 0.66$); Zn with Cd ($R^2 = 0.54$); Mn with Cd ($R^2 = 0.68$) and Cr ($R^2 = 0.53$). The results revealed that metal concentrations rise unnaturally due to the anthropogenic sources of pollution which have been identified to be the human, industrial, and agricultural activities such as sewage effluent, waste combustion, steel processing, fertilizers and pesticides (Wuana et al., 2011). Low positive linear correlations among the concentrations of Cu, Zn, Pb, Cd, and Cr were clearly observed: Cu with Zn ($R^2 = 0.43$), Mn ($R^2 = 0.45$), Pb ($R^2 = 0.41$), Ni ($R^2 = 0.38$); Zn with Ni ($R^2 = 0.42$); Pb with Cd ($R^2 = 0.28$) and Cr ($R^2 = 0.45$); Cd with Cr ($R^2 = 0.45$), Ni ($R^2 = 0.37$); Cr with Ni ($R^2 = 0.15$) respectively. These values revealed the same sources for all of the abovementioned elements. The results indicate that heavy metals are not associated with each other, and that no relationship exists between the variables (Bany Yaseen and Al-Hawari, 2015). Furthermore, these metals have different anthropogenic and natural sources in the sediments of Wadi Al Rayyan (Habes and Nigem, 2006; Bany Yaseen and Elaimat, 2016).

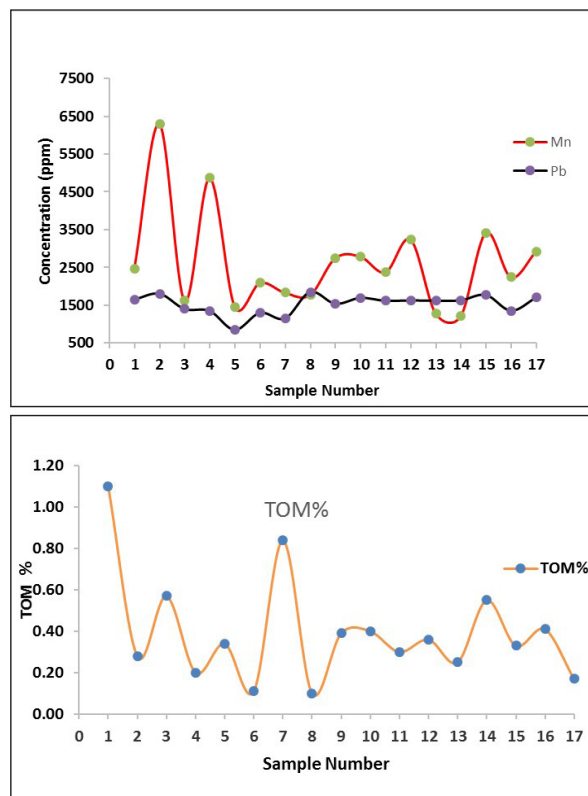
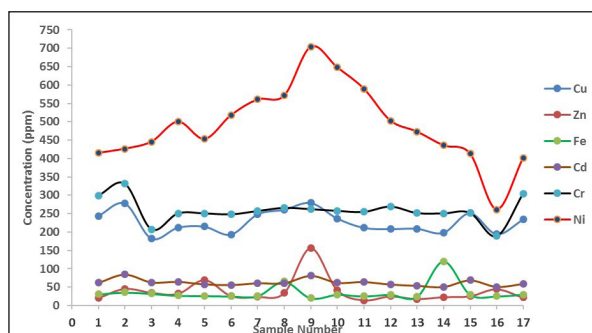


Figure 2. Distribution of metal concentration (ppm) for Cu, Zn, Fe, Cr, Ni, Cd, Mn and Pb and percentage of organic matter (OM%) and CaO wt% for the surfaces sediment samples from Wadi Al Rayyan area.

Table 3. Correlation matrix between metals in the surface sediment samples, from the Wadi Al Rayyan area.

	ppm							
	Cu	Zn	Fe	Mn	Pb	Cd	Cr	Ni
Cu	1							
Zn	0.433	1						
Fe	-0.104	-0.194	1					
Mn	0.447	0.069	-0.248	1				
Pb	0.406	-0.181	0.279	0.324	1			
Cd	0.747	0.537	-0.292	0.687	0.286	1		
Cr	0.658	-0.035	0.025	0.535	0.449	0.496	1	
Ni	0.378	0.424	-0.107	-0.053	0.074	0.372	0.153	1

5.3. Enrichment Factor (EF):

Enrichment factor (EF) was used to assess the degree of contamination and the possible anthropogenic impact on the sediments of Wadi Al Rayyan area. The EF analysis was first presented by Simex and Helz (1981) to evaluate trace element concentration as follows:

$$EF = \frac{(M/Fe)_{\text{sample}}}{(M/Fe)_{\text{background}}}$$
 Where (M/Fe) sample is the ratio of metal and Fe concentration in the sample. (M/Fe) background is the ratio of metal and Fe concentration of a background (Ergin et al., 1991; Chakravarty and Patgiri, 2009; Seshan et al., 2010; Bentum et al., 2011). The geochemical normalization of the heavy metal data was employed for conservative elements such as Fe, Al, and Si. According to Schiff and Weisberg (1999) and Mucha et al., (2003), Fe (reference) was used to normalize heavy metal contaminants. In this study, Fe was used as a conservative tracer to differentiate

natural components from anthropogenic ones. The background concentrations of the studied heavy metals are taken from Turekian and Wedepohl (1961).

The classification of pollution degree based on the enrichment ratio methodology was in a five- category system (Sutherland et al., 2000). If EF is less than 2 ($EF < 2$), it implies depletion to minimal enrichment suggestive of no or minimal pollution. If EF is within the range of 2–5, this indicates a moderate enrichment, suggestive of a moderate pollution, and if EF is in the range 5–20, it means a significant enrichment, suggestive of a significant pollution signal. When EF is in the range 20–40, it means a very high enrichment, indicating a very strong pollution signal, and if EF is more than 40 ($EF > 40$), it means an extreme enrichment, indicating an extreme pollution signal.

The values of EF in the study area are shown in Table 4 and Fig. 3b. The results of EF indicate that high concentrations of Cu, Pb, Cd, Cr, and Ni, are present in the analyzed samples (Table 2). The sediments of Wadi Al Rayyan are moderately-to-strongly polluted and strongly-to extremely polluted. This may result in a risky pollution with Cu, Zn, Mn, Pb, Cd, Cr and Ni, while the values for Zn indicate a minimal pollution in all of the samples excluding sample 9 which shows moderate pollution (Table 4) and Fig.2d (EF ranges between 0.13-5.13 with an average of 0.94). As for Cu, there was significant pollution except in sample 14 which showed a moderate pollution (EF

ranges between 3 and 26.12 with an average of 14.42). There was minimal pollution with Mn in the samples 3, 8, and 14, and moderate pollution with Mn in all of the other samples (EF ranges between 0.46 and 8.25 within an average of 4.1). As for Pb, there was significant pollution in the samples 3, 5, 7, 8, and 14, whereas other samples showed a very strong pollution (EF ranges between 6 and 34.21 with an average of 22.59). There was significant pollution with Cd in all of the samples except in sample 9 which revealed a very strong pollution. As for Cr, there was moderate pollution in samples 8 and 14, and significant pollution in all of the other samples (EF ranges between 2.27 and 14.23 with an average of 9.5). There was significant pollution with Ni in the samples 1,2,3, 8, 14, 15, 16, and 17, while other samples revealed a very strong pollution. The strong pollution of the sediment samples with Cu, Pb, Cd, Cr, and Ni depends on the location of the sample and the contributors to the elements' concentrations. The fluctuation in the EF values can be attributed to the changes in the amount of contribution of each metal in the sediments, or to the variance in the removal rate of each metal from the sediments. These heavy metals can be derived from anthropogenic sources, such as fertilizers and pesticides used in agricultural activities. These dangerous metals can be derived from industrial and agricultural activities such as waste, gasoline additives used in industries and automobiles (Mwamburi, 2003). In addition, they might be derived from corrosion agricultural activities in the wadi.

Table 4. Enrichment Factor (EF) for the heavy metals of the surface sediments of Wadi Al Rayyan area.

S. No.	Enrichment Factor (EF)						Ni
	Cu	Zn	Mn	Pb	Cd	Cr	
1	14.95	0.44	3.68	24.07	13.28	10.65	18.69
2	14.64	0.84	8.05	22.56	16.24	10.13	16.50
3	10.63	0.72	2.29	19.46	13.10	7.04	19.12
4	14.81	0.79	8.25	22.45	16.75	10.17	25.67
5	15.39	1.76	2.54	14.51	11.89	10.44	23.89
6	14.43	0.68	3.80	23.13	11.06	10.77	28.46
7	18.22	0.61	3.26	20.06	14.20	10.95	30.19
8	7.51	0.34	1.24	12.63	5.72	4.44	12.07
9	26.12	5.13	6.23	34.21	27.40	14.23	48.35
10	15.02	0.94	4.29	25.51	14.70	9.48	30.17
11	15.81	0.38	4.31	28.74	18.11	11.06	32.42
12	13.16	0.56	4.97	24.46	10.80	9.89	23.38
13	16.62	0.50	2.48	30.63	11.76	11.62	27.65
14	3.08	0.13	0.46	6.03	2.14	2.27	4.98
15	15.67	0.56	5.17	26.23	16.20	9.12	18.91
16	14.50	1.17	4.07	24.11	11.63	8.19	14.34
17	14.58	0.47	4.42	25.21	10.80	11.01	18.36
Max	26.12	5.13	8.25	34.21	27.40	14.23	48.35
Min	3.08	0.13	0.46	6.03	2.14	2.27	4.98
Average	14.42	0.94	4.09	22.59	13.28	9.50	23.13

5.4. Assessment of Pollution Level

In the present study, Geoaccumulation index (I_{geo}) and Pollution load index (PLI) are reported by Muller, (1981) and Wei et al. (2009). The I_{geo} values for the heavy metals are presented in Table 5, and the distribution I_{geo} of the studied samples are shown in Fig. 3a. The values of I_{geo} range between (1 and 4) according to the type of metal and its location along the Wadi Al Rayyan area. The surface sediments of Wadi Al Rayyan are unpolluted to moderately to strongly polluted with Zn, Fe, Mn, Cd, Cr, Ni, and Pb respectively. As for the metals

of Zn, Fe, and Mn, the sediments were shown as unpolluted ($0 < I_{geo} \leq 1$), and are moderately polluted ($1 < I_{geo} \leq 2$) with Cu, Cd and Cr. The sample sediments were strongly polluted with Ni and Pb ($2 < I_{geo} \leq 3$) (Table 5). While there was a high level pollution with Pb and Ni, depending on the location of the sample and the contributors to the element concentrations. The highest I_{geo} value was attributed to Pb and Ni being ($2 < I_{geo} \leq 4$) in some places such as in samples 1, 2, 7, 8, 9, 10, 11, 12, 13, and 14 respectively. These dangerous metals can be derived from industrial and agricultural activities such as

waste, gasoline additives used in industries and automobiles as well as from fertilizers and pesticides (Mwamburi, 2003).

The Pollution Index (PI) and Pollution Load Index (PLI) were calculated for all metals and the statistical values are given in Table 6. PI is classified by (Faiz et al. 2009). $PI \leq 1$ indicates a low level of pollution; $1 < PI \leq 3$ indicates a middle level of pollution, and $PI > 3$ a high level of pollution. PI of Zn and Fe for all of the samples correspond to the low level ($PI < 1$), except for samples 8 and 9 which show a middle level of pollution. There was a low level of pollution with Cd in the sample 5, 6, 12, 13, 14, 16, 17, while the other samples showed a middle level of pollution (Table 5) and (Fig. 3d). PI for Cu, Pb, Cr and Ni shows a high level of pollution (PI

≥ 3) in all of the samples. PI for Mn shows middle pollution ($PI \leq 1$) except in samples 2, 4, 15 which had a high level of pollution ($PI \geq 3$). Therefore, according to the values of I_{geo} and PI for Pb and Ni there is a high level of pollution; these reflect the same sources of metals in the study area. The average PI for Zn is (0.61), Fe (0.83) and for Cd it is (1.04). These metals cause a low level pollution ($PI < 1$); Cu (9.09), Pb (14.35), Cr (6.02) and Ni (14.37) shows a high level of pollution ($PI \geq 3$); Mn (2.67) shows a middle level of pollution. The PLI value for all the surface sediment samples of Wadi Al Rayyan was less than 1 ($PLI < 1$) (Table 6). The results reveal that the sediments are unpolluted with respect to Cu, Zn, Fe, Mn, Pb, Cd, Cr, and Ni.

Table 5. Geoaccumulation index (I_{geo}) for heavy metals in the surface sediments of Wadi Al Rayyan area.

S. No.	Geoaccumulation Index (I_{geo})							
	Cu	Zn	Fe	Mn	Pb	Cd	Cr	Ni
1	1.96	0.06	0.13	0.48	3.14	1.74	1.39	2.38
2	2.23	0.13	0.15	1.23	3.44	2.48	1.54	2.44
3	1.46	0.10	0.14	0.32	2.68	1.80	0.97	2.55
4	1.7	0.09	0.11	0.95	2.58	1.92	1.17	2.87
5	1.72	0.20	0.11	0.28	1.62	1.33	1.17	2.60
6	1.54	0.07	0.11	0.41	2.48	1.19	1.16	2.97
7	2.28	0.07	0.11	0.36	2.20	1.56	1.20	3.21
8	2.1	0.10	0.28	0.35	3.53	1.60	1.24	3.27
9	2.24	0.44	0.09	0.54	2.94	2.35	1.22	4.04
10	1.9	0.12	0.13	0.54	3.23	1.86	1.20	3.72
11	1.69	0.04	0.11	0.46	3.09	1.95	1.19	3.38
12	1.66	0.07	0.13	0.63	3.11	1.37	1.26	2.88
13	1.67	0.05	0.10	0.25	3.09	1.19	1.17	2.71
14	1.59	0.07	0.52	0.24	3.11	1.11	1.17	2.49
15	2.02	0.07	0.13	0.67	3.38	2.09	1.18	2.37
16	1.55	0.13	0.11	0.44	2.59	1.25	0.88	1.50
17	1.88	0.06	0.13	0.57	3.25	1.39	1.41	2.30
Max	2.28	0.44	0.52	1.23	3.53	2.48	1.54	4.04
Min	1.46	0.04	0.09	0.24	1.62	1.11	0.88	1.50
Average	1.83	0.11	0.17	0.55	2.94	1.70	1.22	2.87
Background	25	71	46.7	1030	105	0.098	43	34

Table 6. Pollution Index (PI) and Pollution load index (PLI) for the heavy metals in the surface sediments of Wadi Al Rayyan area.

S. No.	Pollution Index (PI)								PLI
	Cu	Zn	Fe	Mn	Pb	Cd	Cr	Ni	
1	9.76	0.29	0.65	2.40	15.71	1.03	6.95	12.21	<1
2	11.12	0.64	0.76	6.12	17.14	1.41	7.70	12.54	<1
3	7.28	0.49	0.69	1.57	13.33	1.05	4.83	13.10	<1
4	8.48	0.45	0.57	4.73	12.86	1.08	5.83	14.71	<1
5	8.58	0.98	0.56	1.42	8.10	0.96	5.83	13.32	<1
6	7.72	0.37	0.54	2.03	12.38	0.93	5.77	15.24	<1
7	9.94	0.33	0.55	1.78	10.95	1.01	5.98	16.49	<1
8	10.44	0.48	1.39	1.72	17.58	1.01	6.17	16.79	<1
9	11.18	2.20	0.43	2.67	14.65	1.35	6.09	20.71	<1
10	9.48	0.59	0.63	2.71	16.11	1.03	5.99	19.06	<1
11	8.46	0.20	0.54	2.31	15.38	1.07	5.92	17.35	<1
12	8.32	0.35	0.63	3.15	15.48	0.95	6.26	14.79	<1
13	8.36	0.25	0.50	1.25	15.41	0.89	5.85	13.91	<1
14	7.92	0.32	2.57	1.18	15.50	0.83	5.83	12.81	<1
15	10.06	0.36	0.64	3.32	16.85	1.14	5.86	12.15	<1
16	7.76	0.63	0.54	2.18	12.90	0.84	4.38	7.68	<1
17	9.36	0.30	0.64	2.84	16.19	0.98	7.07	11.79	<1
Max	11.18	2.20	2.57	6.12	17.58	1.41	7.70	20.71	<1
Min	7.28	0.20	0.43	1.18	8.10	0.83	4.38	7.68	<1
Average	9.09	0.61	0.83	2.67	14.33	1.04	6.02	14.37	<1

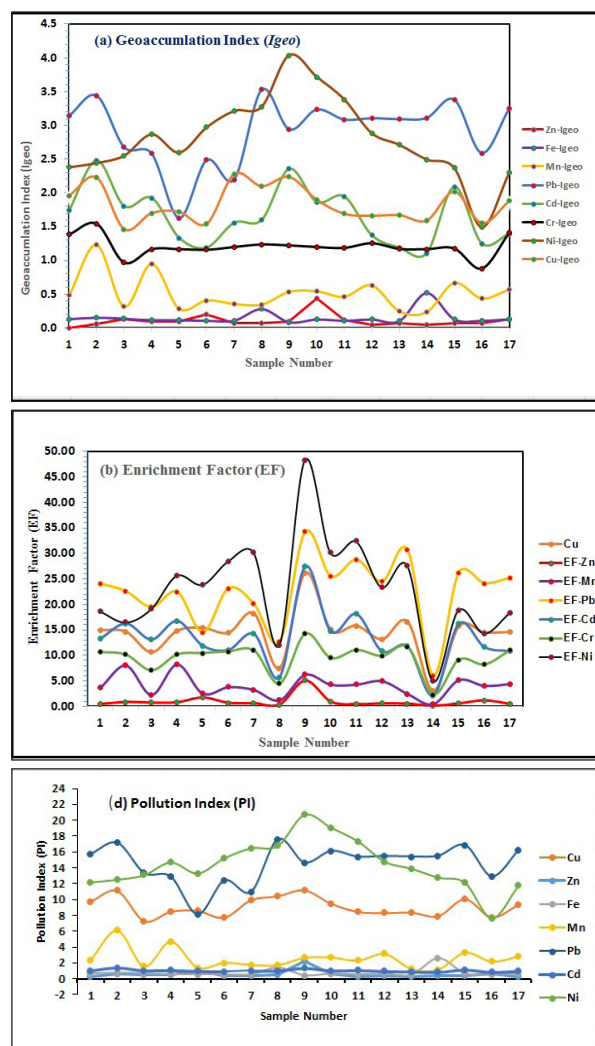


Figure 3. Distribution for (a) Geoaccumulation index (I_{geo}), (b) Enrichment Factor (EF) and (d) Pollution Index (PI) for the surface sediments samples Wadi Al Rayyan area.

6. Conclusions

The data analyses have been performed for this study using several verification methods in order to provide an important tool for a better understanding of the complex dynamics of heavy metal pollution in Wadi Al Rayyan area. These methods include, concentration (ppm) of the heavy metals (Cu, Zn, Fe, Mn, Pb, Cd, Cr, Ni), OM%, CaO wt%, pH and EC $\mu\text{S cm}^{-1}$ and correlation coefficients analyses. Sediment contamination assessment was used for the Enrichment Factor (EF), Geoaccumulation Index (I_{geo}), Pollution Index (PI), and Pollution Load Index (PLI). The main conclusions of this study can be summarized as follows:

1-The heavy mineral concentration in the sample distributions along Wadi Al Rayyan area show the concentration Enrichment of Cu, Mn, Pb, Cd, Cr and Ni along the Wadi Rayyan sediments from upstream to downstream, but a valuable concentration of Zn and Fe was found along the Wadi. The enrichment concentration of these elements are located near the roads across the stream and in areas of human activity along the Wadi. The elevated concentrations of the heavy metals in the sediments of Wadi Al Rayyan may be ascribed to the anthropogenic sources as well

as the human and agricultural activities (Calace et al., 2005). The sources include fertilizers and pesticides used in agricultural activities and sewage for untreated municipal sludge, wastewater discharges and seepage of the running of the surface water for transport and deposition by precipitation of solid particles from suspension (Zhang et al., 2011).

- 2- The Pearson's correlation coefficients for the contents of Cu, Zn, Fe, Mn, Pb, Cd, Cr and Ni for the surface sediments of Wadi Al Rayyan show a positive correlation for Cu with Cd and Cr; Zn with Cd; Cr, Mn with Cd and Cr. The results revealed that the metal concentration rises due to the anthropogenic sources of pollution identified to be the human, industrial, and agricultural activities such as sewage effluents, waste combustion, steel processing, fertilizers and pesticides. Low positive linear correlations have been found among the concentrations of Cu, Zn, Pb, Cd and Cr. These results indicate that these metals have complicated geochemical behaviors and different sources.
- 3- The content of OM% in Wadi Al Rayyan sediments is related to the organic content of the plant remains, farm residues and accumulation of animal manures, adjacent to the Wadi site at various stages of decomposition, such as cells and tissues of plant organisms as well as substances from plant roots and soil microbes which have been considered as additional sources.
- 4- The Enrichment Factor (EF) results reveal the sediments to be moderately-to-strongly polluted and strongly-to-extremely polluted. This may result in risky significant-to-strong pollution with Cu, Mn, Pb, Cd and Ni, while the values for Zn and Cr indicate a moderate level of pollution. The strongly polluted sediments with Cu, Mn, Pb, Cd and Ni, depend on the location of the sample along the Wadi Rayyan area and the contributors to the element concentrations.
- 5- The I_{geo} values of the surface sediments of Wadi Al Rayyan show a strong level of pollution with respect to Zn, Fe, Mn, Cd, Cr, Ni and Pb respectively. As for Zn, Fe, and Mn the values show no pollution ($0 < I_{geo} \leq 1$), and the I_{geo} values of Cu, Cd, and Cr show a moderate level of pollution ($1 < I_{geo} \leq 2$), and those for Ni and Pb show a strong level of pollution ($2 < I_{geo} \leq 3$). The strong level of pollution with respect to Pb and Ni, depends on the location of the sample along the wadi.
- 6- The PI values of Zn, Fe, and Cd for all of the samples show a low level of pollution ($PI < 1$). The PI of Cu, Pb, Cr and Ni shows a high level of pollution ($PI \geq 3$) for all of the samples. PI for Mn shows a middle level of pollution ($PI \leq 1$) except in samples 2, 4, 15 which had a high level of pollution ($PI \geq 3$). The PLI value for all of the surface sediments of Wadi Al Rayyan were found to be less than 1 ($PLI < 1$). These results reveal that the sediments are unpolluted with respect to Cu, Zn, Fe, Mn, Pb, Cd, Cr, and Ni.
- 7- The results of the statistical analysis and distribution of the metal contamination suggest that human activities, as well as industrial and agricultural activities are the most important pollution sources in the study area.

Acknowledgments

The authors are thankful to the Geology Department at The University of Jordan for their assistance in the chemical analyses of the heavy metals using the atomic absorption spectrophotometer. The authors are also grateful to Mrs. Ameenah Al-Kourdi for her help in calculating and the assessment of sediment contamination. The authors also express their immense gratitude to engineers Fatimah Hajawe and Rasha Al Harahsheh for determining the organic matter content. The authors also extend their thanks to the Water Environment and Arid Regions Research Center for the chemical and mineralogical analyses of the samples by XRF and XRD.

References

- Abu Qudaria, M. (2005). Geological Map of Dayr Abu Said Area, Scale (1/50,000). Natural Resources Authority, Geological Mapping Directorate, Amman, Jordan.
- Albanese, S. (2008). Evaluation of the bioavailability of potentially harmful elements in urban soils through ammonium acetate-EDTA extraction: a case study in southern Italy, *Geochemistry: Exploration, Environment, Analysis*, 8: 49-57.
- Al-Khashman, O.A. (2013). Assessment of heavy metals contamination in deposited street dusts in different urbanized areas in the city of Ma'an, Jordan. *Environ Earth Sci.* 70: 2603–2612
- Al-Khashman, O.A., and Shawabkeh R.A. (2006). Metals distribution in soils around the cement factory in southern Jordan. *Environ Pollute* 140: 387–394.
- Al-Khashman, O.A., Shawabkeh, R.A. (2009). Metal distribution in urban soil around steel industry beside Queen Alia Airport, Jordan. *Environ Geochem Health* 31: 717–726.
- Al-Khashman, O.A. (2004). Heavy metal distribution in dust, street dust and soils from the work place in Karak Industrial Estate, Jordan. *Atmos Environ* 38: 6803–6812
- Alloway, B.J., and Ayres, D.C. (1997). *Chemical Principles of Environmental Pollution* 2nd Edition, Blackie academic and professional, 190-203.
- Ankley, G.T., Lodge, K., Call, D.J., Balcer, M.D., Brooke, L.T., Cook, P.M., Kresis Jr., Baptista Neto, J.A., Smith, B.J., McAllister, J.J. (1992). Heavy metal concentrations in surface sediments in a nearshore environment, Jurujuba Sound, Southeast Brazil. *Environ. Pollut.* 109: 1-9.
- Auburn, (2000). Soil Quality-Urban Technical Note No. 3. United States Department of Agriculture (USDA), Natural Resources Conservation Service, Soil Quality Institute, 411 S. 36832, 334-844-4741, X-177,
- Bany Yaseen, I., and Al Elaimat A. (2016). Assessment of the Heavy Metal Pollution in the Surface Sediments along Upstream at Wadi Al-Arab, Jordan. *Journal of Natural Sciences Research*, 6 (20): 1-12.
- Bany Yaseen, I., and Al-Hawari, Z. (2015). Assessment of Heavy Metal Pollution of Surface Sediments in Wadi Shu'ayb, Jordan. *Jordan Journal of Civil Engineering*, 9(3): 303-313.
- Bellucci, L.G., Frignani, M., Paolucci, D., Ravanelli, M. (2002). Distribution of heavy metals in sediments of the Venice Lagoon: The role of the industrial area. *Sci. Total Environ.* 295: 35-49.
- Bentum, J.K., Anang, M., Boadu, K.O., Koranteng Addo, E.J., Antwi, E.O. (2011). Assessment of heavy metals pollution of sediments from Fosu lagoon in Ghana. *Bull. Chem. Soc. Ethiop.* 25 (2): 191-196.
- Biasioli, R., Barberis, R., Marson, F.A. (2006). The influence of a large city on some soil properties and metal content. *The Science of the Total Environment*, 356: 154– 164.
- Bilos, C., Colombo, J.C., Skorupka, C.N., Presa, M.J.P. (2001). Source, distribution and variability of airborne trace metals in La Plata city area, Argentina. *Environmental Pollution*, 111: 149–159.
- Bin Chen, T., Ming Zheng, Y., Lei, M., Chun Huang, Z., Tao Wu, H., Chen, H., et al. (2005). Assessment of heavy metal pollution in surface soils of urban parks in Beijing, China. *Chemosphere*, 60(4): 542–551.
- Bloundi, M.K., Duplay, J., Quaranta, G. (2009). Quaranta heavy metal contamination of coastal lagoon sediments by anthropogenic activities: The case of Nador (East Morocco), *Environ. Geol.*, 56: 833-843.
- Bowen, H.J.M. (1979). *Environmental chemistry of the elements*. Academic Press, New York
- Caccia, V.G., Millero, F.J., Palanques, A. (2003). The distribution of trace metals in Florida Bay sediments. *Marine Pollution Bulletin*, 46(11): 1420–1433.
- Calace, N., Ciardullo, S., Petronio, B.M., Pietrantonio, M., Abbondanzi, F., Campisi, T., Cardellicchio, N. (2005). Influence of chemical parameters (heavy metals, organic matter, sulphur and nitrogen) on toxicity of sediments from the Mar Piccolo (Taranto, Ionian Sea, Italy). *Microchem J.*, 79 (1–2): 243–248.
- Cao, Z., Yang, Y., Lu, J., Zhang, Ch. (2011). Atmospheric particle characterization, distribution and deposition in Xi'an, Shaanxi Province, Central China. *Environ Pollut* 159: 577–584
- Çevik, F., Göksu, M.Z.L., Derici, O.B., Findik, Ö. (2009). An assessment of metal pollution in surface sediments of Seyhan dam by using enrichment factor, geoaccumulation index and statistical analyses. *Environ. Monit. Assess.*, 152: 309- 317.
- Chakravarty, M., and United States Department Patgiri, A.D. (2009). Metal pollution assessment in sediments of the Dikrong River, NE India. *J. Hum. Ecol.*, 27 (1): 63-67.
- Dean. W. (1974). Determination of Carbonate and Organic Matter in Calcareous Sediments and Sedimentary Rocks by Loss on Ignition: Comparison with Other Methods. *Journal of Sedimentary Research*, 44(1): 242-248
- El-Hasan, T., and Jiries, A. (2001). Heavy metal distribution in valley sediments in Wadi Al-Karak catchment area, South Jordan. *Environ. Geochem. Hlth.*, 23: 105-116
- Ergin, M., Saydam, C., Baştürk, Ö., Erdem, E., Yörük, R. (1991). Heavy metal concentrations in surface sediments from the two coastal inlets (Golden Horn Estuary and Izmit Bay) of the northeastern Sea of Marmara, *Chem. Geol.*, 191: 269–285.
- Faiz, Y., Tufail, M., Javed, M.T., Chaudhry, M.M. (2009). Road dust pollution of Cd, Cu, Ni, Pb and Zn along Islamabad Expressway, Pakistan. *Micro chemical Journal*, 92(2): 186-192.
- Gray, C.W., McLaren, R.G., Roberts, A.H.C. (2003). Atmospheric accessions of heavy metals to some New Zealand Pastoral Soils. *The Science of the Total Environment*, 305: 105–115
- Habes, G., and Nigem, Y. (2006). Assessing Mn, Fe, Cu, Zn and Cd pollution in bottom sediments of Wadi Al-Arab Dam, Jordan. *Chemosphere*, 65: 2114-2121.
- Harikumar, P., Nasir, U. Rahman, M.M. (2009). Distribution of heavy metals in the core sediments of a tropical wetland system. *Int. J. Environ. Sci. Tech.*, 6 (2): 225 -232.
- Kim, D., An, K., Kim, K. (2003). Heavy metal pollution in the soils of various land use based on physicochemical characteristics. *J Environ Science Health*, 38:839–853.
- Komarek, M., and Zeman, J. (2004). Dynamics of Cu, Zn, Cd, and Hg release from sediments at surface conditioning. *Bulletin of Geosciences*. 79: 99-106.
- Leivouri, M. (1998). Heavy metal contamination in surface sediment in the Gulf of Finland and comparison with the Gulf of Bothnia. *Chemosphere*, 36: 43-59.

- Li, X.D., Poon, C.S., Pui, S.L. (2001). Heavy metal contamination of urban soils and street dusts in Hong Kong. *Appl. Geochem*, 16: 1361–1368.
- Loska, K., and Wiechula, D. (2003). Application of principal component analysis for the estimation of source heavy metal contamination in surface sediments from Rybnik Reservoir. *Chemosphere*, 51: 723-733.
- Lu, X., Wang, L., Lei, K., Huang, J., Zhai, Y. (2009). Contamination assessment of copper, lead, zinc, manganese and nickel in street dust of Baoji, NW China. *J Hazard Mater* 161: 1058–1062
- MacFarlane, G.R., and Burchett, M.D. (2000). Cellular distribution of Cu, Pb and Zn in the grey angrove *avicennia marina* (Forsk.). *Vierh. Aquat. Bot.*, 68: 45-59.
- Maher, W.A., and Aislabie, J. (1992). Polycyclic aromatic hydrocarbons in nearshore marine sediments of Australia. *Sci. Total Environ.*, 11 (2-3): 143-164.
- Marchand, C., Lalliet, V.E., Baltzer, F., Alberic, P., Cossa, D., Baillif, P. (2006). Heavy Metals Distribution in Mangrove Sediments along the mobile coastline of French Guiana. *Mar. Chem.*, 98: 1-17.
- Martin, A.C., Rivero, V.C., Marin, M.T.L. (1998). Contamination by heavy metals in soils in the neighborhood of a scrapyard of discarded vehicles. *The Science of the Total Environment*, 212: 142–152.
- Mason, B.J. (1966) *Introduction to geochemistry*. 3rd edition, John Wiley, New York.
- Mhamdi, A.A., Choura, M., Maanan, M., Zourarah, B., Robin, M. (2010). Metal fluxes to the sediments of the Moulay Bouselham lagoon, Morocco. *Environ. Earth Sci.*, 61: 275-286.
- Moller, A., Muller, H.W., Abdullah, A., Abdelgawad, G., Utermann, J. (2005). Urban soil pollution in Damascus, Syria: Concentrations and patterns of heavy metals in the soils of the Damascus Ghouta. *Geoderma*, 124: 63–71.
- Mucha, A.P., Vasconcelos, M.T.S.D., Bordalo, A.A. (2003). Macrobenthic community in the Doura estuary: relations with trace metals and natural sediment characteristics. *Environ. Pollut.*, 121: 169-180.
- Muller, G. (1981). The heavy metal content of the sediments of the Neckar and its tributaries: an inventory, *Chem. Zeitung*, 105: 157-164.
- Murray, Ge.Y., Hendershot, W.H. (2000). Trace metal speciation and bioavailability in urban soil. *Environ Pollut.*, 107: 137–144.
- Mwamburi, J. (2003). *Metal Sources and Distribution in Rivers Within The Lake Victoria (Kenya) Catchment Area*. Lake Victoria Fisheries: Status, biodiversity and management. Aquatic Ecosystem Health and Management Society.
- Odat, S., and Alshammari, A. (2011). Spatial Distribution of Soil Pollution along the Main Highways in Hail City, Saudi Arabia, *Jordan Journal of Civil Engineering*, 5(2): 163-172
- Pekey, H. (2006). Heavy Metal Pollution Assessment in Sediments of the Izmit Bay, Turkey. *Environ. Monit. Assess.*, 123: 219-231.
- Rath P., Panda, U.C., Bhatta, D., Sahoo, B.N. (2005). Environmental Quantification of Heavy Metals in the Sediments of the Brahmani and Nandira Rivers, Orissa. *J Geol Soc Ind*, 65: 487-492.
- Saffarini, G.A., and Lahawani, Y. (1992). Multivariate statistical techniques in geochemical exploration applied to Wadi sediments data from an arid region: Wadi Dana, SW Jordan, *J. Afr. Earth Sci.*, 14(3): 417-427.
- Schiff, K.C., and Weisberg, S.B. (1999). Iron as a reference element for determining trace metal enrichment in Southern California coast shelf sediments. *Mar. Environ. Res.*, 48: 161-176.
- Schuermann, G., and Market, B. (1998). *Ectotoxicology, ecological fundamentals, chemical exposure and biological effects*. John Wiley & Sons, Inc., and Spektrum Akademischer Verlag.
- Seshan, B.R.R., Natesan, U., Deepthi, K., (2010). Geochemical and statistical approach for evaluation of heavy metal pollution in core sediments in southeast coast of India. *Int. J. Environ. Sci. Tech.*, 7(2): 291-306.
- Simex, S.A., and Helz, G.R. (1981). Regional geochemistry of trace elements in Chesapeake Bay. *Environ. Geo.*, 3: 315-323.
- Singh, A.K., Hasnain, S.I., Banerjee, D.K. (1999). Grain size and geochemical partitioning of heavy metals in sediments of the Damodar River - a tributary of the lower Ganga, India. *Environmental Geology*, 39(1): 90–98.
- Soares, H.M.V.M., Boaventura, R.A.R., Machado, A.A.S.C., Esteves da Silva, J.C.G. (1999). Sediments as monitors of heavy metal contamination in the Ave river basin (Portugal): Multivariate analysis of data. *Environmental Pollution*, 105(3): 311–323
- Suthar, S., Nema, A.K., Chabukdhara, M., Gupta, S.K. (2009). Assessment of metals in water and sediments of Hindon River, India: Impact of industrial and urban discharges. *J. Hazard. Mater*, 171(1-3): 1088-1095.
- Sutherland, R.A. (2000). Bed sediment-associated trace metals in an urban stream, Oahu, Hawaii. *Environmental Geology*, 39(6): 611–627.
- Tomlinson, D.L., Wilson, J.G., Hariis, C.R., Jeffrey, D.W. (1980). Problems in the assessment of heavy metal levels in estuaries and the formation of a pollution index. *Helgoländer Meeresunters*, 33: 566-575.
- Turekian, K.K., and Wedepohl, K.H. (1961). Distribution of the elements in some major units of the earth's crust. *Bulletin of Geological Society of America*; 72: 175–92.
- Wei, B., Jiang, F., Li, X., Sh, Mu. (2009). Spatial distribution and contamination assessment of heavy metals in urban street dusts from Urumqi, NW China. *Microchem J.*, 93:147–152.
- Wuana, R.A., and Okieimen, F.E. (2011). Heavy metals in contaminated soils: a review of sources, chemistry, risk and best available strategies for remediation. *ISRN Ecology*, 2011, <http://dx.doi.org/10.5402/2011/402647>
- Yang, Z., Lu, W., Long, Y., Bao, X., Yang Q. (2011). Assessment of heavy metals contamination in urban topsoil from Changchun City, China. *J Geochem Explor* 108: 27–38.
- Zarei, I., Pourkhabbaz, A., Khuzestani, R.B. (2014). An assessment of metal contamination risk in sediments of Hara Biosphere Reserve, southern Iran with a focus on application of pollution indicators. *Environ Monit Assess.*, doi: 10.1007/s10661-014-3839-x.
- Zhang, C., Qiao, Q., Piper, J.D., Huang, B. (2011). Assessment of heavy metal pollution from a Fe-smelting plant in urban river, sediments using environmental magnetic and geochemical methods. *Journal Environmental Pollution*, 159: 3057-3070.

Status and Prediction of Nitrogen Oxides in the Air of Shiraz City, Iran

Masoud Masoudi, Fatemeh Ordibeheshti, Neda Rajai Poor

Shiraz University, Department of Natural Resources and Environmental Engineering, Iran.

Received 31 July 2018, Accepted 18 February 2019

Abstract

In the present study, air quality analyses for Nitrogen oxides (NO_x) were conducted in Shiraz, a city in the south of Iran. The measurements were taken over the period from 2011 through 2012 in two different locations to prepare average data in the city. The average concentrations were calculated every twenty-four hours, each month and each season. The results showed that the highest concentration of NO_x occurred generally in the morning while the least concentration was found at mid-night. Monthly concentrations of NO_x showed that the highest value occurred in December, while the least value was recorded in September. The seasonal concentrations showed that the least amounts were in summer, while the highest amounts were found in winter. Unfortunately, most of the time, the concentration of the NO_x showed higher levels than the primary standards of Nitrogen dioxide (0.021 ppm), protecting human health. Relations between air pollutants and some meteorological parameters were calculated statistically using the daily average data. The wind data (velocity, direction), relative humidity, temperature, sunshine periods, evaporation, dew point and rainfall were considered as independent variables. The relationships between the concentration of pollutants and meteorological parameters were expressed by multiple linear regression equations for both annual and seasonal conditions using the SPSS software. The RMSE test showed that among the different prediction models, the stepwise model is the best option.

© 2019 Jordan Journal of Earth and Environmental Sciences. All rights reserved

Keywords: Nitrogen Oxides, Air Pollution, Meteorological Parameters, Regression Model.

1. Introduction

Air sustains life. But the air we breathe is not pure. It contains a lot of pollutants and most of these pollutants are toxic (Sharma, 2001). While developed countries have been making progress during the last century, air quality has been getting much worse especially that in developing countries air pollution exceeds all health standards. For example, in Lahore and Xian (china) dust is ten times higher than health standards (Sharma, 2001).

Nitrogen oxides (NO_x) include different forms of oxides of nitrogen. NO_2 generally derives from emissions of NO (in high temperature). About 95 % of Nitrogen oxides are emitted as NO and 5 % as NO_2 . Other oxides are N_2O , N_2O_3 and N_2O_5 which are not so important in air pollution. Among NO_x , NO_2 leads to respiratory problems, therefore NO_2 is considered the most important of the oxides of nitrogen.

Nitrogen dioxide (NO_2) is one of the seven conventional (criteria) pollutants (including SO_2 , CO, particulates, hydrocarbons, nitrogen oxides, O_3 and lead). These pollutants produce the highest volume of pollutants in the air and the most serious threat for human health and welfare. The concentration of these pollutants, especially in cities, has been regulated by the Clean Air Act since 1970 (Cunningham and Cunningham, 2002).

Some properties of Nitrogen dioxide (NO_2) include: a reddish brown gas, formed as fuel burnt in cars, a strong oxidizing agent and forms Nitric acid in air. Its Sources are divided into two parts: 1) natural emissions including forest fires, volcanoes, bacteria in the soil, lightning, etc. 2)

anthropogenic activities including motor vehicle emissions and power generation. Fuel combustion increases NO_2 production. Half of the emission of HC and NOx in cities comes from Motor vehicles. (Asrari et al., 2007).

The presence of pollutants in the atmosphere, causes a lot of problems, thus the study of pollutant's behavior is necessary. Some of the main health effects of NO_2 include lung and heart problems, NO_2 poisoning, asthma, lowered resistance to infection. Other Effects include damage to plants such as the damages of leaves, retarding photosynthesis activity, chlorosis, damage to various textile fibers, multiplying the photochemical smog problems and those by acid rain (Sharma, 2001).

The status of pollutants' concentration and the effects of meteorological and atmospheric parameters on these pollutants constitute the base for following studies: Ho and Lin (1994) studied semi-statistical models for evaluating the NO_x concentration by considering source emissions and meteorological effects. Moreover, the street levels of NO_x and SPM in Hong Kong have been studied by Lam et al., (1997). In another study, the relationship between monitored air pollutants and meteorological factors, such as wind speed, relative humidity ratio and temperature, was statistically analyzed, using SPSS. According to the results obtained through multiple linear regression analysis, there was a moderate and weak relationship between the air pollutants like the O_3 level and the meteorological factors in Trabzon city during some months (Cuhadaroglu and Demirci, 1997).

Mandal (2000) has shown the progressive decrease of air

* Corresponding author e-mail: masoudi@shirazu.ac.ir

pollution from west to east in Kolkata. Statistical modeling of ambient air pollutants in Delhi has been studied by Chelani et al., (2001). Abdul-Wahab and Al-Alawi (2002) developed a neural network model to predict the tropospheric (surface or ground) ozone concentrations as a function of meteorological conditions and various air quality parameters. The results of this study showed that the artificial neural network (ANN) is a promising method for air-pollution modeling. The observed behavior of pollution concentrations to the prevailing meteorological conditions has been studied for the period from June 13 to September 2, 1994, for the Metropolitan Area of Sao Paulo (Sánchez-Ccoyllo and Andrade, 2002). The results showed low concentrations associated with intense ventilation, precipitation and high relative humidity. While high values of concentrations prevailed due to weak ventilation, absence of precipitation and low relative humidity for some pollutants. Also for predicting CO, Sabah et al., (2003) used a statistical model for carbon monoxide levels.

Elminir (2005) mentioned dependence of air pollutants on meteorology over Cairo in Egypt. The results indicate that wind direction was found to have an influence not only on pollutant concentrations, but also on the correlation between pollutants. As expected, the pollutants associated with traffic were at highest ambient concentration levels when wind speed was low. At higher wind speeds, dust and sand from the surrounding desert was entrained by the wind, thus contributing to ambient particulate matter levels. It was also found that, the highest average concentration for NO₂ and O₃ occurred at humidity ≤ 40 % which is indicative of strong vertical mixing. For CO, SO₂ and PM₁₀, the highest average concentrations occurred at humidity being above 80 %. In another research, data on the concentrations of seven air pollutants (CH₄, NMHC, CO, CO₂, NO, NO₂ and SO₂) and meteorological variables (wind speed and direction, air temperature, relative humidity, and solar radiation) were used to predict the concentration of ozone in the atmosphere using both multiple linear and principal component regression methods (Abdul-Wahab et al., 2005). The results showed that while high temperature and high solar energy tended to increase the day time ozone concentrations, the pollutants NO and SO₂ being emitted to the atmosphere were being depleted. However, the model did not predict the night time ozone concentrations as precisely as it did for day time. Asrari et al., (2007) studied the effect of meteorological factors for predicting CO. Similarly, variations in the concentration of CO at different times have been shown in this study.

Cesaroni et al. (2012) measured NO₂ at 67 locations in Rome during 1995-1996, and seventy-eight sites in 2007, over three one-week-long periods. To develop LUR models, several land-use and traffic variables were used. NO₂ concentration at each residential address was estimated for a cohort of 684,000 adults. They used Cox regression to analyze the association between the two estimated exposures and mortality. Results showed that the measured and predicted NO₂ values from LUR models, from samples collected twelve years apart, had good agreement, and that the exposure estimates were similarly associated with mortality in a large cohort study.

Li et al., (2014) presented the spatial and temporal variation of Air Pollution Index (API) and examined the relationships

between API and meteorological factors over the period between 2001 and 2011 in Guangzhou, China. Relationships were found between API and a variety of meteorological factors. Temperature, relative humidity, precipitation, and wind speed were negatively correlated with API, while the diurnal temperature range and atmospheric pressure were positively correlated with API in the annual condition.

Yoo et al., (2014) mentioned that all of the pollutants show significant negative correlations between their concentrations and rain intensity due to washout or convection. The relative effect of the precipitation on the air pollutant concentrations was estimated to be: PM₁₀ > SO₂ > NO₂ > CO > O₃, indicating that PM₁₀ was most effectively cleaned by rainfall.

Jhun et al., (2015) analyzed hourly O₃ and NOx measurement data between 1994 and 2010 in the continental USA. Nationally, hourly O₃ concentrations decreased by as much as -0.38 ppb/year with a standard error of 0.05 ppb/year during the warm season midday, but increased by as much as +0.30±0.04 ppb/year during the cold season. High O₃ concentrations (≥75th percentile) during the warm season decreased significantly, however, there were notable increases in the cold season as well as warm season nighttime; we found that these increases were largely attributable to NOx decreases as less O₃ is quenched.

Wang et al. (2015) studied air quality in Chongqing, the largest mountainous city in China. Statistical analysis of NO₂ concentrations was conducted over the period from 2002 to 2012. The analysis of Pearson correlation indicated that the concentrations of NO₂ were positively correlated with atmospheric pressure, but were negatively correlated with temperature and wind speed. The analysis of Multi-Pollutant Index (MPI) showed that air quality in Chongqing was serious.

Choi et al., (2017) conducted a nitrogen dioxide (NO₂) exposure assessment with four methods including LUR in the Republic of Korea to compare the model performances, and estimate the empirical NO₂ exposures of a cohort. The LUR models showed high performances in an industrial city in the Republic of Korea, despite the small sample size and limited data. Findings suggest that the LUR method may be useful in similar settings in Asian countries where the target region is small and the availability of data is low.

Statistical modeling of NO₂ was studied in Iranian cities of Ahvaz (Masoudi and Asadifard, 2015), Tehran (Masoudi et al., 2017a) and Isfahan (Masoudi and Gerami, 2018a). According to the results obtained by multiple linear regression analysis for seasonal and annual conditions, there were significant relationships between NO₂ levels and meteorological factors in these cities. Such results between other pollutants and meteorological factors in Shiraz, another Iranian city, were observed: O₃ (Masoudi et al., 2016); CO (Masoudi et al., 2017b) and PM₁₀ (Masoudi et al., 2018b).

The presents study exhibits diurnal, monthly and seasonal variations of the concentration of NOx and also a statistical model that is able to predict the amount of NOx. This is based on multiple linear and nonlinear regression techniques. Multiple Regression estimates the coefficients of the linear equations, involving one or more independent variables that best predict the value of the dependent variable (NO_x amount in this study). Accordingly, a large statistical and graphical

software package (SPSS, Software Package of Social Sciences, V. 20), that is one of the best known statistical packages has been used (Kinneer, 2002).

2. Materials and Methods

2.1. Study Area

The research area, Shiraz, is the biggest city in the southern part of Iran (Fig. 1). It is located around 29° 30' N

and 52° 30' E and the elevation is about 1500 m above the mean sea level. The annual precipitation in Shiraz is about 330 mm. The city of Shiraz has a semi-arid climate, and its residential population amounted to 1,500,000 in 2010. There are lots of cars driven in the city, and also many factories and industrials are built around it. Because of these reasons, Shiraz is one of the most polluted cities in Iran, therefore, there is an urgent need for an ambient air quality analysis to be conducted in this city.



Figure 1. Two photographs from the same place in Shiraz showing impacts of dust pollution during recent years (left one in clean condition and right one in worse condition).

2.2. Data and Methodology

Two available sampling stations in the city, namely Setad and Darvazah-Kazarun, belonging to the Environmental Organization of Iran were selected to represent different traffic loads and activities.

The sampling has been performed every thirty minutes daily for each pollutant during all months of 2011 and 2012. Among the measured data in the two stations, Nitrogen oxides were chosen. Then the averages were calculated for every hour, monthly and seasonally for both stations by Excel. Finally, the averages of data at the two stations were used to show the air pollution situation as diurnal, monthly and seasonal graphs of the concentration of Nitrogen oxides in the city.

studying the correlation of Nitrogen oxides and metrological parameters of the synoptic station of the city was the next step. The metrological parameters studied include: temperature (min., max., and mean), ratio of humidity (min, max), precipitation, sunshine hours, wind direction (max), wind speed (max and mean) and evaporation.

In the next step, the daily average data at the two stations in 2012 was considered as dependent variables in the statistical analysis, while the daily data of the meteorological parameters during this year were selected as independent variables in the SPSS programme. The linear regression equation showed that the concentration of Nitrogen oxides depends on the kind of meteorological parameters and also gives an idea about the levels of this relation. The relationship between the dependent variables and each independent variable should be linear. The significant values in the output are based on fitting a single model. Also, a linear regression equation made for different seasons perhaps show that those relationships are not observed using annual data.

The model for predicting Nitrogen oxides was determined using two multiple regression modeling procedures of the 'enter method' and the 'stepwise method'. In the 'enter method' all

independent variables selected are added to a single regression model. In the 'stepwise method' which is better, all variables can be entered or removed from the model depending on the significance. Therefore, only those variables which have more influence on dependent variable are observed in a regression model.

3. Results and Discussion

In Figs. 2, 3, and 4, the diurnal, monthly and seasonal variations in concentration of NO_x have been presented. As shown in figure 2, the high concentration of NO_x occurs in the morning. Monthly concentration of the NO_x showed that the highest values were in December and the least amounts were recorded in September (Fig. 3). The seasonal concentration of NO_x showed that the highest values were in winter, and that the least amounts were reported in summer (Fig. 4). Unfortunately, all graphs showed that the concentrations of NO_x are higher than the Primary Standards of Nitrogen dioxide (0.021 ppm), recommended by the National Ambient Air Quality Standards (NAAQS) of Iran respectively. These results are almost in good agreement with results obtained regarding other cities including Tehran (Masoudi et al., 2017a), Isfahan (Masoudi and Gerami, 2018a), and Ahvaz (Masoudi and Asadifard, 2015).

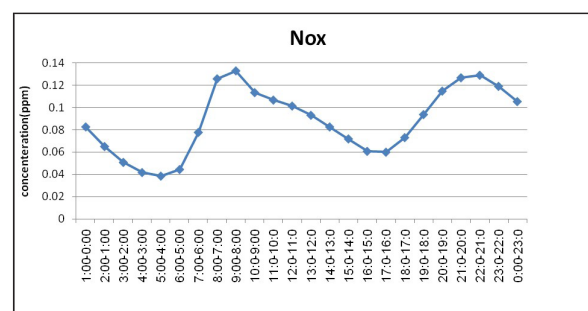


Figure 2. Diurnal variation of Nitrogen oxides' concentrations in Shiraz (2011-2012).

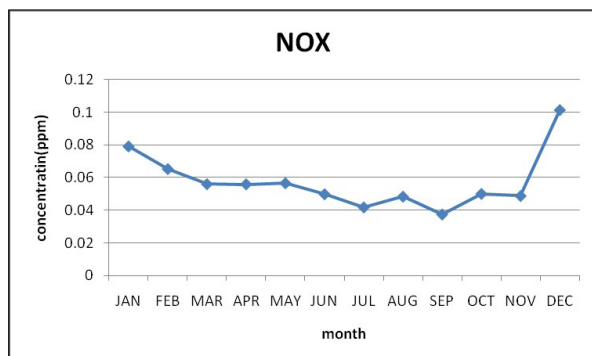


Figure 3. Monthly variation of Nitrogen oxides' concentrations in Shiraz (2011-2012).

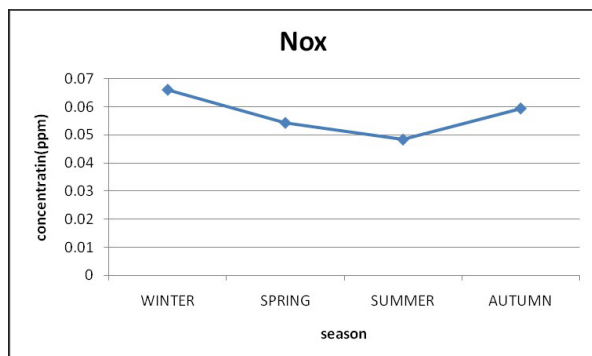


Figure 4. Seasonal variation of Nitrogen oxides' concentrations in Shiraz (2011-2012).

Table 1 shows the relationships between NO_x and other air pollutants. For example, the concentration of NO_x shows a negative correlation with PM and SO_2 , O_3 , while it shows a positive correlation with NO_2 and CO. NO_x , like NO_2 and CO, is increased when traffic increases, while other negative pollutants are related to other resources like SO_2 whose main source is the industrial activities, or PM_{10} whose main source is the detached soils from western neighbors like Iraq, or ozone related to the increasing of sunlight. These results are almost in good agreement with other results regarding NO_x assessment in other cities including Tehran (Masoudi et al., 2017a), and Isfahan (Masoudi and Gerami, 2018a). The correlation

coefficients significant at the 0.05 level are identified with a single asterisk (significant), and those significant at 0.01 level are identified with two asterisks (highly significant).

Table 1. Correlation between air pollutants and ozone.

	CO	PM	NO_2	O_3	SO_2
Pearson Correlation	.145*	-.220**	.895**	-.096	-.402**
Sig. (2-tailed)	.032	.001	.000	.156	.000
N	221	221	221	221	221

Table of analysis of variance (Table 2) shows that both regressions of 'enter' and 'stepwise' methods in annual condition are highly significant, indicating a significant relation between the different variables.

Table 2. Tables of analysis of variance for both regressions of 'enter' (a) and 'stepwise' (b) methods for annual condition.

Analysis of variance (a)

Model	Sum of Squares	df	Mean Square	F	Sig.
Regression	89568.643	11	8142.604	16.190**	.000
Residual	153396.583	305	502.940		
Total	242965.226	316			

Predictors: (Constant), Rain, Wind direction (max), Wind speed (max), Wind speed (mean), Temperature (max), Temperature (min), Temperature (mean), Sunshine Hours, Ratio of Humidity (min), Ratio of Humidity (max), Ratio of Humidity (mean), Evaporation.

Dependent Variable: NO_x

Analysis of variance (b)

Model	Sum of Squares	df	Mean Square	F	Sig.
Regression	87652.374	7	12521.768	24.912**	.000
Residual	155312.852	309	502.631		
Total	242965.226	316			

Predictors: (Constant), Sunshine Hours, Ratio of Humidity (min), Ratio of Humidity (max), Wind direction (max)

Dependent Variable: NO_x

Table 3 presents the coefficients of NO_x pollution model and regression lines for both the enter and stepwise methods in annual conditions. Regression coefficients, standard errors, standardized coefficient beta, t values, and two-tailed significance level of t are presented in the Tables.

Table 3. Coefficients of NO_x pollution model and regression lines for both enter (a) and stepwise (b) methods for annual conditions.

Coefficients (a)

Model	Unstandardized Coefficients		Standardized Coefficients	t	Sig.
	B	Std. Error	Beta		
(Constant)	61.898	17.870		3.464	.001
Temperature (min)	-3.463	.706	-.948	-4.902**	.000
Temperature (max)	-1.336	.703	-.442	-1.901	.058
Temperature (mean)	1.639	.703	.512	2.332*	.020
Ratio of Humidity (min)	.879	.238	.411	3.693**	.000
Ratio of Humidity (max)	-.479	.140	-.338	-3.415**	.001
Rain	-.352	.409	-.050	-.860	.390
Sunshine Hours	1.021	.728	.099	1.402	.162
Evaporation	1.909	.901	.284	2.118*	.035
Wind speed (max)	1.568	.885	.124	1.771	.078
Wind direction (max)	-.005	.015	-.016	-.322	.748
Wind speed (mean)	1.912	1.847	.075	1.035	.301

Dependent Variable: NO_x

Coefficients (b)

Model	Unstandardized Coefficients		Standardized Coefficients	t	Sig.
	B	Std. Error	Beta		
(Constant)	75.492	15.661		4.820	.000
Temperature (max)	-1.326	.664	-.439	-1.998*	.047
Evaporation	2.106	.889	.313	2.369*	.018
Temperature (min)	-3.453	.675	-.945	-5.114**	.000
Wind speed (max)	2.019	.651	.159	3.101**	.002
Temperature (mean)	1.526	.690	.477	2.211*	.028
Ratio of Humidity (max)	-.486	.138	-.343	-3.513**	.001

Dependent Variable: NO_x

The linear regression equations show that NO_x pollution depends on the meteorological parameters, and also gives an idea about the levels of relations. The linear model equations after using the 'enter method' and 'stepwise method' for the annual condition are:

- NO_x amount (ppb) using 'enter method' for annual condition = 61.898 + (-3.463) Temperature_(min) + (-1.336) Temperature_(max) + (1.639) Temperature_(mean) + (0.879) Ratio of humidity_(min) + (-0.479) Ratio of Humidity_(max) + (-0.352) Rain + (1.021) Sunshine Hours + (-0.005) Wind direction_(max) + (1.568) Wind speed_(max) + (1.912) Wind speed_(mean) + (1.909) Evaporation R= 0.607 (significant at 0.01)

- NO_x amount (ppb) using 'stepwise method' for annual condition = 75.492 + (2.019) Wind speed_(max) + (-0.486) Ratio of Humidity_(max) + (-1.326) Temperature_(max) + (-3.453) Temperature_(min) + (1.526) Temperature_(mean) + (2.106) Evaporation R= 0.601 (significant at 0.01)

Results of the linear regression model show that the ratio of humidity (max), temperature_(max) and temperature_(min) have reverse effect on the concentration of NO_x. Accordingly, when these parameters increase, the concentration of NO_x decreases. While, when Evaporation, wind speed_(max) and temperature_(mean) increase the concentration of NO_x significantly increases (Table 3b). Other meteorological parameters show different effects on NO_x amounts although these results are not significant. For example, rainfall has reverse effects on the concentration of NO_x (Table 3a). These results are almost in good agreement with other results regarding NO_x measurements in other cities like Tehran (Masoudi et al., 2017a) and Isfahan (Masoudi and Gerami, 2018a) and Ahvaz (Masoudi and Asadifard, 2015). In fact, some of these events happen in real conditions. The increasing of rainfall, wind speed and temperature (inversion happens in low temperatures) usually decreases most of air pollutants (Asrari et al., 2007).

The values and significance of R (multiple correlation coefficient) in both equations show the capability of them to predict the NO_x amount. The amount of Adjusted R² in both equations is almost 0.346 showing that different parameters used can calculate almost 35 % variability of NO_x. This result

indicates predicting most of air pollutants such as NO_x, taking into consideration the consumption of fossil fuel especially in motor vehicles. Half of emission of (VOC) Hydrocarbons and NO_x in cities is produced by motor vehicles. Automobile exhausts is responsible for 75 % of the total air pollution by releasing poisonous gases of CO (77 %), NO_x (8 %) and Hydrocarbons (14 %) (Sharma, 2001). On the other hand, R in the enter method (0.607) is almost equal to that in the stepwise method (0.601), showing no difference. Therefore, the second equation that is based on the stepwise method can be used to predict NO_x in the city instead of using the first equation which needs more data. On the other hand, the fact that there is no difference between the two R values indicates that the excluded variables in the second equation have less effect on the measurement of NO_x in the city.

Beta in Table 3 shows that those independent variables (meteorological parameters) have more effect on dependent variables (NO_x). Beta in Table 3 shows a highly significant effect of some variables like temperature compared to other meteorological parameters for measuring NO_x which is close to the results of Tehran (Masoudi et al., 2017a) and Isfahan (Masoudi and Gerami, 2018a) and Ahvaz (Masoudi and Asadifard, 2015). Parameter Sig (P-value) from Table 3 shows the degree of relation between NO_x and meteorological parameters. For example, Table 3a shows that evaporation has a higher effect on NO_x than the sunshine hours.

On the other hand, in Table 4, the linear regression equations of NO_x amount are presented for the enter and stepwise methods in different seasonal conditions. Almost all of the models except the autumn model of the enter method are significant. Stepwise methods show that those meteorological parameters are extremely important during these seasons for estimating the pollution. Among the models, the summer models have the highest R, while the R of the autumn models shows the least. These results are slightly different from the results of Tehran (Behzadi and Sakhacai, 2014) and Isfahan (Masoudi and Gerami, 2018a), and Ahvaz (Masoudi and Asadifard, 2015). R in the summer and winter models are higher than in the annual models, also indicating that relations between the pollutant and meteorological parameters are stronger than the whole year during these seasons.

Table 4. NO_x amount (ppb) using the enter and stepwise methods for different seasonal conditions.

season	enter method	R	stepwise method	R
Winter	= 21.446 + (3.431) Tmax + (-3.618) Tmin + (-.296) WSmean + (-.308) WSmax + (-.011) WDmax + (.021) RHmax + (.427) RHmin + (-.023) R + (-.909) SH	.712 (significant at 0.01)	= 5.867 + (.577) RHmin + (-3.655) Tmin + (3.552) Tmax + (-2.793) E	.700 (significant at 0.01)
Spring	= 49.457 + (.815) Tmean + (.599) Tmax + (-1.834) Tmin + (-2.101) WSmean + (.674) WSmax + (-.011) WDmax + (.035) RHmax + (.094) RHmin + (-2.022) R + (-.479) SH	.556 (significant at 0.01)	= 57.417 + (.883) Tmean + (-1.513) Tmin + (-1.302) E	.505 (significant at 0.05)
Summer	= -180.905 + (3.239) Tmax + (.672) Tmin + (-1.590) WSmean + (2.099) WSmax + (-.025) WDmax + (.003) RHmax + (.217) RHmin + (2.766) SH	.745 (significant at 0.01)	= -184.583 + (3.587) Tmax + (4.262) E + (2.972) SH	.724 (significant at 0.01)
Autumn	= .842 + (.030) Tmax + (-.016) Tmin + (-.084) WSmean + (.060) WSmax + (.000) WDmax + (-.001) RHmax + (.002) RHmin + (-.011) R + (-.042) SH	.448 (not Significant)	= .905 + (.036) WSmax	.278 (significant at 0.05)

where Tmean is the Temperature (mean), Tmax is the Temperature (max), Tmin is the Temperature (min), WSmean is the Wind speed (mean), WSmax is the Wind speed (max), WDmax is the Wind direction (max), RHmean is the Ratio of Humidity (mean), RHmax is the Ratio of Humidity (max), RHmin is the Ratio of Humidity (min), SH is the Sunshine Hours, R is the Rainfall, and E is the Evaporation

To test which annual model is better to use, RMSE (Root Mean Square of Error) is calculated for different linear models of the enter and stepwise methods. Predicted amounts using the different annual models for thirty days during 2011 are calculated and compared with the observed data during those days using the RMSE equation:

$$RMSE = \sqrt{\frac{\sum_{i=1}^n (O_{obs} - O_{cal})^2}{n}} \dots\dots\dots (1)$$

where O_{obs} is the observed NO_x value, and O_{cal} is the predicted NO_x value using model

The values of RMSE in both linear models of enter (39.32) and stepwise (37.34) methods show the capability of the stepwise model to predict NO_x amount compared to the enter model. This result is in agreement with the results of some studies conducted on other Iranian cities including Tehran (Masoudi et al., 2017a), Isfahan (Masoudi and Gerami, 2018a) and Ahvaz (Masoudi and Asadifard, 2015) and also other studies of other pollutants in the Shiraz city such as O₃ (Masoudi et al., 2016), CO (Masoudi et al., 2017b) and PM₁₀ (Masoudi et al., 2018b). The results indicate predicting most of air pollutants like NO_x when taking into consideration only the linear models of the stepwise method which need less data in addition to the fact that its calculation is easier than the enter model.

4. Conclusions

Nitrogen oxides are listed among the seven conventional (criteria) pollutants (including SO₂, CO, particulates, hydrocarbons, nitrogen oxides, O₃ and lead). In the current research, air quality analyses for Shiraz were conducted for NO_x. Shiraz is one of the highly polluted cities in Iran. Thus, there is an urgent need for conducting similar studies to analyze air quality in this city. The results of the current research showed that in the Enter and Stepwise models, there were significant relationships between NO_x and some meteorological parameters. The amount of R for both models

was highest during the summer. From the final part of the study, which uses the RMSE (Root Mean Square of Error) value, it can be concluded that the Stepwise model is more suitable for this pollutant. Finally, it can be said that there is a significant relationship between the amount of air pollutants and atmospheric parameters that can be used to predict the amount of contaminants in the coming years. Also, the results almost all times showed that the concentration levels of NO_x were higher than the primary standards of NO_x exhibiting unhealthy conditions.

References

- Abdul-Wahab, S.A., and Al-Alawi, S.M. (2002). Assessment and prediction of tropospheric ozone concentration levels using artificial neural networks, *Environmental Modelling & Software*, 17(3): 219–228
- Abdul-Wahab, S.A., Bakheit, C.S., Al-Alawi, S.M. (2005). Principal component and multiple regression analysis in modelling of ground-level ozone and factors affecting its concentrations, *Environmental Modelling & Software*, 20 (10): 1263–1271
- Asrari, E., Sen, P.N., Masoudi, M., 2007. Status of carbon mono oxide in Tehran City- Iran, *Pollution Research*, 26 (4): 531-535
- Behzadi, F., and Sakhaei, M. (2014). Study of Air Pollution and its relationship with meteorological parameters in Tehran city, Project of B.Sc. degree in Shiraz University.
- Cesaroni, G., Porta, D., Badaloni, C., Stafoggia, M., Eeftens, M., Meliefste, K., Forastiere, F., (2012). Nitrogen dioxide levels estimated from land use regression models several years apart and association with mortality in a large cohort study, *Environmental Health*, 11 (48): 1-10
- Chelani, A.B., Gajghate, D.G., Tamhane, S.M., Hasan, M.Z. (2001). Statistical modeling of ambient air pollutants in Delhi, *Water, Air and Soil Pollution*, 132: 315-331
- Choi, C., Bell, M., Lee, J. (2017). A study on modeling nitrogen dioxide concentrations using land-use regression and conventionally used exposure assessment methods, *Environmental Research. Letter*, 12: 1-11
- Cunningham, W.P., and Cunningham, M.A. (2002). Principles of Environmental Science inquiry and applications. MxGraw Hill Company.
- Cuhadaroglu, B., and Demirci, E. (1997). Influence of some meteorological factors on air pollution in Trabzon city, *Energy and Buildings*, 25 (3): 179–184
- Elminir, H.K. (2005). Dependence of urban air pollutants on meteorology, *Science of The Total Environment*, 350: 225–237

- Ho, L.C., and Lin, W.Y. (1994). Semi-statistical model for evaluating the effects of source emissions and meteorological effects on daily average NO_x concentrations in South Taiwan, *Atmospheric Environment*, 37: 2051-2059
- Jhun, I., Coull, B., Zanutti, A., Koutrakis, P. (2015). The impact of nitrogen oxides concentration decreases on ozone trends in the USA, *Air Quality Atmosphere and Health*, 8(3): 283–292
- Lam, G.C.K., Leong, D.Y.C., Niewiadomski, M., Pang, S.W., Lee, A.W.F., Louie, P.K.K., (1997). Street level concentration of NO_x and suspended particulate matter in Hong Kong, *Atmospheric Environment*, 31: 1-11
- Li, L., Qian, J., Ou, C.Q., Zhou, Y.X., Guo, C., Guo, Y., (2014). Spatial and temporal analysis of Air Pollution Index and its timescale-dependent relationship with meteorological factors in Guangzhou, China, 2001–2011, *Environmental Pollution*, 190: 75-81
- Kinney, P.R. (2002). SPSS for windows made simple release 10. Psychology press.
- Mandal, S. (2000). Progressive decrease of air pollution level from west to east at Calcutta, *Indian Journal of Environmental Protection*, 20: 6-10
- Masoudi, M., and Asadifard, E. (2015). Status and prediction of Nitrogen Dioxide as an air pollutant in Ahvaz City, Iran, *Pollution Atmosphérique*, 225: 1-10
- Masoudi, M., Ordibeheshti, F., Rajaipoor, N., Sakhaei, M. (2016). Status and preparation of prediction models for ozone as an air pollutant in Shiraz, Iran, *Pollution*, 2(4):387-397
- Masoudi, M., Behzadi, F., Sakhaei, M. (2017a). Concentration of NO₂ in the Air over Tehran, Iran, *Russian Meteorology and Hydrology*, 42: 728–730
- Masoudi, M., Rajaipoor, N., Ordibeheshti, F. (2017b). Status and prediction of CO as an air pollutant in Shiraz, Iran, *Fresenius Environmental Bulletin*, 26:3697-3704.
- Masoudi, M., and Gerami, M. (2018a). Status and prediction of NO₂ as an air pollutant in Isfahan, Iran, *Fresenius Environmental Bulletin*, 27: 2743-2750
- Masoudi, M., Rajaipoor, N., Ordibeheshti, F. (2018b). Status of PM₁₀ as an air pollutant and prediction using meteorological indexes in Shiraz, Iran, *Advances in Environmental Research*, 7: 109-120
- Sabah, A., Al-Rubiei, R., Al-Shamsi, A. (2003). A statistical model for predicting carbon monoxide levels, *International Journal of Environment and Pollution*, 19: 209-224
- Sánchez-Ccoyllo, O.R., and Andrade, M.F. (2002). The influence of meteorological conditions on the behavior of pollutants concentrations in São Paulo, Brazil, *Environmental Pollution*, 116 (2): 257–263
- Sharma, B.K. (2001). An Introduction to environmental pollution. Krishna prakashan media (p) ltd.
- Wang, S.M., Yu, H., Song, L., Xie, Y., Zhu, Q. (2015). Air Quality In A Mountainous City: A Case Study In Chongqing, China. *Fresenius Environmental Bulletin*, 24(9): 2699-2706.
- Yoo, J.M., Lee, Y.R., Kim, D., Jeong, M.J., Stockwell, W.R., Kundu, P.K., Oh, S.M., Shin, D.B., Lee, S.J. (2014). New indices for wet scavenging of air pollutants (O₃, CO, NO₂, SO₂, and PM₁₀) by summertime rain, *Atmospheric Environment*, 82: 226-237

Morphometric Analysis of Lake Ruma, Song, Adamawa State in Northeastern Nigeria

Yonnana Ezekiel^{1*}, Apollos Thandime², James Thomas¹

¹ Adamawa State University Mubi, Department of Geography, Nigeria.

² Adamawa State University Mubi, Department of Fisheries and Aquaculture, Nigeria.

Received 2 December 2018, Accepted 19 February 2019

Abstract

The morphometric analysis of lakes is vital for vast limnologic, ecologic and sustainable use of the lake resources. In this study, a morphometric analysis assessment of Lake Ruma was conducted using an integrated approach of hydrographic survey, mathematical computations and field observations. Results revealed that the lake is characterized by a Surface Area (A_0) of 0.56km²; a Volume (V) of 0.80mcm and a Mean Depth (Z_{Mean}) of 1.43m. Its Relative Depth (Z_r) of 0.88% and 0.18 Index of Basin Permanence (IBP) are clear indications of the lake's shallow status, susceptibility to mixing and the littoral effect on the basin volume. The lake's Development of Volume index (1.19) portrays the conical depression nature of its basin as also presented by its bathymetric map, while its Shoreline Development Factor (D_L) of 1.64 indicates its crenulated nature and potential for development of littoral community. Major identified uses of the lake are the small scale (local) fishing and water supply for livestock consumption and domestic uses. The lake is recommended for proper conservation and management to support a longer term and a larger scale of fish farming, irrigation for agriculture and water supply for livestock and domestic uses.

© 2019 Jordan Journal of Earth and Environmental Sciences. All rights reserved

Keywords: Lake Ruma, Morphometry, Hydrographic, Bathymetry, Mathematical computation.

1. Introduction

With the increased focus on integration and holistic approaches to water management across the world, the need for lake resources management is not left out. At the World Summit on Sustainable Development in Johannesburg in 2002, Integrated Water Resources Management (IWRM) and Water Efficiency Plans were proposed in order to overcome the world's essential water resources issues including those of the lake ecosystems (UNEP Collaborating Centre on Water and Environment, 2007). Therefore, Lake Resources Management is regarded as an integral component of IWRM with lake morphometric assessment as a vital activity that provides relevant information on lake basin morphology and water content.

Lakes are primarily water storage bodies with a considerable variation in size, shape and depth (UNEP Collaborating Centre on Water and Environment, 2007) having a great significance to humans and many other organisms. They are found throughout the world, most especially in North America, Africa, and Asia where about 70 % of the world's total lake water exist (Lake, 2010). Among the world's largest lakes are Lake Baikal (Central Asia), the Caspian Sea (Central Asia), Lake Tanganyika (Eastern Africa), Lake Superior and the Great Lakes (North America), Crater Lake (Oregon, USA), and Aral Sea (Western Asia). Others include Lake Eyre (Australia), Lake Vanern Northern Europe, Lake Titicaca (Western South America) and Great Slave Lake (Canada). Containing over 90 % of the world's liquid surface freshwater, natural and artificial lakes provide many uses for sustainable human livelihood and economic

developments (International Lake Environment Committee-ILEC, 2007) as well as uses for socio-cultural developments, while serving as habitats for a great variety of flora and fauna.

In the recent decades, the human impact on lake ecosystems has increased due to the intensification of agriculture, irrigation, water consumption, and electrical purposes, in a way that noticeable environmental changes have been observed in the shallowest lakes (Ławniczak et al., 2011). Furthermore, it has been noted that the majority of such changes within lakes are associated with changes in the water level, progressing degradation, or plant succession leading to lake disappearance taking place within the littoral zone. The United Nations World Water Assessment Programme, (2010) has earlier commented on the alarming deteriorating state of most lakes in the world, which calls for a timely and periodic monitoring and conservation measures that include bathymetric mapping and morphometric analysis. In this line of thought, studies conducted on the fluvial lakes of the Upper Benue Valley area of Adamawa State, in Northeastern Nigeria showed that the lakes are subjected to gradual changes in their basin morphology and loss in their hydrological potentials over time as they gradually shrink and dry up or accumulate mineral and organic materials, filling up their basins through the combined influences of natural and anthropogenic processes of climate change as well as catchment erosion and deposition rates associated with changing land uses (Yonnana, 2015; Yonnana and Hyellamada, 2016).

Lake Morphometry is simply the measurement and description of lake morphology (shapes and size of lakes)

* Corresponding author e-mail: ezekiel97@adsu.edu.ng

(Wetzel and Likens, 1991; Kalff, 2002). It is a very vital concept used in detailed analyses of the limnologic properties of freshwater lakes (Wetzel, 2001; Kalff, 2002). The Morphometric characteristics of lakes are paramount in the assessments of numerous limnologic properties of the lake ecosystem, ranging from status and changes in the lake basin morphology to the quantity and quality of its waters in relation to the biological productivity and human uses. Stefanidis and Papastergiadou (2012) added that the morphology of lakes is one of the most important factors controlling the trophic status, physicochemistry, productivity, and distribution of aquatic organisms, and that lake morphometric properties such as surface area, volume, maximum and average depths are strongly related to nutrient cycling and the lake water chemistry. Expressing the usefulness of Lake Morphometry in Limnology, Hakanson (2005) noted that the size and form of lakes regulate many general transport processes, such as sedimentation, re-suspension, diffusion, mixing, burial and outflow, which in turn regulate many abiotic and chemical variables. More so, by influencing water clarity, Lake Morphometry regulates both the primary and secondary biological productions of the lake, for example the production of zooplankton and fish. Management techniques, such as the loading capacity for effluents and the selective removal of undesirable components of the biota, are also heavily dependent on a detailed knowledge of the morphometry and water retention times in freshwater ecosystems (Wetzel and Likens, 1991). Morphometric studies conducted on natural lakes in Brasil revealed that Lake Palmas was the deepest (Barroso et al., 2014). Similarly, studies carried out on lakes Mbemun and Goro Dong in Lamurde and Numan areas of Adamawa State in Nigeria (Yonnana and Raji, 2017; Yonnana et al., 2018), respectively, showed that variations in their morphometric properties are responsible for variations in their suitability for socio-cultural fishing festival in the Bachama Chiefdom, even though they both possess good potentials for fish production. While Lake Mbemun was found to be shallower in its water level and more muddy and sticky, Lake Goro Dong was discovered to be deeper in the water level, and less muddy and not sticky.

Considering the importance of lake morphometry as well as the craving for surface freshwater resources by humans on one hand and the fast depletion tendencies of lakes on the other hand, there is a serious and urgent need for inventory and conservation methods of the existing freshwater lakes, most especially in the sub Saharan African countries (including Nigeria) where the rages of climate change and anthropogenic degradation prevail (Serdeczny, et al., 2015; Yunana et al., 2017). Though a very important and the only existing lentic surface water body in Song Local Government Area of Adamawa State, Lake Ruma lacks detailed and documented morphometry information for proper planning and management. It is against this background that the current study was conducted on the lake with the sole aim of ascertaining its morphometric properties. The objectives of the study are to prepare a bathymetric map that portrays the lake basin morphology, examines its morphometric properties and identifies its major potentials. The study constitutes part of an ongoing research and information gathering exercise by

the researchers on lakes' and ponds' potentials in Adamawa State for the purpose of conservation and sustainable use of the state's water resources.

2. Materials and Methods

2.1. Study Area

Lake Ruma and its immediate environs are located between latitudes $09^{\circ}31'30''\text{N}$ and $09^{\circ}43'30''\text{N}$ and longitudes $12^{\circ}40'00''\text{E}$ and $12^{\circ}44'30''\text{E}$. The lake is situated in Song Local Government Area of Adamawa State, Northeastern Nigeria; about 15km Southeast of Song Town, on the right bank floodplain of River Kilange, southwards of Wuro Daudu settlement (Fig. 1).

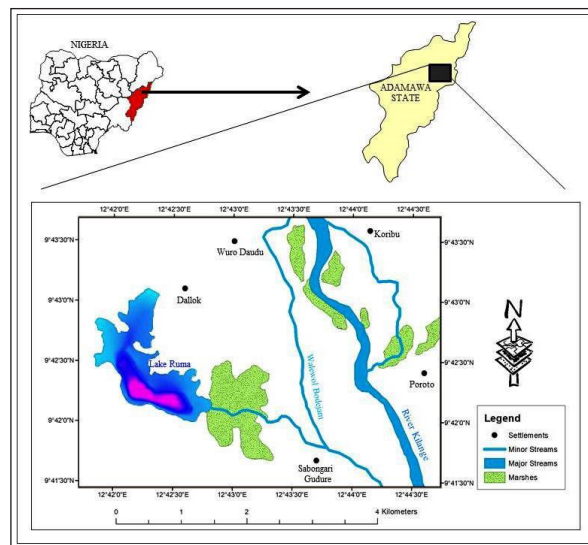


Figure 1. Study Area Map showing the location of Lake Ruma

The major sources of its water are direct rainfall, stream inflows from the Kilange River, most especially at periods of peak discharges and runoffs from the immediate surroundings during periods of high and intensive rainfalls. The lake area is surrounded by riverine alluvium soils with its littoral zones dominated by vast species of submerged, floating and emerged aquatic plants; prominent among which are *Ipomea aquatica* (Floating Morning Glory), *Nymphaea nouchali* (Water Lilly) and *Typhalatifolia* (Typha grass) and *Pistia stratiotes* (Water lettuce). The lake environs are characterized by a large expanse of a grazing land with few farmlands and few isolated human settlements.

2.2. Data Collection

Both process and historical methods of lake system studies in geomorphology as suggested by Kashiwaya (2017) were employed in this study. Therefore, an integrated approach involving the applications of hydrographic survey, GIS analyses, mathematical computations using relevant mathematical formulae, field observation and oral interviews were employed for the sake of assessing the morphometric characteristics and functionality of the lake.

The hydrographic survey of the lake basin involved a combined sounding routine over the lake in which HONDEX PS-7 Portable Handheld Depth Sounder and the Sounding Rod Method as described by Davis et al., (1981) and Basak (1994) were used. The Handheld Depth Sounder was used for most of the depth measurements owing to its accuracy propensity at the depth range of 0.6m to 80m, while the Sounding Rod

procedure was employed as an alternative measure at the lake portions of less than a 0.6m depth. The soundings were randomly conducted at 478 sampling points over the lake covering the portion of open water and parts with less littoral vegetation. The sounding sample size (462 points) was tied to the small size state of the lake. At each sounding point, depth was recorded as Z coordinate alongside its corresponding X, Y coordinates (Northing and Easting) obtained in Universal Traverse Mercator (UTM) format using the Global Positioning System (GPS-Garmin etrex 20) owing to the small nature of the study lake. With a 2.0m to 3.0m range of accuracy, the GPS used had a very minimal effect on the results of spatial variations.

The hydrographic survey data were compiled in a Microsoft Excel sheet and then converted into a point-shape file in ArcGIS 10.0 for preparation of the lake bathymetry. Through geo-processing procedures involving the use of the Nearest Neighbor Interpolation method, the Lake's Bathymetric map was generated from the imported hydrographic survey data. From the generated bathymetric map, the lake's morphometric parameters such as Shoreline Length (SL), Surface Area (A), Maximum Length (L_{Max}) and Maximum Width (W_{Max}) were directly measured on the generated bathymetric map in ArcGIS 10.0 using the measure tool of the Arc Map.

While the lake's shoreline elevation and maximum depth values were obtained directly from the hydrographic survey data, other parameters such as the Relative Depth (Z_r), Mean Depth (Z_{Mean}), Development of Volume (D_v), Lake Volume (V), Shoreline Development Index (D_{SL}) and Index of Basin Permanence (IBP) were obtained by mathematical computations using the appropriate formulae as shown in Table 1.

Table 1. Lake Morphometric parameters and corresponding mathematical formulae

Morphometric Parameter	Symbol/Formulæ	Source
Shoreline Elevation	H	Wetzel, 2001;
Shoreline Length	SL	Wetzel, 2001; Kalf, 2002; SWCSMH, 2015
Surface Area	A_0	Wetzel, 2001; Kalf, 2002; SWCSMH, 2015
Maximum Length	L_{Max}	Wetzel, 2001; Kalf, 2002; SWCSMH, 2015
Maximum Width	W_{Max}	Wetzel, 2001; SWCSMH, 2015
Maximum Depth	Z_{Max}	
Mean Depth	$Z_{Mean} = V / A_0$ V = Lake Volume	Wetzel, 2001; Kalf, 2002; SWCSMH, 2015
Depth Ratio	$R_z = Z_{Mean} / Z_{Max}$	Kalf, 2002
Relative Depth	$Z_r = \frac{50(z_{max})\sqrt{\pi}}{\sqrt{A_0}}$	Wetzel, 2001; SWCSMH, 2015
Shoreline Development Factor	$D_{SL} = \frac{SL}{2\sqrt{\pi A_0}}$	Wetzel, 2001; SWCSMH, 2015
Development of Volume	$D_v = 3Z_{Mean}/Z_{Max}$	Wetzel, 2001; Kalf, 2002; SWCSMH, 2015
Volume (V)	$V_{z_0-z_1} = \frac{1}{3}(A_{z_0} + A_{z_1} + \sqrt{A_{z_0} \times A_{z_1}})(z_0 - z_1)$ z_0 = Zero depth (Shoreline) z_1 = Next successive area at depth z_0	Wetzel, 2001; Kalf, 2002; SWCSMH, 2015
Index of Basin Permanence	IBP = V/SL	Wetzel, 2001; Kalf, 2002; SWCSMH, 2015

Information on the functional relevance of the lake was obtained by observation and historic inquiries through a focus group discussion with fishermen and settlers in the lake environs.

3. Results and Discussion

Results of the lake's morphometric parameters as obtained are provided in Table 2. The results revealed that the lake is characterized by a surface area (A_0) of 560,000.00m² (0.56km²), a maximum length (L_{max}) or fetch of 1.22km, and a maximum width (W_{max}) of 0.34km, resulting in a length-width ratio (Extension) of 3.59. The maximum length value indicates a good lake surface state, adequate for the development of water waves by wind action as well as the enhancement of adequate water mixing which promotes a good circulation of oxygen within the lake.

While the Shoreline Length (SL) is the farthest distance of the lake's entire marginal line that marks the water and land boundary, the Shoreline Development Index (D_{SL}) is the ratio of the shoreline length to the length of the circumference of a circle of area equal to that of the lake, which is a measure of the lake's shape and a morphometric parameter that reflects the lake's potential for development of littoral communities, which are usually of high biological productivity (Soil and Water Conservation Society of Metro Halifax - SWCSMH, 2015). Analysis and mathematical computations yielded a Shoreline Length of 4.34km and a Shoreline Development Factor of 1.64, which is an indication of its crenulated state and potential for littoral community development. This property is a relevant pointer to the lake's viable potential for fishery development.

Table 2. Morphometric Parameters of Lake Ruma estimated in January, 2019

Morphometric Parameter	Symbol/Formulæ	Dimension
Shoreline Elevation	H	215 m a.s.l
Shoreline Length	SL	4.34 km
Surface Area	A_0	0.56km ²
Maximum Length	L_{Max}	1.22 km
Maximum Width	W_{Max}	0.34 km
Maximum Depth	Z_{Max}	3.60 m
Mean Depth	$Z_{Mean} = V / A_0$	1.43 m
Depth Ratio	$R_z = Z_{Mean} / Z_{Max}$	0.40
Relative Depth	$Z_r = \frac{50(z_{max})\sqrt{\pi}}{\sqrt{A_0}}$	0.43
Development of Volume	$D_v = 3Z_{Mean}/Z_{Max}$	1.19
Shoreline Development Factor	$D_{SL} = \frac{SL}{2\sqrt{\pi A_0}}$	1.64
Volume	$V_{z_0-z_1} = \frac{1}{3}(A_{z_0} + A_{z_1} + \sqrt{A_{z_0} \times A_{z_1}})(z_0 - z_1)$	0.80mcm ³
Index of Basin Permanence	IBP = V/SL	0.18

The mean depth of a lake serves a common parameter used for depth comparison among lakes, while the relative depth (a ratio of the lake maximum depth to its mean diameter) portrays general shallow or deep characteristics of the lake (SWCSMH, 2015; Kalf, 2002). A Maximum Depth (Z_{max}) of 3.60m was obtained from the hydrological survey data, while mathematical computations revealed a Mean Depth (Z_{mean}) of 1.43m and a Relative Depth of 0.43%, all indicating the lake's

shallow status. Comparing the lake's mean depth with those of other fluvial lakes in the Benue valley area of Adamawa State, the lake was found to be substantially deeper than Lakes Geriyo-Yola North (0.70m), Gwakra-Girei (0.75m), Pariya-Fufore (0.79m) and Mbemun-Lamurde (0.82m) and in the ranges of Lakes Pariya Ribadu-Fufore (1.41m) and Goro Dong-Numan (1.20m) (Yonnana et al., 2015; Yonnana and Raji, 2017; Yonnana et al., 2018). The relative depth value (0.43%) obtained for the lake indicates its relatively very shallow status (<15ft or 4.60m) as asserted by Bischoff (2014) and Wenk News (2017) and thus its susceptibility to mixing and exposure to sunlight and nutrients which could enhance aquatic plant productivity by photosynthesis.

Lake volume (V) is a measure of the water content of the lake in cubic meters (m^3) or million cubic meters (mcm). It is normally computed from the lake bathymetry map information using the formula provided on table 1. A volume of 0.80mcm was computed for the studied lake. In comparison to the volumes of Lakes Mbemun (2.99mcm), Goro Dong (1.98mcm), Geriyo (1.12mcm) and Pariya Ribadu (1.08mcm) (Yonnana et al., 2015; Yonnana and Raji, 2017; Yonnana et al., 2018), Lake Ruma was found to be smaller, yet confirmed as another substantial lentic water body of great aquatic potentials in Adamawa State, though smaller in volume compared to other lakes.

Two important morphometric parameters that provide good estimates of the Lake Basin form are

the Depth Ratio (R_z) and Development of Volume (D_v). Depth Ratio (R_z) relates the lake basin depression to that of a perfect cone with the same height and basal area as that of the lake's maximum depth and surface area, respectively (Neumann, 1959 in Kalff, 2002). R_z values from 0.33 to 0.35 indicate elliptical cone-shaped basins, while values from 0.66 to 0.67 indicate ellipsoid-shaped basins (Kalff, 2002). As such, the Depth Ratio value (0.40) obtained for Lake Ruma indicates the departure of its basin form and elliptical cone-shape towards an ellipsoid form as also portrayed by the Bathymetric map (Fig. 2) and the lake's Hypsographic Curve (Fig. 3).

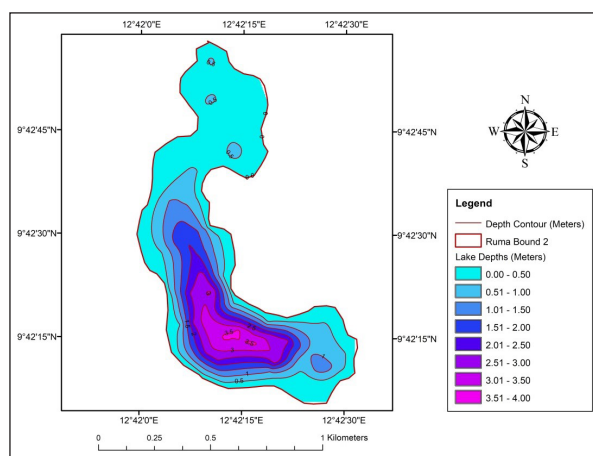


Figure 2. Bathymetric Map of Lake Ruma for January, 2019

Development of Volume is a measure of departure of the shape of a lake basin from that of a cone, in that the value is greater than 1.0 for the majority of lakes and greatest in shallow lakes with flat bottoms (SWCSMH, 2015). Lake

Ruma yielded a D_v value of 1.19 depicting the slight conical shape of its basin.

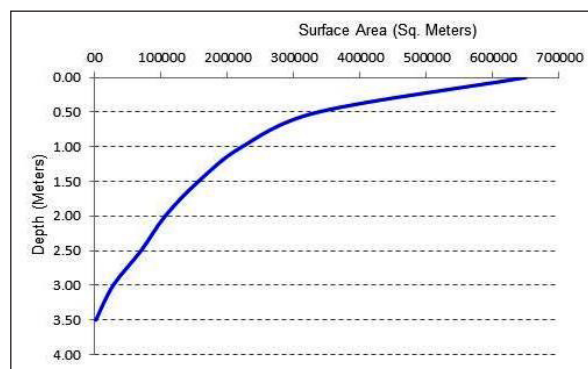


Figure 3. Hypsographic Curve of the lake

A parameter that reflects the littoral effect on lake volume is the Index of Basin Permanence (IBP). It is the ratio of the lake volume to its shoreline length in kilometers. It also indicates a state of shallowness so that lakes with IBPs in the vicinity of 0.1 and below are commonly dominated by rooted aquatic macrophytes, while values of 0.2 and above indicate a level of more water permanence (SWCSMH, 2015). The 0.18 IBP value obtained for Lake Ruma therefore indicates its shallow and non-permanence status as well as the dominance of its littoral zone by rooted aquatic plants; prominent among which are *Typha latifolia*, *Nymphaea nouchali* *Oryza* Spp and *Pistia stratiotes* as found from field studies.

Field studies revealed that besides its ecological function as a habitat for vast aquatic flora and fauna, Lake Ruma serves as an important fishing site that supports over fifty occupational fishermen on an annual basis. It also serves as a major source of drinking water for livestock and domestic uses for humans living in its vicinity, most especially in the dry seasons. Even though irrigation agricultural practices were observed to be very minimal in the area, animal rearing and rain-fed agriculture were found to be the most prominent land uses in the lake environs. It was also observed that sheet wash and surface runoff in form of rills from the surrounding farmlands drain water and some quantity of sediments into the lake at several points. Thus, the encroachment of farming activities closer to the lake shore is capable of intensifying sediment loading and focusing in the lake basin, which in time can eventually lead to gradual siltation of the lake.

4. Conclusions

The morphometric properties of Lake Ruma were found to be similar to those of the fluvial lakes in the Benue River valley area of Yola. It is a shallow and elongated fluvial lake of a concise surface area, volume and maximum length, adequate for supporting aquatic productivity with viable potentials for fisheries and aquaculture as well as substantial water quantity for livestock production in the area. However, the encroachment of farming practices closer to the lake shores poses the dangers of siltation in the near future. Therefore, proper management of the lake against sediment generating land uses in the area is recommended. Besides, the data and information generated from this study will be very useful for the monitoring and management of the lake, most particularly, with regards to the aspects of water budget and siltation abatement.

References

- Barroso, G.F., Gonçalves, M.A., Garcia, F.C. (2014). The Morphometry of Lake Palmas; A deep Natural Lake in Brazil. *PLoS One*, 9(11). doi:10.1371/journal.pone.0111469
- Basak, N.N. (1994). Survey and leveling. New Delhi, MacGraw Hill Ltd. 1994;475-476
- Bischoff, J. (2014). Shallow Lake Ecology. Retrieved July 14, 2018 from <https://minnehahacreek.org/sites/minnehahacreek.org/files/Shallow%20Lake%20Forum%204-12-14%20Bischoff.pdf>
- Davis, R.E., Foote, F.S., Anderson, J.M., Mikbail, E. M. (1981). *Surveying Theory and Practice* (6th ed). New York, McGraw-Hill, p 878.
- Hakanson, L. (2005). The Importance of Lake Morphometry for the Structure and Function of Lakes. *International Review of Hydrobiology*, 90(4): 433-461. doi. 10.1002/iroh.200410775
- International Lake Environment Committee (ILEC) Foundation (2007). How can we stop
- Degradation of the World's Lake Environments? Retrieved July 12, 2018 from <http://www.ilec.or.jp>
- Kalff, J. (2002). *Limnology: Inland Water Ecosystems*. New Jersey, Prentice Hall; pp85-91
- Kashiwaya, K. (2017). *Geomorphology of Lake-Catchment Systems: A New Perspective from Limnogeomorphology*. Singapore, Springer Nature Ltd.
- Lake (2010). In the *Encyclopaedia Britannica Student and Home Edition*. Chicago: Retrieved July 14, 2018] from <https://www.britannica.com/science/lake>
- Ławniczak, A.E., Choiński, A., Kurzyca, I. (2011). Dynamics of Lake Morphometry and Bathymetry in Various Hydrological Conditions. *Polish J. of Environ. Stud.* 20(4): 931-940. <http://www.pjoes.com/pdf-88636-22495>.
- Serdeczny, O., Adams, S., Baarsch, F., Coumou, D., Robinson, A., Hare, W., Schaeffer, M., Perrette, M. (2015). Climate change impacts in Sub-Saharan Africa: from physical changes to their social repercussions. *Regional Environmental Change*, 15(8). DOI 10.1007/s10113-015-0910-2
- Soil and Water Conservation Society of Metro Halifax - SWCSMH (2015). *Lake Morphology*. Retrieved July 12, 2018 from www.3dflags.com.
- Stefanidis, K., and Papastergiadou, E. (2012). Relationships between Lake Morphometry, Water Quality, and Aquatic Macrophytes, in Greek Lakes. *Fresenius Environmental Bulletin PSP*, 21(10a): 3018 - 3026
- UNEP Collaborating Centre on Water and Environment (UCC Water). (2007). *Sustainable Management of Lake Basins in the Context of IWRM Concepts and Issues*. Paper No.2. <https://www.gwp.org/.../sustainable-management-of-lake-basins-in-the-context-of-iwr.../pdf>
- United Nations World Water Assessment Programme (2010). *Lakes: Freshwater Storehouses and Mirrors of Human Activities*. Retrieved, July 2, 2018 from www.unesdoc.unesco.org/images/0018/001863/186316e.pdf.
- Wenk News (2017). *Carp and Shallow Lake Ecology*. Retrieved July 19, 2018 from <https://www.wenk.com/news/off-the-hook-carp-and-shallow-lake-ecology/>
- Wetzel, G. R. (2001). *Limnology; Lake and River Ecosystems*, 3rd ed. Academic Press, California.
- Wetzel, R.G. and Likens, G.E. (1991) *Limnological Analysis*. 2nd Edition, New York, Springer Verlag,
- Yonnana, E. (2015). *Assessment of Hydrogeomorphic characteristics of lakes in the Upper Benue Valley of Adamawa State, Nigeria*. Unpublished PhD Thesis, Department of Geography, Modibbo Adama University of Technology Yola, Adamawa State.
- Yonnana, E., Tukur, A.L., Mubi, A.M. (2015). Morphometric Characteristics of Selected Fluvial Lakes in the Upper Benue Valley Area of Adamawa State, Northeastern Nigeria *Journal of Geography and Regional Planning*, 8(3): 56-64. DOI: 10.5897/JGRP2014.0470.
- Yonnana, E., and Hyellamada J.S. (2016). Land Use Impacts on Hydrogeomorphology of Lakes in the Upper Benue Valley Area of Adamawa State, Nigeria. *International Journal of Research in Geography*. 2(1): 26-33. www.arcjournals.org.
- Yonnana, E., and Raji, A. (2017). Assessment of Hydrogeomorphic Suitability of Lake Mbemun for Socio-cultural Fishing Festival in the Bachama Chiefdom, Adamawa State, Northeastern Nigeria. *Journal of Geography, Environment and Earth Science International*, 10(3): 1-9. <http://www.sciencedomain.org/review-history/19206>. doi: 10.9734/JGEESI/2017/33534
- Yonnana, E., Raji, A., Alikidon, A.V. (2018) Hydrogeomorphologic and Limnologic Characteristics of Goro Dong (Lake) in Numan Area, Adamawa State, Northeastern Nigeria. *Asian Journal of Environment and Ecology*, 6(3): 1-9. <http://www.sciencedomain.org/review-history/24368>, doi: 10.9734/AJEE/2018/4117
- Yunana, D. A., Shittu A. A., Ayuba, S., Bassah, E.J., Joshua, W.K. (2017). Climate change and lake water resources in sub-Saharan Africa: Case Study of Lake Chad and Lake Victoria. *Nigerian Journal of Technology (NIJOTECH)*, 36(2): 648 – 654. www.nijotech.com; <http://dx.doi.org/10.4314/njt.v36i2.42>.

Estimation of Global Solar Radiation, Sunshine Hour Distribution and Clearness Index in Three Geopolitical Regions of Southern Nigeria

Adeniji Nathaniel^{*1,2}, Akinpelu Jacob¹, Adeniji Joshua³, Adeola Solomon²

¹ Bowen University, Department of Physics and Solar Energy, Iwo, Osun State, Nigeria

² Solar Energy Research and Application Centre, Iwo, Osun State, Nigeria

³ Bowen University, Department of Computer and Information Technology, Iwo, Osun State, Nigeria

Received 23 January 2019; Accepted 3 March, 2019

Abstract

The concept of solar energy and its applications in this present day world would come to be one of the solutions to the present problem of instability and epileptic power supply in Nigeria. In this research work, the baseline data for the mean monthly global solar radiation (H) and sunshine hours (S) for three geopolitical regions of Nigeria, namely Port-Harcourt (South-southern Nigeria) (5.00°N, 6.950°E), Enugu (South-eastern Nigeria) (6.7°N, 7.6°E) and Ikeja (South-western Nigeria) (6.58°N, 3.32°E), were obtained from the Nigeria Metrological Agency (NIMET) in Nigeria over the period from 1996 to 2010. The data for global solar radiation were measured using a Gunn-Bellani radiometer, and a linear regression correlation model was developed. The clearness index estimated for each station and other surrounding towns/villages with similar meteorological conditions was also developed. The results show that using the Angstrom-Prescott model, the Angstrom coefficients (a and b) for estimating the global solar radiation were: 0.07 and 0.12; 0.27 and 0.58; 0.25 and 0.63 for Port-Harcourt, Enugu and Ikeja respectively. The average sunshine hour for the period of the study was estimated to be four hours, five hours, forty minutes and five hours, 0 minutes and six seconds for the three meteorological stations in this study. The average global solar radiation for these stations was estimated to be 10.003 MJm⁻²day⁻¹, 15.006 MJm⁻²day⁻¹ and 14.440 MJm⁻²day⁻¹ respectively. The results show that the root-mean-squared-error, mean-bias-error and mean percentage error were generally less than 0.6, 0.2 and 3.84 respectively for all of the stations considered. The study concluded that the Angstrom- Prescott model plays a significant role in predicting and estimating solar energy potentials in these geopolitical zones

© 2019 Jordan Journal of Earth and Environmental Sciences. All rights reserved

Keywords: Angstrom-Prescott model, Global solar radiation, Sunshine Hour, Clearness Index.

1. Introduction

Solar radiation can be considered as the most important meteorological element which affects all climatological and biological processes such as evaporation and transpiration, snowmelt (increase in sea level) and plant growth either directly or indirectly (Mojarrad et al., 2015). In addition, the global solar radiation is the sun total of all radiation reaching the earth surface i.e. it includes both the direct and the diffused solar radiation reaching the earth surface measured at any location. It has been established that sunshine duration has a direct correlation with global solar radiation (Okonkwo, 2014). Moreover, solar radiation data over the years have been used in different solar applications such as solar ovens, solar water heaters, photovoltaic systems, atmospheric energy balance studies, meteorological forecasting among others. However, for most developing countries, solar radiation measurements are not easy to obtain due to the shortage of measurement instruments. To overcome this limitation, most estimates of Global solar radiation (GSR) are focused on readily available meteorological parameters. However, the number of weather stations recording the different meteorological parameters are becoming rapidly increasing in recent times but even so, data for previous years (going back 50 years) on global radiation are still very rare in Nigeria. Solar Energy, which is a

renewable energy, is one of the foremost and ancient sources of underutilized energy. It forms the basis for the fundamental elements of most fossil and renewable energies (Innocent et al., 2015). Radiation from the sun (solar and atmospheric) has been identified as the largest renewable energy resource on earth (Gana and Akpootu, 2013).

Solar radiation reaching the earth is considered to be affected by some parameters like diffusion, reflection, and so on. Most of the time, this radiation is reflected or scattered by air molecules, clouds, aerosols (dust) (Aweda et al., 2016). The application/utilization of renewable energy resources has increased largely in recent times owing to the ever increasing need for electrical/thermal energy (Sanusi and Abisoye, 2013). However, fossil fuel resources needed for the generation of conventional electrical power are quite limited and there is also the problem of the global environmental concerns over the use of fossil fuels. The over dependency of present day Nigeria on hydro power generation, transmission and distribution of electricity has failed to satisfy the citizens' demands for an uninterruptable power supply, hence, there is a big need to search for other forms of renewable energy sources. The estimation of the clear sky irradiance components of solar radiation is very important in many solar energy applications (systems design and simulation,

* Corresponding author e-mail: nathaniel.adeniji@bowenuniversity.edu.ng

control process of the accuracy of radiometers, data quality control, gaps filling process, etc.), as well as in some routine engineering practices (e.g., the peak cooling load of buildings is determined for a hot, cloudless, summer day) (Islahi et al., 2015).

The south southern part of Nigeria is characterised by cloudiness conditions which occur frequently even during the dry seasons of the year. This could be attributed to the influence of the Inter-Tropical Convergence Zone (ITCZ), producing Tropical Continental (TC) associated with dry and dusty North-Easterly winds which blow from the Sahara Desert and finally prevail over Nigeria producing the dry season conditions (Sunday et al., 2016). The clearness index for the south southern part of Nigeria was estimated to be 0.40 using the two major cities of Calabar and Port-Harcourt in a research carried out by Augustine and Nnabuchi, 2009. The city of Enugu, along sides its south eastern counterpart cities of Awka, Owerri, was seen to have Angstrom Constants of 0.226 and 0.677; 0.259 and 0.589; and 0.251 and 0.617 respectively in a research carried out by (Elekalachi et al., 2016). Enugu was seen to have a correlation percentage of 65.9 % between the measured and the estimated global solar radiation; 69.6 % correlation for Awka and 83.1 % for Owerri carried out by values in the research.

The average values of the angstrom Constant for South eastern Nigeria using Akwa, Owerri and Enugu were given to be 0.24 and 0.62. The clearness index for the south eastern part of Nigeria was estimated using the two major cities of Uyo and Warri to be 0.5 in a research carried out on the Correlation of cloudiness index with a clearness index for four selected cities in Nigeria by (Augustine and Nnabuchi, 2009). Other researchers investigated the monthly average clearness index and the sunshine duration for Iseyin in the southwest region of Nigeria. The clearness index, which is a fraction of the solar radiation at the top of the atmosphere that reaches the city of Iseyin varied between 0.34 in August and 0.65 in November, with an annual average of 0.53 these findings were part of a research carried out by (Yusuf, 2017) on the characterization of sky conditions using clearness index and relative sunshine duration for Iseyin, Nigeria Similarly, the current research investigates the global solar radiation, sunshine hour distribution and clearness index of Enugu, Port Harcourt and Ikeja respectively.

In a research carried out on the Empirical model for the estimation of global radiation from sunshine duration in Ijebu-Ode in south western Nigeria, it was discovered that the angstrom constants were found to be 0.18 and 0.79 with a correlation of about 89.13 % (Ogunsanwo et al., 2016). The clearness index for the south western Nigeria is given to be 0.59 by another research carried out on the evaluation of clearness index and diffuse ratio of some locations in south western, Nigeria using solar radiation data (Sanusi and Ojo, 2015). This slight difference in the patterns may be attributed to the latitudinal difference that exists between the locations. Hence, the global solar radiation in the locations varied from $12.248 - 20.844 \text{ MJm}^{-2} \text{ day}^{-1}$ in Abeokuta, $12.880 - 21.744 \text{ MJm}^{-2} \text{ day}^{-1}$ in Ado Ekiti, $12.064 - 21.888 \text{ MJm}^{-2} \text{ day}^{-1}$ in Akure, $12.600 - 19.224 \text{ MJm}^{-2} \text{ day}^{-1}$ in Ikeja, $12.960 - 22.916 \text{ MJm}^{-2} \text{ day}^{-1}$ in Ogbomoso, $12.420 - 21.276 \text{ MJm}^{-2} \text{ day}^{-1}$ in Osogbo .

The clearness index (K_t) value ranges between 0.35 – 0.59 (Abeokuta), 0.36 – 0.61 (Ado Ekiti), 0.34 – 0.61 (Akure), 0.32 – 0.48 (Ikeja), 0.39 – 0.61 (Ogbomoso) and 0.34 -0.53 (Osogbo). In Abeokuta, the highest K_t (0.59) was observed in January and December, while the lowest K_t (0.35) occurred in August. In Ado Ekiti, the highest value of K_t (0.613) was observed in January and December, and the lowest value of K_t (0.38) was observed in July. The highest value of K_t (0.61) was observed in Akure in January, while the lowest K_t (0.35) occurred in August. In Ikeja, the highest value of K_t (0.57) was observed in December and the lowest value of K_t (0.38) was in July. In Ogbomoso, the highest value of K_t (0.617) was observed in January and December, and the lowest value of K_t (0.37) was observed in August (Sanusi and Ojo, 2015). In Osogbo, the highest value of K_t (0.60) occurred in January, while the lowest value of K_t (0.34) was observed in August. This indicates that the sky is very clear over Akure, Ado Ekiti, Ogbomoso and Osogbo in south western Nigeria throughout the year except in June to September. This study is aimed at estimating the global solar radiation, sunshine hour distribution and clearness index in three geopolitical regions of southern Nigeria. The model used in this study is the principal Angstrom-PreScott model on which other empirical models such as El – Metwally Model (2005), Bakirci Model (Exponential) (2009), Glower and McCulloch Model (1958) have been built over time for estimating solar radiation using sunshine hour data.

2. Methodology

In this study, the baseline data for the mean monthly global solar radiation (H) and sunshine hours (S) for Port-Harcourt (5.00°N , 6.95°E), Enugu (6.7°N , 7.6°E) and Ikeja (6.58°N , 3.32°E) were obtained from the Nigeria Metrological Agency (NIMET) in Oshodi Lagos, Nigeria over the period from 1996 to 2010.

The regression coefficients, a and b , the monthly average daily global radiation H , the monthly extraterrestrial solar radiation H_0 , the sunset hour angle W_s , the aolar declination angle δ , and the monthly average of the maximum possible daily hours of bright sunshine S_0 ,

$$\left[H, H_0, \frac{H}{H_0}, w_s, S_0, \delta \right]$$

were calculated by means of simulation of the corresponding equations into Java program compatible with netbeans which served as a calculator for the parameters.

a:	0.0	H/Ho:	0.0	d	0.0
b:	0.0	Ws:	0.0	Eo:	0.0
H:	0.0	Kt:	0.0		
Ho:	0.0	So:	0.0		

Figure 1. Number Code generation interface used in the estimation by means of Java scripts.

Graphical analyses were also exploited by plotting graphs of monthly mean estimated and calculated global solar radiation, monthly mean sunshine hour data and yearly mean sunshine hour data.

The original Angstrom-type regression equation relates the monthly average daily radiation to the clear day radiation at any station and the average fraction of possible sunshine hours:

$$\frac{\bar{H}}{\bar{H}_c} = a' + b' \frac{\bar{n}}{\bar{N}} \quad (1)$$

where \bar{H} = the monthly average of daily solar radiation on a horizontal surface

\bar{H}_c = the average clear sky daily solar radiation for the location and month

a', b' = empirical constants

\bar{n} = monthly average daily hours of bright sunshine

\bar{N} = monthly average of the maximum possible daily hours of bright sunshine.

Equation (1) has been modified to be based on extraterrestrial radiation on a horizontal surface rather than on a clear day radiation and was given as equations (2a) and (2b):

$$\frac{H}{H_0} = \left(a + b \frac{S}{S_0} \right) \quad (2a)$$

$$H = H_0 \left(a + b \frac{S}{S_0} \right) \quad (2b)$$

where H_0 is the radiation outside of the atmosphere subject to latitude of the location

$$a = -0.1 + 0.235(\phi) + 0.323 \left(\frac{S}{S_0} \right) \text{ and}$$

$$b = 1.449 - 0.553 \cos(\phi) - 0.694 \left(\frac{S}{S_0} \right)$$

S is the monthly average daily hours of bright sunshine, and S_0 is the monthly average of the maximum possible daily hours of bright sunshine, and ϕ is the latitude of the locations in consideration.

$$S_0 = \frac{2}{15} \omega_s \quad (3)$$

$\frac{H}{H_0}$ gives the clearness index over a particular location and denoted by K_t

$$H_0 = \frac{24 \times 3600 G_{sc}}{\pi} \left[1 + 0.033 \cos \left(\frac{360n}{365} \right) \right] \times \left[\cos \phi \cos \delta \sin \omega_s + \frac{2\pi \omega_s}{360} \sin \phi \sin \delta \right] \quad (4)$$

Where $\omega_s = \cos^{-1}(-\tan \phi \tan \delta)$ and $\delta = 23.45 \sin \left(360 \frac{284 + n}{365} \right)$

3. Statistical Analysis

Mean Bias Error (MBE) helps to calculate the error or the deviation of the calculated values from the measured values, and provides information on long-term performance. A low mean bias error value is desired. A negative value gives the average amount of underestimation in the calculated value.

$$MBE = \frac{1}{n} \sum_{i=1}^n (H_{est} - H_{meas}) \quad (5)$$

The value of Root Mean Square Error is always positive, representing zero in the ideal case. The normalized root mean square error gives information on the short-term performance of the correlations by allowing a term by term comparison of the actual deviation between the predicted and measured values. The smaller the value is, the better the correlation will be (Namrata, 2012).

$$RMSE = \left[\frac{1}{2} \sum_{i=1}^n (H_{est} - H_{meas})^2 \right]^{1/2} \quad (6)$$

The Mean Percentage Error is one of the measures used to evaluate forecasts using forecast errors. A forecast error is defined as the actual observation minus forecast. The mean percentage error is the average or mean of all the percentage errors. A percentage error between -10 % and +10 % is considered acceptable (Muzathik et al., 2011).

$$MPE(\%) = \frac{1}{n} \sum_{i=1}^n \left(\frac{H_{est} - H_{meas}}{H_{meas}} \right) \times 100 \quad (7)$$

The majority of the equations used in this study were taken from (Duffie and Beckman, 2013).

4. Results and Discussion

Tables 1, 2, and 3 show the estimated monthly global solar radiation, Angstrom coefficient, sunshine hour, and clearness index for each station in the study.

Table 1. Estimated monthly global solar radiation, Angstrom coefficient, Sunshine hour and Clearness index for Port-Harcourt

Month	Mean Sunshine Hour S	H_{est} ($MJm^{-2}day^{-1}$)	Mean Anomaly	H_{meas} ($MJm^{-2}day^{-1}$)	a	b	$\frac{S}{S_0}$	K_t
JAN	4.55	13.40	-1.67	13.40	0.039	0.112	0.387	0.474
FEB	4.52	16.90	1.83	15.30	0.037	0.112	0.382	0.468
MAR	3.94	16.10	1.03	14.10	0.020	0.116	0.328	0.402
APR	4.50	15.80	0.73	13.70	0.034	0.138	0.372	0.456
MAY	4.90	15.30	0.23	12.90	0.043	0.113	0.400	0.490
JUN	3.19	15.10	0.03	11.50	0.018	0.121	0.260	0.313
JUL	2.24	13.80	-1.27	7.90	0.026	0.126	0.183	0.205
AUG	2.38	12.30	-2.77	8.80	0.022	0.125	0.196	0.224
SEP	2.93	14.30	-0.77	9.10	0.007	0.122	0.244	0.291
OCT	3.87	14.80	-0.27	10.20	0.019	0.116	0.325	0.399
NOV	4.79	17.10	2.03	11.50	0.457	0.110	0.407	0.497
DEC	5.53	15.90	0.83	12.80	0.066	0.106	0.472	0.569

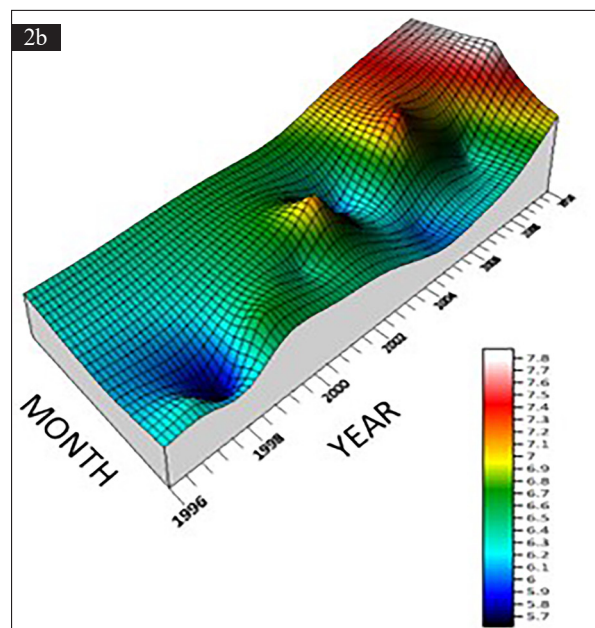
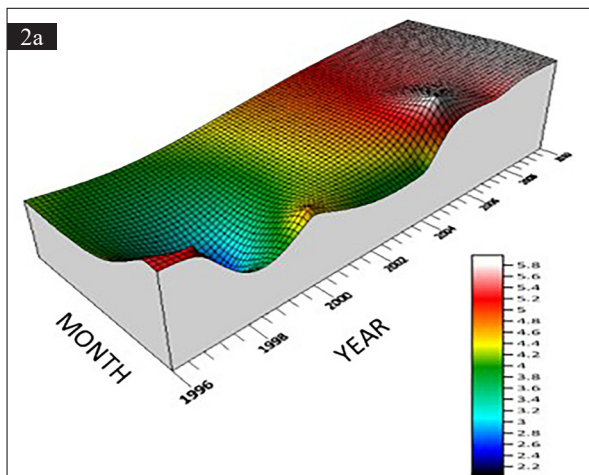
Table 2. Estimated monthly global solar radiation, Angstrom coefficient, Sunshine hour and Clearness index for Enugu

Month	Mean Sunshine Hour S	H_{est} ($MJm^{-2}day^{-1}$)	Mean Anomaly	H_{meas} ($MJm^{-2}day^{-1}$)	a	b	$\frac{S}{S_0}$	K_t
JAN	6.45	13.9	-0.54	14.27	0.300	0.520	0.553	0.588
FEB	6.58	15.4	0.96	15.89	0.301	0.517	0.557	0.590
MAR	6.02	16.6	2.16	15.30	0.283	0.557	0.500	0.561
APR	6.15	14.7	0.26	14.39	0.285	0.553	0.506	0.561
MAY	6.30	15.3	0.86	14.70	0.286	0.549	0.513	0.565
JUN	5.10	14.1	-0.34	13.62	0.255	0.618	0.412	0.568
JUL	3.78	12.5	-1.94	11.62	0.221	0.689	0.309	0.435
AUG	3.77	11.3	-3.14	11.12	0.221	0.689	0.309	0.434
SEP	4.20	13.1	-1.34	13.00	0.234	0.662	0.349	0.465
OCT	5.64	14.7	0.26	14.34	0.275	0.574	0.476	0.548
NOV	7.08	16.7	2.26	15.71	0.316	0.484	0.605	0.610
DEC	6.98	15.0	0.56	15.13	0.315	0.487	0.600	0.608

Table 3. Estimated monthly global solar radiation, Angstrom coefficient, Sunshine hour and Clearness index for Ikeja

Month	Mean Sunshine Hour S	H_{est} ($MJm^{-2}day^{-1}$)	Mean Anomaly	H_{meas} ($MJm^{-2}day^{-1}$)	a	b	$\frac{S}{S_0}$	K_t
JAN	5.86	10.80	0.77	10.76	0.275	0.575	0.502	0.56
FEB	6.54	10.80	0.77	12.34	0.292	0.538	0.555	0.59
MAR	5.82	12.80	2.77	13.06	0.269	0.588	0.483	0.55
APR	5.64	13.10	3.07	13.29	0.263	0.601	0.464	0.54
MAY	5.82	12.70	2.67	11.94	0.265	0.595	0.472	0.54
JUN	3.71	11.20	1.17	10.28	0.209	0.715	0.299	0.42
JUL	2.68	7.60	-2.43	8.140	0.183	0.773	0.217	0.35
AUG	3.12	5.10	-4.93	7.35	0.195	0.746	0.256	0.38
SEP	3.86	6.90	-3.13	8.95	0.217	0.700	0.321	0.44
OCT	5.24	8.50	-1.53	10.32	0.256	0.616	0.443	0.52
NOV	6.28	10.20	0.17	11.80	0.286	0.550	0.537	0.58
DEC	6.36	10.70	0.67	12.13	0.290	0.543	0.548	0.58

Figs 2a, 2b, and 2c show the yearly averages mean monthly sunshine hour distribution, mean monthly variation in Sunshine hour, and the mean yearly variation for sunshine hour for the three different stations in the study from 1996 to 2010. In each case, the sunshine hour varies from 2.68 hours to 7.8 hours.



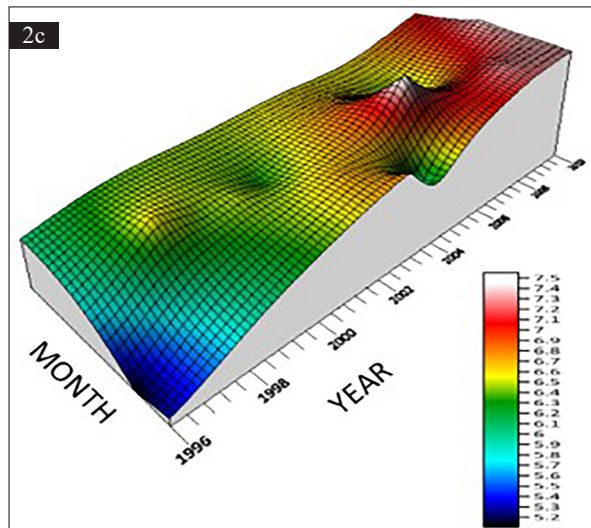


Figure 2. Plots of (a) Distribution of Sunshine Hour for Port-Harcourt, (b) Distribution of Sunshine Hour for Enugu, (c) Distribution of Sunshine Hour for Ikeja.

Fig 2a shows Port-Harcourt with the minimum value of sunshine hour for this study with values ranging from 2.2 to 5.8 maximum values for sunshine hour. The years 2005, 2006, 2007, 2008, 2009, and 2010 have the highest value for sunshine hour with February of 2006 as highest for the whole period of study as seen by the monthly distribution along the z axis and the yearly distribution along the x-axis. The month of January of 1996 also showed a high value of sunshine hour, while the month of February 1999 showed a very low value of 2.2 average sunshine hours as in Fig 2a. From the distribution, the green colour code (3 to 4.2 sunshine hours) is seen to dominate the period from 1996 to 2004, while 2005 to 2010 is on the high side. The Early part of 1996 showed a low sunshine hour measurement as shown by Fig 1b with the distribution of sunshine hour for Enugu improving along the year 2002 up to 2010 for which the study is carried out. January for the following years of 2005, 2006, 2007, 2008, 2009, and 2010 in Enugu showed values of sunshine hour as 7.0 to 7.8 compared to 5.2 to 5.8 sunshine hours for 1996 to 1998. The year 2010 showed a favourable distribution of sunshine hour throughout the year. Fig 2c shows the distribution of sunshine hour for Ikeja. To a large extent the distribution of sunshine hour ranges from 5.7 to 6.1 hours. The month of October to December 2005, October to December 2008, and April to December 2010 showed higher values of 7.1 to 7.8 hours of sunshine duration as shown for Ikeja. Fig 2c shows that the minimum value of sunshine hour was recorded in the month of February 1998.

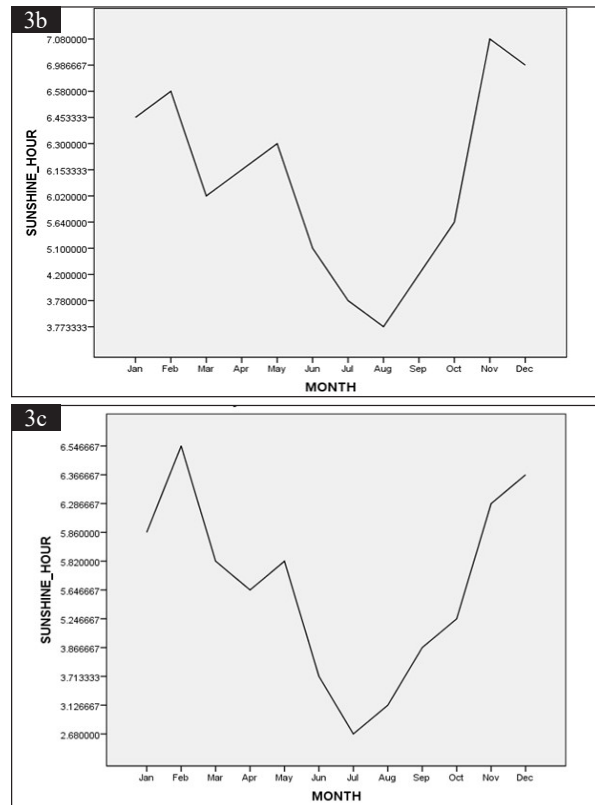
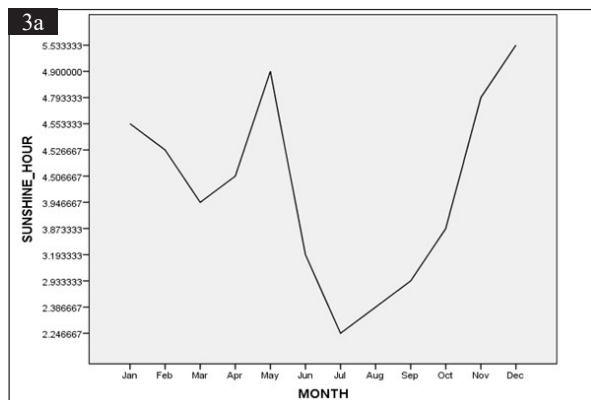


Figure 3. Plots of (a) Mean monthly variation in sunshine hour for Port-Harcourt, (b) Mean monthly variation in sunshine hour for Enugu, (c) Mean monthly variation in sunshine hour for Ikeja.

Fig 3a shows that December has the mean highest sunshine hour. The notable south-southern city of Nigeria has its lowest sunshine in July. December is associated with little or no rainfall whereby making clouds over this station thin and allowing for high sunshine hour reaching Port-Harcourt during the Month. The months of June, July, September and October would be noticed to have low sunshine duration in Port-Harcourt. This is as a result of the raining season which is associated with a heavy cloud cover and hence, little sunshine recordings are gotten as rainfall could take hours of the day during these months. The mean monthly sunshine hour for Enugu happens to be highest in the month of November, and the lowest in the month of August as reported by Fig 3b. The maximum average rainfall for Enugu falls in the Month of August which explains the fall in the number of possible sunshine hours for this location. The month of August for Ikeja happens to be the month with the lowest mean sunshine hour recorded for the fifteen-year study period of 1996 to 2010 as shown in Fig 3c. These can be associated with heavy rainfall in the area during the Month, thereby reducing the sunshine hour due to more absorption, reflection or scattering of solar radiation over Ikeja in this Month. Fig 3 is characterised by a significant fall in the sunshine hour in the months of June, July, August, and September. This fall is predominantly noticed in the month of July and August. This significant fall can be associated with the August break (period of heavy rainfall) in Nigeria. Port-Harcourt has the month of July characterised by low sunshine hours from 1996 to 2010 according to Fig 3a which formed a pattern of sunshine hour distribution for this region (south-southern) of Nigeria.

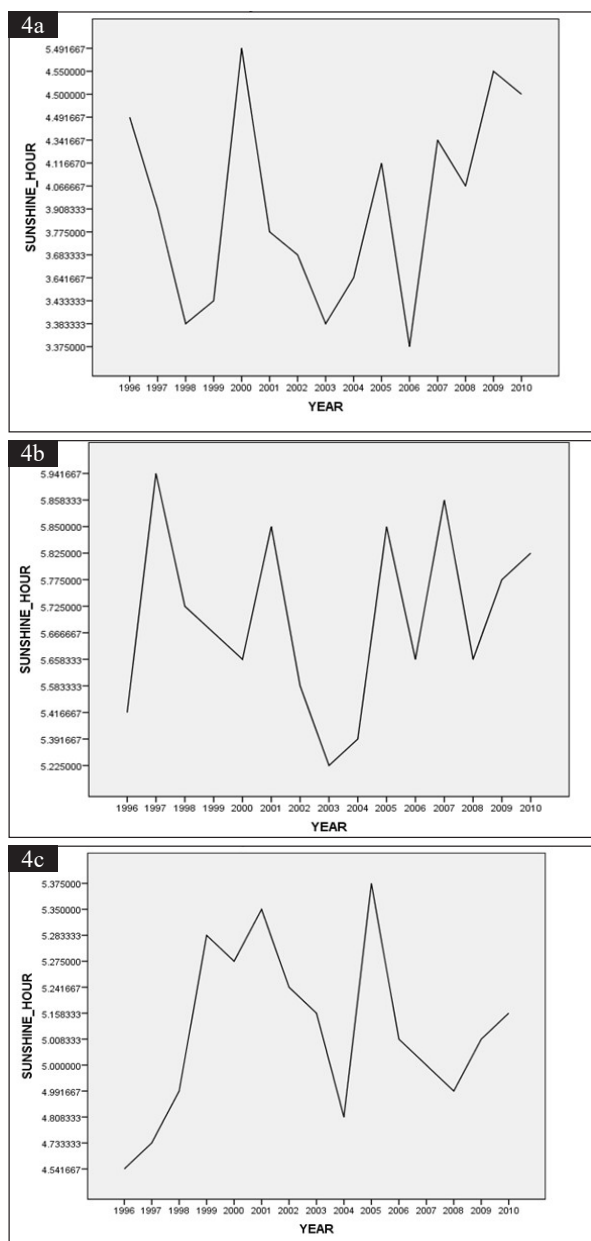


Figure 4. Plots of (a) Mean yearly variation in Sunshine Hour for Port-Harcourt, (b) Mean yearly variation in Sunshine Hour for Enugu, (c) Mean yearly variation for Sunshine Hour in Ikeja.

The yearly estimation of mean sunshine hour for Port-Harcourt reported by Fig 4a shows that the year 2000 has the highest value of sunshine hour, while the years 1998 and 2003 have the same sunshine values and happen to have the lowest sunshine hour for this station. This could be associated with rainfall, humidity, and cloud cover over this location for the various years. For the years 1998 and 2003, the average rainfall recorded was 214.09mm and 208.46mm respectively compared with the value of 166.19mm for average rainfall in year 2000. The value for the average rainfall for 2000 explains why the year had high sunshine duration for this location. According to Fig 4b, the year 2003 had the least sunshine hour recorded between 1996 and 2010, while 1997 can be seen to have the highest value of sunshine hour in Enugu. The years 2003 and 2004 are characterised by an average rainfall of 205.6mm and 171.9mm respectively compared with 147.5mm average rainfall in 1997. This clearly shows that the years 2003 and 2004 should normally have low sunshine

duration as days in this year have abundant rainfall. The year 2005 was very favourable for Ikeja for recording the highest sunshine hour under the width band of the study. With the year 1996 having the lowest sunshine hour, Ikeja also had a major drop in 2004 as seen in Fig 4c.

The graphs of the correlation between the measured and estimated global solar radiation for the various stations in the study were plotted and shown in Fig 5. This representation shows the degree of agreement and variation between the measured and the estimated values of global solar radiation for these stations. Fig 5 shows the various values (measured and estimated) for each month of the year. Generally, the months of June, July, August and September have considerably low values of global solar radiation which can be attributed to the raining season in Nigeria which is characterised by thick cloud covers.

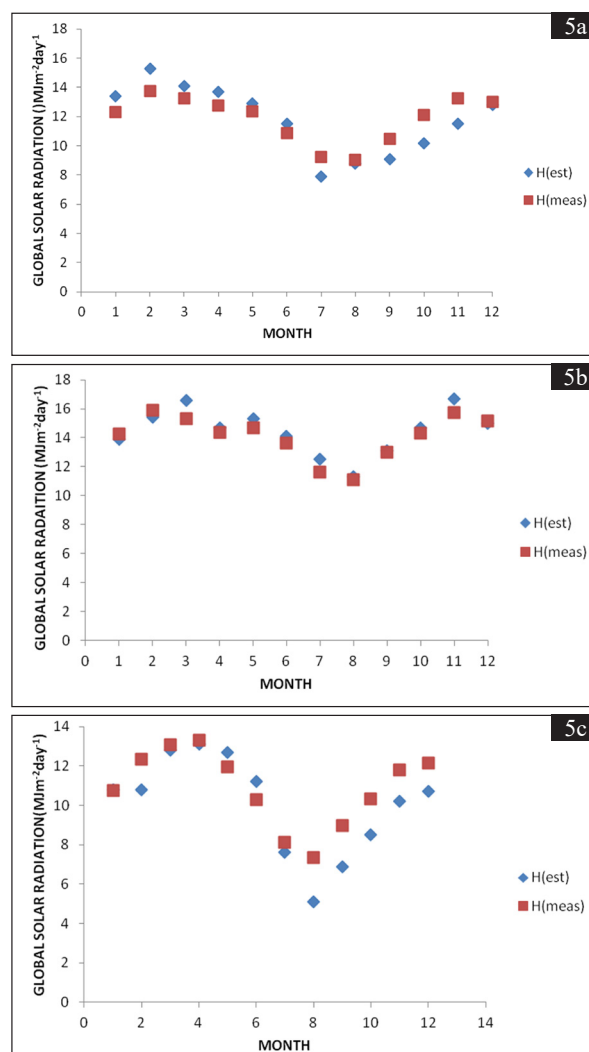


Figure 5. Plots of (a) Correlation between estimated global solar radiation and measured global solar radiation for Port-Harcourt (b) Correlation between estimated global solar radiation and measured global solar radiation for Enugu (c) Correlation between estimated global solar radiation and measured global solar radiation for Ikeja.

Fig 5a shows a correlation of 0.88 between the measured and estimated values of global solar radiation in Port-Harcourt. The 0.88 value for correlation makes the angstroms constants good estimates for finding values of global solar radiation in Port-Harcourt and the nearby cities with similar latitude and sunshine duration. The correlation also serves as a means

of checking the correctness of the values of the angstrom constants in relation to the estimation of global solar radiation for this station. In Fig 5b, the 0.94 value for correlation between the measured and estimated values of global solar radiation in Enugu makes the angstroms constants estimated in this study for Enugu good estimates for finding values of global solar radiation in Enugu and the nearby cities with similar latitude and sunshine duration. The correlation also serves as a means of checking the correctness of the values of the angstrom constants in relation to the estimation of global solar radiation for Enugu. For Ikeja (South-Western Nigeria), the correlation between the measured and the estimated values of global solar radiation was found to be 0.91 which makes the results of the current study regarding the estimated solar radiation very good estimates as shown in fig 5c.

Statistical Test Results

Mean Bias Error (MBE) helps to calculate the error or the deviation of the calculated values from the measured values, and provides information on long-term performance. A low mean bias error value is desired. A negative value gives the average amount of underestimation in the calculated value.

Table 4. Statistical Error result presentation

STATION	$H_{est} (MJm^{-2}day^{-1})$	$H_{meas} (MJm^{-2}day^{-1})$	MBE	RMSE	MPE (%)
PORT-HARCOURT	11.76667	11.87000	-0.0589	0.0730	0.43
ENUGU	14.44167	14.09277	0.1744	0.2467	1.23
IKEJA	10.03333	10.86722	-0.4169	0.5896	3.83

Table 5. Clearness index for different locations of study

Station	$K_t (Max)$	$K_t (Min)$	K_t
PORT-HARCOURT	0.4902	0.2053	0.3992
ENUGU	0.6101	0.4350	0.5447
IKEJA	0.5915	0.3511	0.5087

The clearness index for the south southern part of Nigeria was estimated to be 0.399 in this study which agrees strongly with that of Augustine and Nnabuchi in their research which investigates the clearness index using the cities of Calabar and Port-Harcourt in 2009 in the south southern Nigeria which was found to be 0.40.[9]

The monthly average of Angstrom Constants for Port-Harcourt, Enugu, and Ikeja were estimated to be 0.07 and 0.12; 0.27 and 0.58; 0.25 and 0.63, respectively. The values of 0.23 and 0.68 were Angstrom constants obtained for Enugu by [10] and agree with the values of 0.27 and 0.575 recorded in this study.

5. Conclusions

The trend of global solar radiation, sunshine hour, and clearness index were investigated in this study. The results obtained in this research clearly indicate the importance of developing empirical models for estimating global solar radiation reaching a particular geographical location. The Angstrom Prescott type model presented can also be used to predict the global solar radiation of nearby cities with a latitude, climate, vegetation, elevation and topography similar to those of Enugu.

The results obtained from this research clearly show that the level of sunshine hour distribution and clearness index in Enugu are sufficiently adequate to support solar energy application in this geographical location, and can, therefore, be utilized in the evaluations of their design and performance.

References

- Augustine, C., and Nnabuchi, M. (2009). Correlation of cloudiness index with clearness index for four selected cities in Nigeria. *The Pacific Journal of Science and Technology*, 10(2): 568–573. Retrieved from http://www.akamaiuniversity.us/PJST10_2_568.pdf
- Aweda, F., Akinpelu, J., Falaiye, O., Adegboye, J.O. (2016). Temperature Performance Evaluation of Parabolic Dishes Covered With Different Materials in Iwo, Nigeria. *Osun State, Nigeria: Department of Physics and Solar Energy, Bowen University, Iwo. Nigerian Journal of Basic and Applied Science*, 24(1): 90–97.
- Duffie, J.A., and Beckman, W.A. (2013). *Solar Engineering of Thermal Processes (Fourth)*. Hoboken, New Jersey, Canada: John Wiley and Sons, Inc., Hoboken, New Jersey.
- Elekalachi, C.I., Nwokoye, A.O.C., Ezenwa, I.A., Okoli, N.L. (2016). Estimation of Global Solar Radiation from Monthly Mean Sunshine Hour Data in Some Cities in South Eastern Zone of Nigeria. *Physics Journal*, 2(2): 96–103.
- Gana, N.N., and Akpootu, D.O. (2013). Estimation of global solar radiation using four sunshine based models in Kebbi, North-Western, Nigeria. *Advances in Science Research*, 4(5): 409–421.
- Innocent, A.J., Jacob, O.E., Chibuzo, G.C., James, I., Odeh, D.O. (2015). Estimation of Global Solar Radiation in Gusau, Nigeria. *International Journal of Research in Engineering and Technology*, 3(2): 27–32.
- Islahi, A., Shakil, S., Hamed, M. (2015). Hottel's Clear Day Model for a typical arid city - Jeddah. *International Journal of Engineering Science Invention*, 4(6): 32–37.
- Mojarrad, F., Fathnia, A., Rajae, S. (2015). The Estimation of Receiving Solar Radiation at Earth's Surface in Kermanshah Province. *Arid Regions Geography Studies*, 5(19).
- Muzathik, A.M., Nik, W.B.W., Ibrahim, M.Z., K.B. Samo, K. Sopian and Alghoul M.A., (2011). Daily global solar radiation estimate based on sunshine hours. *International Journal of Mechanical and Materials Engineering (IJMME)*, 6(1): 75–80.
- Namrata, K. (2012). Estimation of Global and Diffuse Solar Radiation for Jamshedpur, Jharkhand, India, 2(1): 44–47.
- Ogunsanwo, F.O., Adepitan, J.O., Ozebo, V.C., Ayanda, J. (2016). Empirical model for estimation of global radiation from sunshine duration of Ijebu-Ode. *International Journal of Physical Sciences*, 11(3): 32–39. <https://doi.org/10.5897/IJPS2015.4422>
- Okonkwo, G. N. (2014). Relationship between Global Solar Radiation and Sunshine Hour Duration for Bida in Nigeria. *International Journal of Renewable and Sustainable Energy*, 3(2): 43–46. <https://doi.org/10.11648/j.ijrse.20140302.12>
- Sanusi, Y.K., and Abisoye, S.G. (2013). Estimation of Diffuse Solar Radiation in Lagos. In *2nd International Conference on Chemical, Environment and Biological Sciences* (pp. 6–9). Lagos.
- Sanusi, Y.K., and Ojo, A.M.O. (2015). Evaluation of Clearness Index and Diffuse Ratio of Some Locations In South Western, Nigeria using Solar Radiation Data. *IOSR Journal of Applied Physics*, 7(5), 45–51. <https://doi.org/10.9790/4861-07524551>
- Sunday, E., Agbasi, O., Samuel, N. (2016). Modelling and Estimating Photosynthetically Active Radiation from Measured Global Solar Radiation at Calabar, Nigeria. *Physical Science International Journal*, 12(2), 1–12. <https://doi.org/10.9734/PSIJ/2016/28446>
- Yusuf, A. (2017). Characterization of sky conditions using clearness index and relative sunshine duration for Iseyin, Nigeria. *International Journal of Physical Sciences Research*, 1(1), 53–60.

Assessment of Heavy Metal Pollution in the Sediments of the Lower Litani River Basin, Lebanon

Nada Nehme¹, Chaden Haidar¹, Walaa Diab¹, Khaled Tarawneh^{2*}, Frédéric Villieras³

¹ Lebanese University, Faculty of Agriculture and Veterinary Medicine, Beirut-Lebanon.

² Amman Arab University, Faculty of Engineering, Amman, Jordan.

³ Laboratoire Interdisciplinaire Des Environments Continentaux (LIEC), Université de Lorraine Nancy, France.

Received 12 January 2019; Accepted 5 March, 2019

Abstract

Concentrations of eight heavy metals (Cu, Fe, Cd, Mn, Cr, Zn, Ni, and Pb) were determined in this study to evaluate their levels and spatial distribution in sediments from the Lower Litani River Basin (LLRB) in six sites, during the dry seasons for the period from 2011 to 2012. Consensus-based sediments quality guidelines of Wisconsin Department of Natural Resources were applied to assess metal contamination in these sediments. The range of the measured concentrations in the total sediments were determined for dry weights to the total sediments. The samples were characterized by a set of cation exchange capacity, granulometric, X-Ray diffraction (XRD) and Fourier Transformed Infrared Spectroscopy (FTIR). Pearson's correlation was also performed in this study to compare and determine the correlation between heavy metals in these sediments. Geo-accumulation (Igeo) index, Contamination Factor (Cf), and contamination degree (Cd) were also applied to assess the level of contamination in these sites. The results of this study show that the concentrations of Pb and Fe are high in the sites S5 and S6, and the values of Cr and Ni are high in site S6. All of the investigated sites are characterized by a moderate to a highly-polluted range of contamination, with the degree of contamination increasing during the dry season.

© 2019 Jordan Journal of Earth and Environmental Sciences. All rights reserved

Keywords: Lebanon, Litani, sediments, granulometric, heavy metals, pollution.

1. Introduction

Heavy metals in the environment may accumulate to toxic levels without visible signs. The accumulation of the trace metals occurs in the upper sediments of an aquatic environment by biological and geochemical mechanisms. They can become toxic to the sediments, organisms and fish, resulting in death, reduced growth, or in impaired reproduction and lower species diversity (Praveena et al., 2007). This may occur naturally from normal geological processes such as weathering and the leaching of rocks or due to increased urban and industrial activities, agricultural practices, exploration and exploitation of natural resources (Ajayi and Osibanjo, 1981). Hence, trace metals may be used as sensitive indicators for the monitoring of the changes in the water environment (Iwashita and Shimamura, 2003).

The anthropogenic sources are mainly associated with industrial and domestic effluents, urban storm, runoff, landfills, the mining of coal, atmospheric sources and inputs from rural areas (Biney et al., 1994). The nutrition requirements of heavy elements differ substantially among species or elements, and the optimum ranges of concentrations are generally narrow given the fact that heavy elements exhibit extreme toxicity even at trace levels (Nicolau et al., 2006). Exposure to heavy metals has been linked to several human diseases such as development retardation or malformation, kidney damage, cancer, abortion. It also has been said to have effects on intelligence and behavior, and may even lead to death in cases of exposure to very high concentrations. The degree of particulate heavy-metal pollution can be evaluated in terms of the geochemical background of the element value in a

drainage network, normally obtained in the headwater region without anthropogenic influences, according to Salomons and Forstner (1984), using an Igeo-accumulation index (Müller 1979; Simonovski et al., 2003; Audry et al., 2004; Yan et al. 2007).

2. Study Area

2.1. Description of the Study Area

The discharge of the Lower Litani River varies across seasons, and also according to different localities, where the average annual discharge is about 360 million m³ (LRA, 1999). There are eighteen measuring stations along the lower Litani river course. In this study, four stations are included along the investigated river course. They are situated from north to south as: Qelia, Gandourieh, Khardali and Qasmieh. The average discharge from these stations is 31.7, 224.2, 227.5 and 176.3 Mm³, respectively.

In addition to water pollution by nutrients and bacteria, the heavy-metal content in sediments has become one of the most important problems, because of its toxic effect even at minor concentrations. This is the case in the Litani River, the largest of its type in Lebanon with a basin area of about 2180 km² and a length exceeding 174 km.

The Litani River is divided into two sub-basins with its upper basin stretching from the north of the Bekaa plain to the Qaraaoun dam, where a lake (8km²) exists. Its lower sub-basin extends from the dam along Qelia Village down to the Qasmieh where it outlets into the sea north to Tyre city (Fig. 1-A and Fig. 1-B). The river water in the lower basin is used mainly for irrigation proposes, particularly in highly agricultural areas (Khoury et al., 2006).

* Corresponding author e-mail: khtarawneh62@yahoo.com

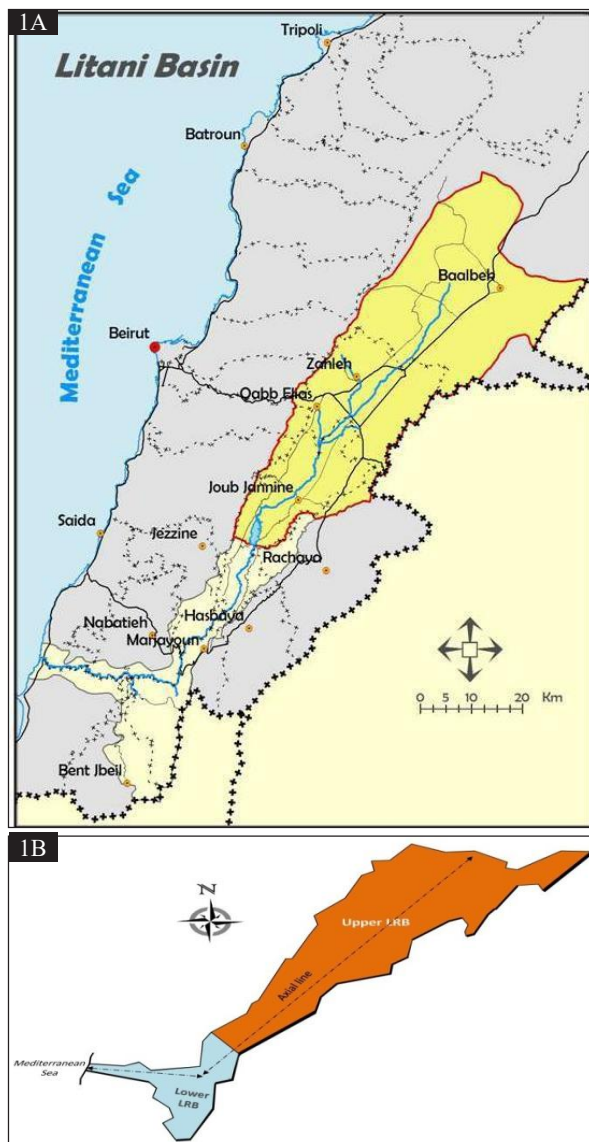


Figure 1. A: Map of Litani river basin location in Lebanon (BAMAS, 2005). B: Schematic figure for the LRB with its axial line (Shaban et al., 2018).

According to Beydoun (1988), the eastern Mediterranean basin, including Lebanon, represents a terrain mass for the unstable tectonic shelf of the Middle East Region, which is affected by plate tectonic movements of the Dead Sea Rift System, and has its extension forming the Bekaa Plain. Therefore, the folded mountain ranges with uplifted blocks created the three elongated and parallel physiographic units of Lebanon (Mount-Lebanon, Anti-Lebanon, and Bekaa Plain).

The Bekaa depression (wide plain), where the LRB is extended, is almost a graben structure located between the two uplifted mountain chains. The western side of the graben structure is marked by a well-defined fault boundary (i.e., Yammounh Fault). Beydoun (1972) described the eastern side of this graben as a sharp flexure, in place, partly formed by en-echelon faults. The exposed stratigraphic rock sequence among the LRB is similar to the one representing the entire sequence of Lebanon. It reveals rocks from Middle Jurassic up to the quaternary deposits. This stratigraphic rock sequence shows sedimentation in a marine environment until the Middle Eocene, with carbonate rocks building up the largest part of the stratigraphic column separated by continental clastic rocks

at the Lower Cretaceous and some intercalated volcanic rocks up to the Pliocene.

Several aspects of rock deformations exist in the LRB. They are considered as complicated as the geological structures, notably because the area of concern is affected by the presence of the Yammounh Fault, which is characterized by lateral displacement, accompanied by diagonal sliding of the adjacent rock formations. The orientation of the LRB is mainly controlled by the presence of the extension of the Yammounh Fault and the Serghaya Fault along the western and eastern sides of the Bekaa Plain, respectively (Fig. 2). As a result of these two major faults, however, several secondary fault systems, with different scales and magnitude, are developed and sometimes with diagonal/or lateral displacement. However, the existing faults, among the LRB in the southern part are different from those in the Bekaa area, and they are often of the wrench type. These faults cut for several tens of kilometers from outside the Litani catchment and almost terminate into the sea (Shaban et al., 2018). In the LRB, there are many other aspects of rock deformation, including small and moderate-scale faults, folding flexures structures, which are often accompanied by intensive fissuring and jointing systems. Additionally, sharp dips of bedding planes exist in several localities (Shaban et al., 2018). Karstification is well pronounced among the carbonate rocks in the LRB. These are on surface karsts, with special emphasis on sinkholes. In addition, subsurface karst is well-developed, including the cavities, conduits, and galleries, which are characterized by water transport for long distances and water that creates many karstic springs, such as the springs of Berdaouni, Anjar, Yammounh and Khayrat (Shaban et al., 2018).

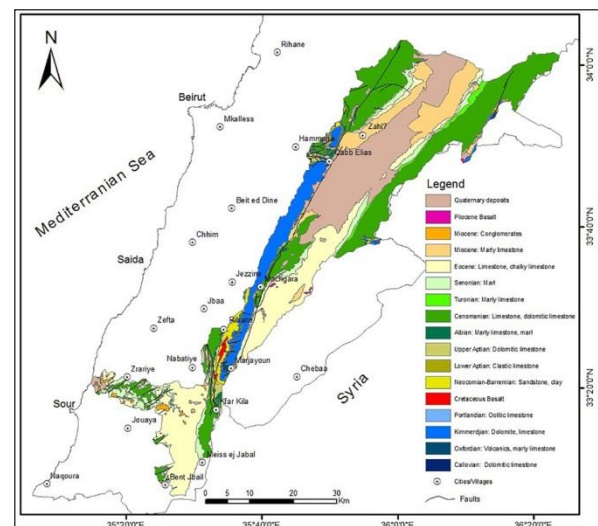


Figure 2. Geological map of Litani River Basin (Shaban et al., 2018).

The heavy metals were investigated during the dry seasons for the period from 2011 to 2012. During this study, the estimation focuses on how much the sediments are impacted (naturally and anthropogenic) by heavy metals. Pollution levels will be measured as the ratio of the sample metal enrichment above the concentration present in the reference station or materials (Abraham and Parker, 2008; Mediolla et al., 2008).

In this study, the influence of minerals and geochemical characteristics on the natural radiation level of the sediments

were considered; the contamination factor (Cf) or enrichment ratio (ER) and the degree of contamination (Cd) have been used to determine the contamination status of the sediments. The Igeo – accumulation index (Igeo) is used to evaluate the heavy-metal pollution in the sediments and to measure the degree of metal contamination or pollution in terrestrial, aquatic and marine environments (Tijani and Onodera, 2009). The Igeo of a metal in sediments can be calculated by the formula obtained by Mediolla et al., (2008) and Asaah and Abimbola (2005).

The main objective of this study is to analyze heavy- metal concentrations in sediments, and thus to assess their geochemical characteristics in the LLRB by calculating the geo – accumulation index (Igeo) and (Cf) in order to detect their relative distribution and to know the influence of mineral content using XRD and FTIR on the geochemical characterization and the level of contamination in the river using multivariate analysis.

3. Sampling and Analytical Techniques

3.1. Sample Collection

The sediment samples were collected from six sites along the LLRB as shown in Figure 3. Coordinates and the distribution of the main activity for each site are illustrated in Table 1. Approximately 2 kg of sediment were collected from

each site at the sediment – water interface (i.e. surface river sediments) using polyethylene bags. The bed sediments from the LLRB were collected by scooping up 10 cm of the bed sediments, 10 m away from the riverbank at the point, where the water samples were taken, using anti-rust scoops. The sediments were naturally dried at room temperature ($25^{\circ}\text{C} \pm 2$) in the laboratory prior to analysis.

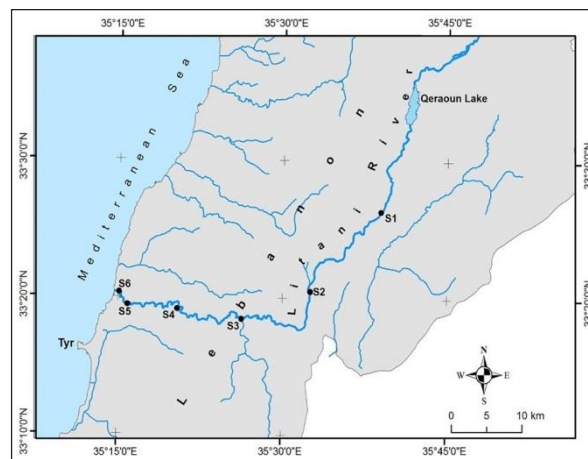


Figure 3. The Lower Litani River Basin (LLRB) shows the sample locations.

Table 1. Location of the sediment samples in the LLRB.

Sampling site	Latitude	Longitude	Other activities
S1= Qelia	33°26'21"N	35°38'55"E	Quarry site and Touristic zones. There are many pumping stations.
S2= Kardali	33°20'34"N	33°32'34"E	Agriculture and touristic zones.
S3=Kaekaeyat eljiser	33°18'31"N	35°26'18"E	Interfered touristic and agricultural zones, near small village
S4=Tair flsaiy	33°19'0"N	35°20'27"E	Touristic zone.
S5=Abouabdellah	33°19'26"N	35°15'50"E	Vegetated sites with citrus trees
S6= Qasmieh	33°20'22"N	35°15'04"E	Road with high traffic is in the proximity of the site. There is an irrigation canal and an agricultural land of banana.

3.2. Sediments' Metal Digestion

The concentrations of Pb, Cd, Fe, Mn, Cr, Cu, Ni, and Zn were measured using the Inductively Coupled Plasma – Optical Emission Spectrometry (ICP-OES) with Ultra Sonic Nebulizer (USN) (model: Perkin Elmer optima 3000). The samples were filtered by a membrane filter of a pore size of $0.45\mu\text{m}$ before analyses using Standard Methods (APHA, 1995). The samples were digested using microwave digestion techniques (Siaka et al., 1998) in which 0.5 g of each sample was placed in Teflon vessel with 5ml HNO_3 (65 %), 2ml HF (40 %), and 2ml H_2O_2 (30 %) using a microwave digestion system (model: MILESTONE mls-1200 mega). An aliquot of the filtration of the samples was taken (about 100ml). Digestion solutions were measured for the total heavy metals using ICP-OES (APHA, 1995). The extraction method was used to analyze the total metal concentrations by atomic absorption Spectrophotometer. Blanks containing all the components except sediments were analyzed to determine background interferences. All of the measurements were performed in triplicate and their average values were reported.

3.3. pH, TDS and EC Analysis

Approximately 10g of the air-dried sediments was suspended in 50mL of deionized water and manually agitated

for five minutes. The suspension was allowed to rest for about one hour with occasional shaking until the pH, TDS and EC were measured.

3.4. CEC, XDR and FTIR Measurements

Cation-Exchange Capacity was measured after exchange with cobalt hexamine ($\text{Co}(\text{NH}_3)_6 \text{Cl}_3$) and the dosage of its residual concentration in the equilibrium solution (Mantin, 1969; Morel, 1957). An amount of 1.5g of the samples was dispersed and shaken during two hours at 30°C in a 30mL of cobalt hexamine solution. The samples were then centrifuged for one hour at 46.251g. The supernatants were analyzed on a UV-Visible spectrophotometer, using a Cobalt absorption band at 472nm to derive CEC from the residual concentrations in Cobalt hexamine. Measurements were always carried out in duplicate to check for reproducibility.

The sediment samples were analyzed by XRD using 1g of a randomly-oriented powder, put on a rotating sample holder, and leveled with a glass slice to obtain a flat surface. XRD were also acquired using Zincite (ZnO) as internal standard. In the latter case, the samples were first mixed with 0.111g of ZnO and ground in an agate mortar for five minutes. XRD patterns were collected on a D8 Advance Bruker AXS diffractometer equipped with a Lynx Eye fast

linear detector using Cobalt K radiation ($R=0.17903$ nm) at 35 kV and 45 mA. Intensities were recorded from 3 to 64° with a 0.035° using a three-second counting time per step. Data reduction and analysis were performed with the EVA software (DIFFRAC plus from Bruker) and diffraction peaks were identified by comparing them with the powder diffraction files.

FTIR spectra were collected on the bulk powder samples mixed with KBr as a transparent matrix. Diffuse reflectance Fourier transform infrared spectra were recorded on a Bruker IFS-55 spectrometer in the range from 4,000 to 600cm^{-1} with a resolution of 2cm^{-1} . Spectra were obtained from the average of 200 scans collected over two minutes. Data reduction and analysis were performed using OPUS program (Russel, 1987).

3.5. Chemical and Statistical Analysis

The concentrations of Cu, Fe, Cd, Mg, Zn, Pb, Al, Ba, Ni, Mn, Ag, and Cr were measured using the Atomic Absorption Spectrophotometric method, (Spectrophotometer (RAYLEICH – MFX-210) with an air/acetylene flame and background correction and a deuterium lamp to remove any solid impurities before testing (AOAC 974.27). The samples were filtered through a membrane filter of a pore size of $0.45\mu\text{m}$ before analyses using Standard Methods (APHA, 1992).

Bed sediment samples were digested using microwave digestion techniques as reported by Made Siaka et al. (1998), where 0.25gm of the samples was placed in a Teflon vessel with 5 ml HNO_3 (65 %), 2ml HF (40 %) and 2ml H_2O_2 (30 %) using the Microwave digestion system (model: MILESTONE mls- 200mega). An aliquot of the filtration of the samples was taken (about 100 ml). Digestion solutions were measured for the total heavy metals using ICP-OES (APHA, 1995). Correlation coefficients were calculated between all pairs of measured elements' concentrations.

Multivariate statistical analyses such as Pearson Correlation Analysis, the degree of dispersion distribution of different metals were performed. Pearson's correlation analysis was carried out using SPSS, 2007. Cluster analysis (CA) is a multivariate technique, whose primary purpose is to classify the objects of the system into categories or clusters based on their similarities.

3.6. Granulometric Analysis:

The samples were also tested to measure their granulometric fractions, such as the content of the sand, silt and clay using an ASTM sieve. About 100g of the sediments were taken for separation of sand, silt and clay fractions by wet sieving.

4. Results and Discussion

4.1. Physical Parameters and CEC Analysis of the Sediments

The tested sediments of LLRB have pH values ranging between 7.4 and 8.09, which is slightly alkaline (Table2), the alkaline nature is mainly pronounced in sediments in LLRB during the dry season, and this can be attributed to heavy metal enrichment, EC and TDS are related together and they increased, EC ranged from 204 to $707\mu\text{s}/\text{cm}$, and TDS varies between 94 and $352\text{ mg}/\text{l}$.

4.2. CEC (Cation Exchange Capacity)

The CEC is defined as the ability of a particle to change its positive bases with the environment in which the particle interacts (Huu et al., 2010). Cations have the ability to be exchanged for another positively-charged ion from the surfaces of clay minerals and organic matter.

Knowledge of the CEC in the soil can be of great importance in order to characterize the soil content of ionic elements, concentration of clay and mud, texture, degree of compaction, levels of porosity and permeability. It also provides information about possible needs for fertilizers and correction of the soil acidity. CEC is an important soil property, and the high CEC may indicate clay content, low permeability and internal drainage, due to the high soil compaction. Low levels of CEC may indicate a soil texture ranging from clayey-sandy to sandy, with variable grain sizes and high permeability. Soils with low CEC can be attributed to the higher content of clay minerals and organic matter.

Table 2 shows that the CEC is decreased in the sites as this order ($\text{S6} > \text{S2} > \text{S1} > \text{S5} > \text{S3} > \text{S4}$), and this identifies the agricultural activity present substantially in the sites S6, S2 and S5. Generally, soils with high CEC have a color ranging from dark brown to black, due to the high lignin content of the organic matter. Soil with a high organic matter content are not necessarily productive in agriculture.

Table 2. Physical parameters of sediments and CEC

Sites	S1	S2	S3	S4	S5	S6
pH	4.7	7.8	8.09	8.04	8.04	7.4
TDS (mg/l)	183	155	94	104	150	352
EC 1500 ($\mu\text{s}/\text{cm}$)	364	313	186	204	300	707
CEC (meq/100g)	13.54	16.94	4.11	3.56	11.38	17.32

4.3. Heavy Metal Distribution in Sediments

The results obtained from the total metal concentrations for each sample are shown in Tables 3 and 4. Metal content ranged according to the following intervals, whereas 1.5-17.5 mg/kg for Cu; 890-40477 mg/kg for Fe; 5-37.5 mg/kg for Cd; 5-90 mg/kg for Zn; 2.5-45 mg/kg for Pb; 4-24.5 mg/kg for Ni; 3.5-55 mg/kg; Cr and 4-451 mg/kg for Mn. This allows for the arrangement of the metals from the higher to lower mean content in this area as follow: $\text{Fe} > \text{Zn} > \text{Cr} > \text{Pb} > \text{Cd} > \text{Ni} > \text{Cu}$.

The results show that the concentration of Cd is higher in all sediments, whereas the contents of Fe, Pb, Ni were higher in the sites 5 and 6 due to the steep slopping and deposition of pollutants in these sites. The sediments are contaminated with Cd, Fe, Zn, Cr, Pb, Ni and Cr exceeding the standard levels.

Standard (CBSQG), is considered harmful for farming and human health, and commonly, Cd is believed to affect human health. The retention of alarming exchangeable levels of cadmium may be related to the leaching of soil particles containing certain types of fungicides employed through agricultural practices. This argument is valid, because the sediments containing cadmium were collected during the rainy seasons, a period in which erosion and leaching processes are often observed.

Table 3. Concentration of heavy metals in the investigated sites (mg /Kg dry weight)

Site	Concentration of heavy metals							
	Cu	Fe	Cd	Mn	Cr	Zn	Ni	Pb
1	16	890	5	416	3.5	90	4	17
2	2.5	8049	16	4	12.5	47	4	3.5
3	1.5	17559	36	190	12.5	5	4.5	23.5
4	2.5	11460	26	39	26.5	43	11	2.5
5	3.5	35070	32	261	25	13.5	7	45
6	17.5	40477	37.5	451	55	71.5	24.5	143
Range	1.5-17.5	890-40477	5-37.5	4-451	3.5-55	5-90	4-24.5	2.5- 45
Minum	1.5	890	5	4	3.5	5	4	2.5
Maximum	17.5	40477	37.5	451	55	90	24.5	45
Average	9.5	40.9	21.2	227.5	29.2	50	14.2	25

Table 4. Consensus-Based Sediment Quality Guidelines of Wisconsin (CBSQG, 2003)

Metal	Consensus-Based Sediment Value (mg/kg)
Cu	32
Fe	20000
Cd	0.99
Mn	460
Cr	43
Zn	120
Ni	23
Pb	36

Pearson's correlation coefficient matrix among the selected heavy metals is presented in Table 5. Significant correlations between the contaminants of Cu and Zn ($r = 0.84$), Cd and Cr ($r = 0.68$), Zn and Cu ($r = 0.84$), Pb and Mn ($r = 0.71$), Cr and Fe ($r = 0.83$), Ni and Cr ($r = 0.96$), almost

indicate the similar source of the inputs. Fe and Cr ($r=0.83$), presumed that the association of the two elements originates from a common source and also during the transportation or deposition processes, and this also confirms the results in Table 5.

The major source of Zn is the domestic and municipal wastes followed by dumping and atmospheric deposition. The positive correlation in Cd and Cr may be attributed to the industrial origin of these metals. According to the samples' location, the elevated levels of "urban" elements Cu, Zn, Mn, Pb and Ni are associated with the direct supply of untreated urban and industrial wastes. Thus, it can be concluded that the anthropogenic inputs resulted in the exceeding levels of Cu, and Zn. These metals were also positively-correlated with the percentage of quartz, dolomite, calcite and kaolinite in these sediments. Calcite and dolomite were significant positively correlated ($r = 0.98$), because they represent the widespread rocks nearby the study area.

Table 5. Correlation matrix between heavy metals in the sediment samples of the LLRB

Matrix	Cu	Fe	Cd	Zn	Pb	Ni	Mn	Cr	pH	Ec	TDS	CEC	Q	K	C	D
Cu	1.00															
Fe	0.17	1.00														
Cd	-0.21	0.82	1.00													
Zn	0.84	-0.27	-0.60	1.00												
Pb	0.37	0.87	0.58	-0.15	1.00											
Ni	0.55	0.70	0.55	0.32	0.47	1.00										
Mn	0.87	0.40	0.06	0.49	0.71	0.45	1.00									
Cr	0.36	0.83	0.68	0.10	0.55	0.96	0.33	1.00								
pH	-0.78	-0.38	-0.05	-0.68	-0.31	-0.76	-0.54	-0.65	1.00							
EC	0.82	0.56	0.18	0.60	0.54	0.82	0.69	0.74	-0.96	1.00						
TDS	0.83	0.56	0.18	0.60	0.55	0.82	0.70	0.74	-0.96	1.00	1.00					
CEC	0.59	0.20	-0.28	0.58	0.27	0.29	0.40	0.25	-0.79	0.74	0.74	1.00				
Q	0.77	-0.06	-0.58	0.77	0.24	0.12	0.65	0.00	-0.43	0.49	0.49	0.60	1.00			
K	0.94	0.30	-0.18	0.73	0.55	0.50	0.90	0.37	-0.68	0.79	0.79	0.62	0.87	1.00		
C	0.90	0.46	-0.03	0.61	0.69	0.55	0.92	0.46	-0.68	0.82	0.82	0.62	0.80	0.98	1.00	
D	0.89	0.50	0.03	0.58	0.71	0.59	0.93	0.50	-0.69	0.84	0.84	0.60	0.77	0.97	1.00	1.00

Q = quartz; C = calcite; D = dolomite; K = kaolinite

4.4. Mineralogical characterization

4.4.1. XRD Analysis

Six samples were performed by using XRD. The results show that the major minerals are quartz and calcite, whereas kaolinite and dolomite are secondary minerals (Fig. 4).

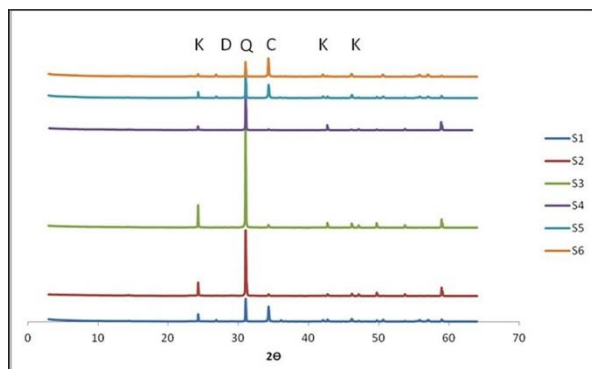


Figure 4. XRD results of major and secondary minerals of the sediments in LLRB. (Q=Quartz, C=Calcite, K=Kaolinite, D=Dolomite)

According to Figure 4, quartz is the dominant mineral in all of the tested sites particularly in site S3; while calcite occurs in site S1, and then leached in water and again reappears in sites S5 and S6. Calcite is decreased from the first two sites in the downstream of the river and the percentage of quartz is increased. This is due to the leaching of CaCO_3 by the agricultural soils. This soil is originated from sandy deposits, justifying the expressive contents of quartz in the sediments. The presence of kaolinite could be explained by the chemical weathering of primary minerals such as feldspar (KAlSi_3O_8), which makes up the solid phase of all soils as described in Figure 4. Dolomite is present with low concentrations and occurs as a result of small leaching processes.

4.4.2. Granulometric Analysis

Granulometric analysis has been carried out for the sake of this study. The contents of sand, silt, and clay are shown in

Figure 5. The particle size distribution in the samples indicated that sand is the main constituent in all of the samples with an average of 66.5 %, whereas the average of silt content is 16.3 %, and clay reaches up to 17 %. The particle size constituent in the samples is sand; the least important constituent is clay except in site S6. The results show that the content of sand is important, and the content of silt and clay are gradually increased in sites S1, S5 and S6. Hence, this figure shows that the important content of the clay is present in site S6 with a high value of CEC due to the high clay content.

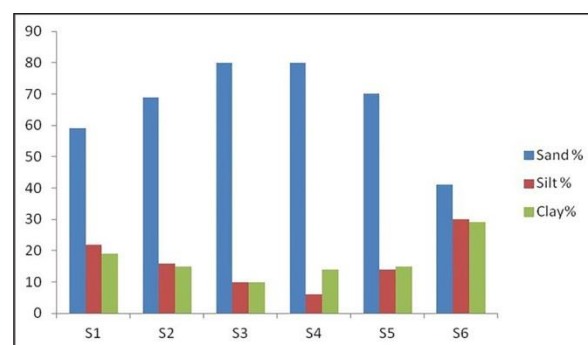


Figure 5. Sand, silt and clay contents in the investigated sites of the LLRB.

4.4.3. FTIR Analysis Frequencies

Minerals of quartz, calcite, kaolinite, dolomite and other components such as feldspar, organic compound are identified by comparing the observed wave numbers with the available literature (Ramasamy et al., 2009; Russell, 1987; Farmer, 1974). The relative distribution of major minerals can be quantified by calculating the extinction coefficient for the characteristic peaks of quartz and kaolinite at around 464cm^{-1} and 1032cm^{-1} , respectively, and for calcite at 1428cm^{-1} . In general, the amount of montmorillonite is less than kaolinite and less than quartz and calcite. The results of FTIR show the presence of montmorillonite and feldspar and some organic compounds (Table 6).

Table 6. Observed absorption wave numbers and corresponding minerals from FTIR spectra.

Mineral	Site	Observed wave (cm-1)
Quartz: SiO_2	S1- S2 S3- S4- S5-S6	468.6 -790-465.7-784
		461.8-690,4 -463.7-691.4-1081
		469.5-707-790
Kaolinite: $\text{Al}_2\text{Si}_2\text{O}_5(\text{OH})_4$	S1-S2- S3 S4- S5- S6	3694-3620- 3695-3621
Calcite: CaCO_3	S1-S2-S3-S4-S5-S6	1424-1425-1426-1427- 1428-1429
Montmorillonite $(\text{Na}, \text{Ca})_{0.3}(\text{Al}, \text{Mg})_2\text{Si}_4\text{O}_{10}(\text{OH})_2 \cdot n\text{H}_2\text{O}$	S1,S4,S5,S4	875.5-877.4-873.6-873.6
Feldspar $(\text{KAlSi}_3\text{O}_8)$	S1,S2,S6	536-533-536
Organic compounds	S1,S5	2872.4-2514.7-2872.4

5. Assessment of Heavy Metal Contamination

5.1. Contamination Factor (Cf)

In this study, the Contamination Factor (Cf) or enrichment ratio (ER) and the degree of contamination (Cd) were used to determine the contamination level of the sediments by applying the following equations:

$$CF = \frac{(Cn)\text{Concentration of the heavy metal in the soil sample}}{(Bn)\text{Background concentration of the same metal}}$$

Or $CF = C_{\text{metal}} / C_{\text{background}}$

$EF = (\text{Metal}/RE)_{\text{Soil}} / (\text{Metal}/RE)_{\text{Background}}$

The maximum contamination factor was found in site S3, where the degree of contaminations is 38.88. The contamination factor $CF > 6$ indicates a very high contamination found in all sites: Site 3 by Cd, S5 by Cd, Fe, Ni, Pb and S6 by Cd, Pb, Fe and Mn. In all stations, the contamination factor was $(Cf) > 6$ for all of the tested heavy metals. The mean values of Cf are found: Cd: 25.67 (high contamination); Ni: 3.7 (Low contamination). On the basis of the mean values of

Cf sediments are enriched with metals in the following order: Cd> Pb >Fe > Ni (Table 7).

Table 7. Contamination factor (Cf) values for the sediments of the LLRB

Sample site	Cf									Contamination factor and level of contamination (Hakanson, 1980)	
	(Cu)	(Fe)	(Cd)	(Mn)	(Cr)	(Zn)	(Ni)	(Pb)	Cf	Contamination fact	Contamination Level
S1	0.5	0.045	5.05	0.90	0.08	0.75	0.17	0.47	7.42	Cf < 1	low
S2	0.08	0.4	16.17	0.86	0.29	0.39	0.17	0.1	17.20	1 ≤ Cf < 3	moderate
S3	0.05	0.88	36.37	0.41	0.29	0.04	0.19	0.65	38.88	3 ≤ Cf < 6	Considerable
S4	0.08	0.57	26.26	0.08	0.62	0.36	0.48	0.07	28.52	Cf > 6	Very high
S5	0.11	1.75	32.32	0.57	0.58	0.11	0.30	1.25	36.99		
S6	0.55	2.02	37.88	0.98	1.28	0.59	1.06	3.97	48.33		
Mean	0.23	0.94	25.67	0.49	0.52	0.37	3.7	1.08	29.55		

5.2. Assessment of Sediments According to Geoaccumulation index (I_{geo})

A common criterion to evaluate the heavy metal pollution in the sediments is the geo-accumulation index (I_{geo}), which was originally defined by Müller (1979). It is applied to determine metal contamination in the sediments by comparing current concentrations with pre-industrial levels and can be calculated by the following equation (Müller, 1979):

$$I_{geo} = \log_2 \left[\frac{C_n}{1.5 B_n} \right]$$

where C_n is the concentration of element 'n' and B_n is the geochemical background value. In this study, it was

considered that B_n =world surface rock average given by Martin and Meybeck (1979). The factor 1.5 is incorporated in the relationship to account for possible variation in the background data due to lithologic effects. The geo-accumulation index (I_{geo}) scale consists of seven grades (0-6) ranging from unpolluted to highly-polluted (Table 8). According to the Müller scale, the calculated results of I_{geo} values indicate that the Cd sediment quality is reported as very strongly polluted, I_{geo} is strongly to very strongly polluted in the sites: S3, S4, S5 and S6 ($I_{geo}>6$) for all stations, while as for the sites S1 and S2, sediment quality was recorded as moderately polluted ($I_{geo}>2$).

Table 8. I_{geo} –accumulation index values for the sediment samples of the LLRB.

Sample site	I_{geo}									Grade standards for I_{geo} (Rahman et al., 2012)		
	Cu	Fe	Cd	Mn	Cr	Zn	Ni	Pb	I_{geo}	I_{geo}	Class	Sediment quality
S 1	0.10	8.9×10^{-3}	1.01	0.18	0.01	0.15	0.03	0.09	1.58	<0	0	Practically Uncontaminated
S2	0.01	0.08	3.24	1.74×10^{-3}	0.06	0.08	0.03	0.02	3.52	>0-1	1	Uncontaminated to moderate
S3	9.40×10^{-3}	0.18	7.23	0.08	0.06	8.36×10^{-3}	0.04	0.13	7.73	>1-2	2	Moderate
S4	0.02	0.12	5.27	0.02	0.12	0.07	0.09	0.01	5.72	>2-3	3	Moderate to strong
S5	0.02	0.35	6.49	0.11	0.12	0.02	0.06	0.25	7.42	>3-4	4	Strong
S6	0.11	0.41	7.60	0.19	0.26	0.12	0.21	0.78	9.68	>4-6	6	Strong to very strong

6. Conclusions

Heavy metal contamination in the Litani river sediments was assessed in this study. The results reveal significant information about heavy metal contents and physical characteristics of sediments from different sampling sites of the LLRB. The characteristics of quality sediment show that the sediments of LLRB have pH ranging between 7.4 and 8.09, which is slightly alkaline. EC ranged from 204 to 707 $\mu\text{S}/\text{cm}$, while TDS varies from 94 to 352 mg/l.

The CEC is decreased in the sites in the following order S6>S2>S1>S5>S3>S4), which indicates that agricultural

activities are present substantially in sites S6, S2 and S5.

The results obtained from the sediment analysis regarding the total metal concentrations for each site allowing for the arrangement of metals from a higher to a lower mean content as follows: Fe > Mn > Zn>Cr>Pb>Ni>Cr. The results show that the concentration of Cd was higher in all sediments which can affect human health and the environment as well, whereas the Fe, Pb and Ni were higher in sites 5 and 6 due to the higher slopping and deposition of pollutants in the tested sites as a result of waste water infiltration into the soil.

In order to evaluate the minerals in the sediments for the

collected samples, X-ray diffraction was carried out. XRD revealed that quartz and calcite are major minerals, whereas kaolinite and dolomite are minor minerals. Quartz is dominant in all of the selected sites, particularly in site S3, while calcite is present in site S1, and then leached in water and reappears again in sites S5 and S6. Calcite is decreased in the first two sites in the downstream of the river; the percentage of quartz is also increased. This can be attributed to the leaching of CaCO_3 by the agricultural soils.

The FTIR analysis shows that the amount of montmorillonite is less than that of kaolinite and is lesser than quartz and calcite. The results of FTIR shows the presence of montmorillonite and feldspar and some organic compounds. The presence of the solid minerals is related to weathering processes, while the organic materials are related to agricultural additives.

Heavy metal contamination of the sediments was assessed with respect to metal pollution load contamination factor of heavy metal concentration and Igeo-accumulated risk. Based upon the used indices, a proposed priority index (Pindex) was used to rank the utmost contaminated sites.

In the present study, the maximum contamination factor was found in site S3, where the degree of contamination is 38.88. Contamination factor, $C_f > 6$ indicates very high contamination for all sites (S3 with Cd, S5 with Cd, Fe, Ni and Pb and S6 with Cd, Pb, Fe, Mn). In all of the tested sites, there are a contamination factor (C_f) > 6 for all of the tested heavy metals. The mean values of the C_f was found as: Cd: 25.67 (high contamination); Ni: 3.7 (low contamination). On the basis of the mean values of C_f , sediments are enriched by metals in the following order: $\text{Cd} > \text{Pb} > \text{Fe} > \text{Ni}$.

The calculated results of Igeo values indicate that Cd sediments are strongly polluted, Igeo is strongly to very strongly polluted in sites S3, S4, S5 and S6 (i.e. $\text{Igeo} > 6$) for all stations, while as for sites S1 and S2, the sediments' quality were recorded as moderately polluted (i.e. $\text{Igeo} > 2$). It can be argued that the high concentrations of heavy metals across different sites can be related to the industrial waste and agricultural additives. In can be concluded that in addition to the problem of water pollution by nutrients and bacteria, the heavy metal content in the sediments has become one of the most serious problems as well, because of heavy metal toxic effects even at minor concentrations.

Acknowledgment:

The authors would like to thank Dr Amin Shaban from the National Council for Scientific Research in Libanon for his help in this work and his advice. Many thanks for all the colleagues who continuously support our work. Thanks are also extended to anonymous reviewers for their valuable comments.

References

Abraham, G.M.S., and Parker, P.J. (2008). Assessment of heavy metal enrichment factors and the degree of contamination in marine sediment from Tamaki Estuary, Auckland, New Zealand.

Ajayi, S.O., and Osibanjo O. (1981). Pollution studies in Nigerian Rivers. Water quality of some Nigerian rivers. Environ. Pollut. (Series B) 2: 87-95.

APHA (1992). American Public Health Association (APHA). Standard methods for the examination of water and wastewater. Washington, D.C. USA, 18th ed. 536 pp.

APHA (1995). American Public Health Association (APHA). Standard methods for the examination of water and wastewater. Washington, D.C. USA, 19th ed. 698 pp.

Audry, S., Schafer, J., Blanc, G., Jouanneau, J.M. (2004). Fifty-year sedimentary record of heavy metal pollution (Cd, Zn, Cu, Pb) in the Lot River reservoirs (France). Environment. Pollution, 132: 413-426.

Asaah, A.V., and Abimbola, A.F. (2005). Heavy metal concentrations and distribution in surface soils of the Bassa Industrial Zone I, Doula, Cameroon. The Journal for Science and Engineering 31(2A): 147-158.

BAMAS (2005). Litani Water Quality Management Project, P17.

Beydoun, Z. (1972). A new evaluation of the petroleum prospects of Lebanon with special reference to the Pre-Jurassic. 18th Arab Pet. Cong., Algeria, 80(B-3).

Beydoun, Z. (1988). The Middle East: Regional Geology and Petroleum Resources. Scientific Press Ltd., London, 296p.

Biney, C., Amuzu, A.T., Calamari, D., Kaba, N., Mbome, I.L., Naeve, H., Ochumba, P.B.O., Osibanjo, O., Radegonde, V., Saad, M.A.H. (1994). Review of pollution in the African aquatic environment, FAO, Rome.

Farmer, V.C. (1974). Layer silicates. In Infrared Spectra of Minerals, Farmer V.C. ed., Mineralogical Society, London, pp. 331-363.

Huu, H.H., Rudy, S. An Van Damme. (2010). Distribution and contamination status of heavy metals in estuarine sediments near Cau Ong harbor, Ha Long Bay, Vietnam. Geology Belgica 13(1-2): 37-47.

Iwashita, M., and Shimamura, T. (2003). Long-term variations in dissolved trace elements in the Sagami River and its tributaries (upstream area), Japan, The Science of the Total Environment, 312: 167-179.

Khoury, R., Doummar, J., Khawlie, M., Doumit, A. Chaaban, A., Abdallah, C. (2006). Using the Water Resources Model (WRM) for Optimization: the Lebanon Lower Litani River Case Study, WatMed3, Tripoli, Liban, November pp 6.

LRA (1999). Technical Report, Litani River Authority.

Martin, J.M., and Meybeck, M. (1979). Elemental mass balance of material carried by world major rivers, Marine Chemistry 7: 173-206.

Siaka, M., Owens, C.M., Birch, G.F. (1998). Evaluation of Some Digestion Methods for the Determination of Heavy Metals in Sediment Samples by Flame-AAS Analytical Letters, 31(4):703-718, DOI: 10.1080/00032719808001873.

Mediolla, L.L., Domingues, M.C.D., Sandoval, M.R.G. (2008). Environmental Assessment of and Active Tailings Pile in the State of Mexico (Central Mexico). Research Journal of Environmental sciences 2(3): 197-208.

Mantin, I., and Glaeser, R. (1969). Fixation des ions cobaltih examines par les montmorillonites acides. Bull.Groupe Fr. Argiles 12, 188.

Morel, L.R. (1957). Étude expérimentale des phénomènes d'échange sur différents minéraux argileux. Ann. Agr., 8: 5-90.

Müller, G. (1979). Schwermetalle in den sedimenten des rheins-veränderungen seit.Umschav, 79: 133-149.

Nicolau, R., Galera, C.A., Lucas, Y. (2006). Transfer of nutrients and labile metals from the continent to the sea by a small Mediterranean river, Chemosphere, 63: 469-476.

- Praveena, S.M., Radojevic, M., Abdullah, M.H., Avis, A.Z. (2007). Factor-cluster analysis and enrichment study of mangrove sediments – An example from Mengkabong Sabah. *The Malaysian Journal of Analytical Sciences*, 2(2): 421-430.
- Rahman, S., Khanam, D., Adyel, T., Islam, M., Mohammad, A., Akbor, M. (2012). Assessment of heavy metal contamination of agricultural soil around Dhaka Export Processing Zone (DEPZ), Bangladesh: Implication of seasonal processing zone, Bangladesh, *Appl. Sci.*, 2(3): 584-601.
- Ramasamy, V., Rajkumar, P., Ponnusamy, V. (2009). Depth wise analysis of recently excavated Vellar river sediments through FTIR and XRD studies. *Indian Journal of Physics* 83: 1295-1308.
- Russell, J.D. (1987). In: Wilson, M. J.(Ed.), *Infrared Methods—A Hand Book of Determinative Methods in Clay Mineralogy*. Blackie and Son Ltd., NewYork, p. 133.
- Salomons, W. and Forstner, U. (1984). *Metals in the hydrocycle*. Berlin, Springer-Verlag, p 349.
- Shaban, A., Faour, G., Awad, M. (2018). *Physical Characteristics and Water Resources of Litani River Basin. The litani River, Lebanon: An assessment and current challenges*, Springer- ISBN 978-3-319-76299-9. pp. 43-47.
- Simonovski, J., Owens, C., Birch, G. (2003). Heavy metals in sediments of the upper Hawkesbury-Nepean river. *Austral Geograph. Studies*, 41(2): 196-207.
- Tijani, M.N., and Onodera, S. (2009). Hydrogeochemical Assessment of metals contamination in an urban drainage system: A case study of Osogbo township, SW-Nigeria. *J. Water Resource and Protection* 3: 164-173.
- CBSQG. (2003). *Consensus based sediment quality guidelines*. Wisconsin Department of Natural Resources. Recommendations for use and application. Department of interior, Washington D.C. 20240, p:17.
- Yan J.P., Yong H., and Huang, H. (2007). Characteristics of heavy metals and their evaluation in sediments from middle and lower reaches of the Huaihe river. *J. China Univ. Mining Techno.*, 17(3):414-417.

Road Rehabilitation Using Mobile Mapping System and Building Information Model

Omar Al-Bayari

AL-Balqa' Applied University, Department of Surveying and Geomatics Engineering, Al-Salt, Jordan

Received 30 January 2019; Accepted 21 March, 2019

Abstract

Road rehabilitation is considered as one of the most important infrastructure projects worldwide. Road rehabilitation requires the Building Information Model (BIM) at different project phases. The most important step in road rehabilitation is building the existing 3D model to be used in the project phases. BIM will help to follow the advancement of the reconstruction field operations, and control the quality and performance of the project based on a predefined time schedule and an approved design. The objective of this research is to obtain optimal quality of a 3D model using state of the art technologies. Mobile Mapping System (MMS) and the number of control points will be used to achieve an accurate 3D model. The 3D model will be used as initial data in the BIM. The Scan to BIM process using laser scanning technology for building the road 3D model and connecting it to the BIM, is becoming an essential part of most engineering projects.

© 2019 Jordan Journal of Earth and Environmental Sciences. All rights reserved

Keywords: lidar technology, Building Information Model, Mobile Mapping System, GNSS technology, right of way, Virtual Reference Station.

1. Introduction

Mobile Mapping System (MMS) is becoming a well-known technology for corridor surveying and for the creation of 3D models in most engineering projects. Lately, several researches have discussed the accuracy, capability, and speed of the lidar technology in field surveying (El-Sheimy, 2005; Klaus et al., 2012).

The accuracy of MMS is based on the GNSS technology. Consequently, the integration between different sensors of MMS is affected directly by the quality of the GNSS data which may create some difficulties regarding accuracy (less than 3cm) in the final survey results. This is caused by a GNSS failure due to some obstacles along the roads including trucks, buildings, trees, etc. Integration between different sensors in MMS such as GNSS/IMU and DMI, in addition to the usage of known control points to reach a reliable combined solution that could be used in the road project life cycle (Sairam et al., 2016).

The current research focuses on the quality of MMS data for BIM and the correct methodology to adjust the obtained Lidar Data (point cloud) using some additional classical survey measurements.

1.1. Building an Information Model and a Mobile Mapping System

Presently, there has been an increased interest in using BIM in engineering project life cycles (Design phase, construction phase, and maintenance period). BIM is defined as a process to share and use data during the life-time of a structure including the maintenance period. A BIM is an intelligent 3D model-based process that provides physical and functional characteristics for a facility (Fernandez, 2015).

MMS is considered one of the best methods to create the initial data requirement for Roads BIM based processes. However, a BIM-based process needs a 3D model of a high

quality to be used in the automation process during the construction or maintenance of roads such as using milling machine and asphalt paver (Heikkilä and Martinen, 2013; Schwarzbach, 2014).

The field operations of MMS are not complicated and most of the field work can be done in automatic steps using a good field operation software installed on the system. However, data processing is the most critical issue in MMS in order to get perfect results in a quick and efficient manner (Sairam et al., 2016). Generally, no single solution is used to obtain the final results including feature extraction and a final 3D model. Mostly, more than one software is used to get the desired results of the 3D model and the extracted road features.

There have been many benefits for using MMS or laser scanning in surveying to BIM. The scanning operations bring the real scanned site into office desktop and extract the 3D model and all the required features without going back to the field. It delivers, as well, a wide variety of formats to accommodate the workflow of the BIM model, solid model, 2D cad files, sections etc.

The planning of field works is important for determining the number of missions, number of GNSS reference stations that are needed to complete and cover the ROW of the road, and to define the Level of details (LOD) of every scanned element.

1.2. Quality of Data and Building Information Model Projects

It's well-known that a quality BIM project requires a quality information sysetem. The increase interest in using work machines in road construction and maintenance requires a good quality 3D model of an existing road to be used as a reference model in BIM.

MMS helps create the 3D model for an existing road. However, any created model needs a preprocessing procedure

* Corresponding author e-mail: o.bayari@bau.edu.jo

in order to be of a good quality and enough accuracy to be used in BIM process. This process needs to combine classical topographic surveys, by means of total station measurements, for identified points or cross sections along the roads to adjust the point cloud before extracting the features and creating the 3D Model from the lidar survey data.

Several experiments will be needed to test data quality and define the minimum number of the identified cross sections needed to get a reliable 3D model to be used for BIM.

GNSS trajectory is considered as one of the most important elements of data quality. Thus, in order to have a reliable GNSS solution, the distance between the MMS car and the GNSS reference station should not exceed 10 km in each mission. Moreover, more than one reference station should be used during the field operation to avoid any failure of data.

1.3. Mobile Mapping System Project Workflow

Using MMS in road surveying is not a strait forward technique that can provide a high quality point cloud and a 3D model without using well-known control points along the surveyed corridor. The number of control points or known cross sections depend on many factors such as the requested accuracy and the quality of combined GNSS/INS trajectory (Kennedy et al., 2006; Qian et al., 2017).

Many researchers explained the work flow to get a good quality point cloud using MMS (Soininen, 2012; Yang et al., 2016; Gandolfi et al., 2008; Barbarella et al., 2011; Al-Bayari, 2018). The current research employs the general procedure for GNSS/INS data processing using the Inertial Explorer software from Novatel (Waypoint Products Group, 2018), in addition to using the terrasolid package (terrascan and terramatch), for pointcloud adjustment, processing, and classification (Soininen, 2018). This research also uses the ORBIT software (Orbitgt, 2018) or TopoDot software (TopoDOT, 2018), for data extraction and the exporting of the extracted data to be used in Civil 3D for the BIM process.

The Terramatch software package is used for point cloud pre-processing to correct the drift of the trajectory at locations, where the accuracy of the trajectory solution is weak due to failures in the GNSS signal. A good number of control points are needed in order to achieve accurate results (Soininen, 2018).

2. Case Study: Rehabilitation of Amman-Aqaba Desert Highway

This case study is part of the reconstruction and rehabilitation project of Highway 15 (Amman-Aqaba Deseret Highway). The project involves a complete reconstruction of 220kms of the road, which runs from Queen Alia airport intersection to Maan governorate (Figure 1).

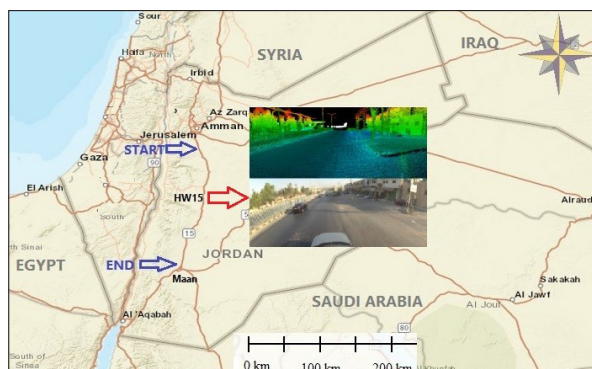


Figure 1. Amman-Aqaba Deseret Highway (Highway 15), in Jordan

The MMS technology for surveying started twenty years ago. Unfortunately, this is the first time for this technology to be used in Jordan. Maverick MMS from Teledyne Optech is used in this pilot project to survey the first section of the Deseret highway (Teledyne Optech, 2017). Figure 2 presents the main component of the Maverick system used in this pilot project.

The quality and testing of MMS results were possible because the whole Highway has been surveyed using highly-accurate surveying techniques in addition to MMS.



Figure 2. Maverick Mobile Mapping System Used for Pilot Project in Jordan

2.1. Highway Surveying Techniques

This research has used a general surveying procedure that guarantees highly-accurate spatial data information for the design and construction phases. This procedure is summarized as follows:

- 1- Establishing a highly-accurate static GNSS traverse network along the road right of way (ROW). The spacing distance between the established points is 500m and is connected with the National Jordanian network.
- 2- The highly-precise geometric leveling of traverse Bench mark points is done using digital level. The accuracy of loop closure is 3mm* $\sqrt{\text{km}}$ (First order class I).
- 3- Surveying of the cross sections every 25m along the Highway using highly-precise Total Station, based on Traverse network (Figure 3).
- 4- Surveying the existing features and terrain points using total Station and the GNSS RTK observation technique (to create a good digital terrain model of the Road ROW).

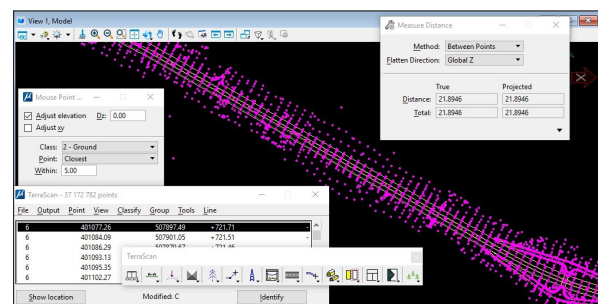


Figure 3. Cross section points measured using Total station every 25m along the Road.

3. Data Processing and Building the 3D Model

Due to high traffic on the road, the surveying of 65kms of the Deseret Highway was done over the period of two days; peak hours were avoided. The total working hours were less than seven hours. Moreover, the road was divided in sessions based on six GNSS reference stations (Three main and three auxiliary stations).

Figure 4 presents the GNSS Reference station used during the MMS surveying. Instead of VRS stations, separate GNSS reference stations were used placed on the same traverse network established by the contractor. This is to avoid any errors in data processing due to datum shift, and to get a better ambiguity resolution in the GNSS data processing, where the baselines do not exceed 10km between the reference stations and MMS.

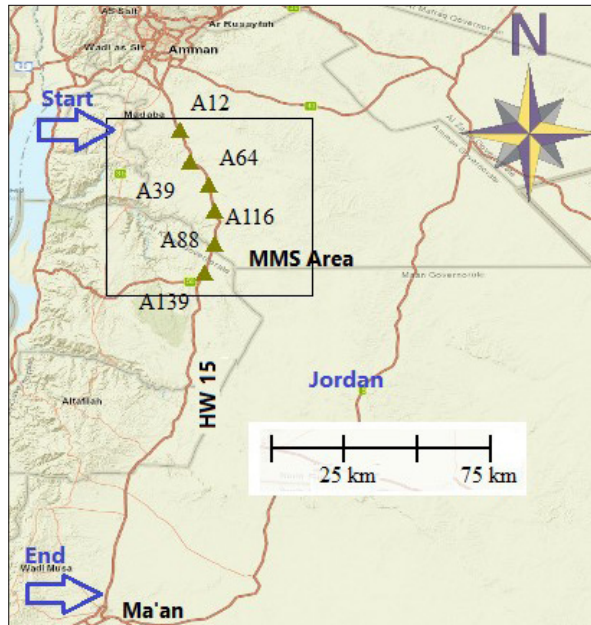


Figure 4. GNSS Reference stations used during the MMS survey.

Data processing of trajectory had been done using the Inertial explorer software package by Novatel to produce a combined GNSS/INS solution and then the Distillery software package was used to process and adjust the trajectory and lidar data and finally to export georeferenced point cloud and images (Figure 5).

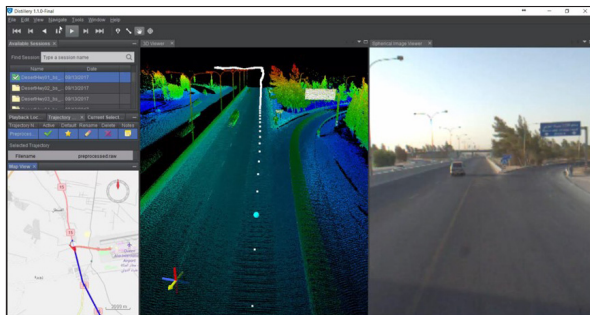


Figure 5. Distillery software for lidar data processing and image visualization

Strip adjustment and matching from different missions were done using Terramatch software package by Terrasolid. Some problems were encountered due to false ambiguity resolution in some places caused by the loss of look of GNSS data (Al Madani et al., 2016). Apparently, the loss of look was caused by heavy traffic of trucks, or when the MMS car passes under steel bridges. Figure 6 presents the difference in different strips due to error in GNSS solution.

The processing of GNSS/INS data using separate reference stations for different missions and adjusting the point cloud using Terramatch can give better results than processing the data using all reference stations and producing one trajectory. This is attributed to the positioning accuracy of

the trajectory, which can vary a lot during one drive mission. Thus, the dominant error source for inaccurate data is that the trajectory positioning will increase using more than one reference station in different missions.

Figure 6 presents the difference in trajectory processed with respect to different reference GNSS stations. The significant differences are just in the height component (1-2cm), but this could produce a larger error in the point cloud and this error is not acceptable for quantity surveying in road rehabilitation and maintenance in BIM process.

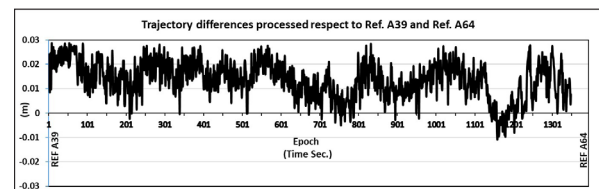


Figure 6. Differences in the Height of trajectory processed using different Reference Stations with a 10km-distance from each other

Terrascan software package provided by Terrasolid company has been used to adjust the point cloud to known points of cross sections. The cross sections have been surveyed using total station every 25m, then the point cloud has been exported for feature extraction to Orbit software (Figure 7) and TopoDOT software package by C3D (Figure 8). Civil 3D software package by Autodesk was used to create the 3D model using extracted features (Figure 9), and to export the final model to BIM software.

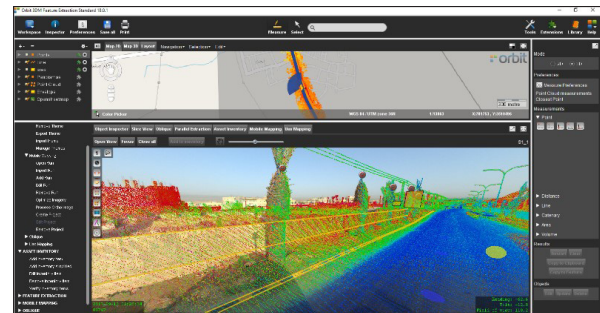


Figure 7. Orbit Software and feature extraction

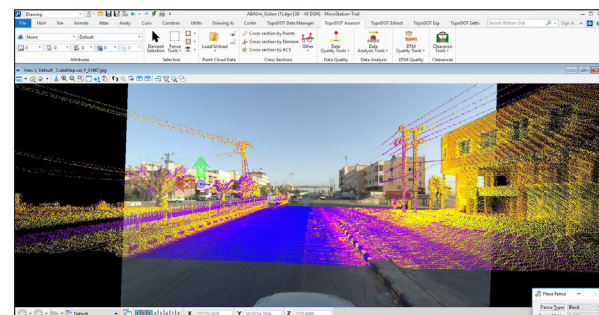


Figure 8. TopoDOT software point cloud overlaid over images

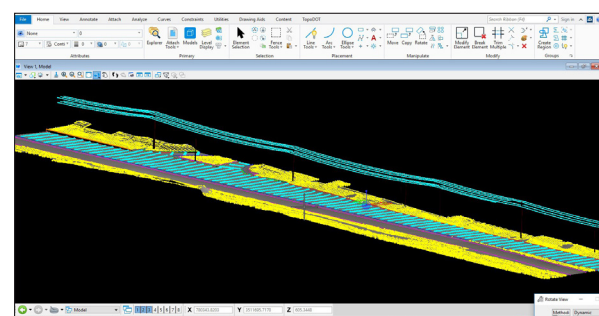


Figure 9. Road extracted features in CAD format

4. Results and Discussion

Several tests have been performed along the road to define the quality of the extracted 3D- model (to be used in the BIM process) and to minimize the effort of control points surveying using classical topographic surveys and/or GNSSRTK observation techniques. The point cloud has been adjusted using different cross sections at different spacing (25m, 50m, 100m, 150m, and 200m). Table 1, Figure 10 and Figure 11, present the differences between point clouds and total station results.

Table 1. Analysis of MMS point cloud and known cross sections measured at different spacing.

Known points Cross Section Spacing	25m	50m	100m	150m	200m
Standard Deviation (m)	0.006	0.007	0.008	0.015	0.026
RMS (m)	0.006	0.007	0.008	0.015	0.026
Min dz (m)	-0.005	-0.007	-0.008	-0.019	-0.028
Max dz (m)	+0.006	+0.007	+0.012	+0.022	+0.027

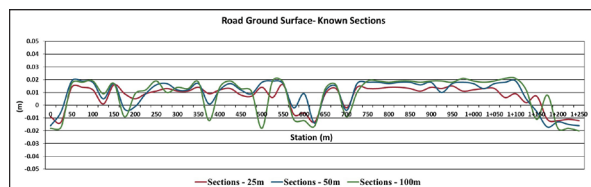


Figure 10. Differences between Ground Road Surface and known points measured at different spacings (25m, 50m, and 100m), road surface match the surface at 25m.

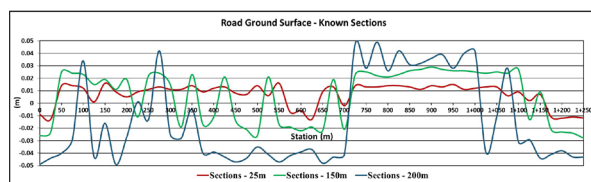


Figure 11. Differences between Ground Road Surface and known points measured at different spacing (25m, 150m, and 200m), road surface match the surface at 25m

Using known cross sections every 100m gives good results and is efficient for adjusting the MMS point clouds to create a reliable and accurate 3D model and road surface that could be used for all road applications in the BIM processes. The created model should be used as initial data model for BIM process, and the easiest way to start utilizing BIM in maintenance is to connect the already existing databank information to geo-spatial locations such as the model created by MMS.

The created Road surface model by MMS permits to perform many analyses related to the road condition such as road surface damage: ruts, cracks, and potholes that will be useful to be integrated in BIM process for maintenance and road rehabilitation:

- 1- Road surface damage analysis: Figure 12 presents damage on the road surface and the field verification using images of the road.
- 2- Cross sections could be created and compared with the designed drawing and calculation of quantities for the needed materials in the construction or rehabilitation phase (Figure 13).
- 3- Feature extraction: point cloud supports the extraction

of all features and objects such as bridges, road signs, electrical poles, etc. Figure 14 presents extracted features and a bridge model created using MMS data.

- 4- Moreover, the Desert road is in the phase of reconstruction, but the MMS survey revealed an urgent need for renewing the asphalt. Therefore, the original 3D model could be thinned and used for creating a new design surface which could be imported into a machine control system and used for resurfacing the road (Schwarzach, 2014).
- 5- Finally, the data allowed an accurate estimation of the quantities of materials needed for the surface renewal (Martinen and Heikkilä, 2015).

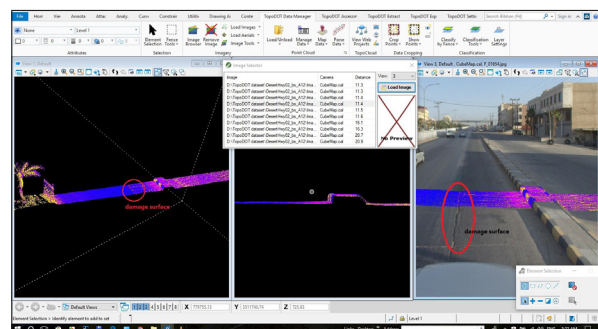


Figure 12. Road surface condition analysis and verification using point cloud and images

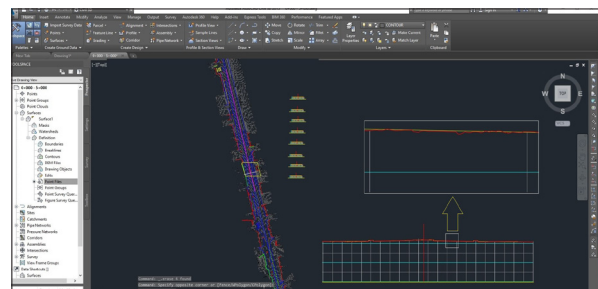


Figure 13. Road surface and Designed cross sections in AutoCAD Civil 3D

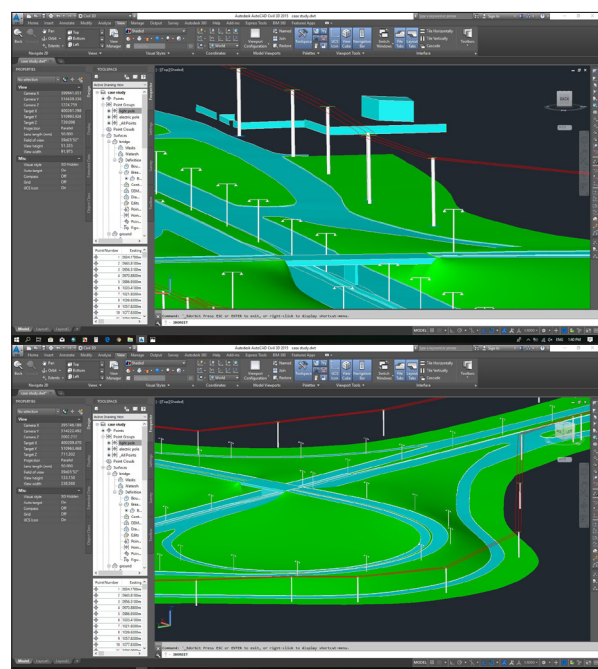


Figure 14. Extracted 3D Model in Civil 3D

5. Conclusions

MMS perhaps constitutes the best technique to create roads 3D model to be used in BIM, but there are important considerations that have to be taken into account during the surveying and data preprocessing phase, and these include:

- 1- Strip matching and adjustment is an essential step in point cloud data pre-processing and it should be done for different missions and different surveying directions as well as for overlapping between different strips and missions.
- 2- To get a reliable precise 3D model to be used in the BIM process, the point cloud for this purpose should be adjusted and corrected with known cross-section points distributed every 100m along the road corridor.
- 3- Processing the GNSS/INS data to create an MMS trajectory should be done based on the nearest GNSS reference station. To avoid corruption in the ambiguity resolution, the processing of data for baselines with more than a 15km-distance between the MMS car and the GNSS reference station must be avoided.
- 4- Finally, the Scan to BIM process in the road project is efficient and accurate to create the initial 3D model to be used in the BIM process, but, often, the office work and production time are relatively long.

References

- Al Madani, S., Sadoun, B., Al Bayari O. (2016). Continuously operating reference station and surveying applications in KSA. *International Journal of Communication Systems*, Volume 29, Issue 6, pp 1046–1056
- Al-Bayari, O. (2018). Mobile mapping systems in civil engineering projects (case studies) *Appl Geomat* (2018). Volume 11, Issue 1, pp 1-13
- Barbarella, M., Gandolfi, S., Meffe, A., Burchi, A. (2011). A Test Field for Mobile Mapping System: design, set up and first test results, *Proceeding of the 7th International Symposium on Mobile Mapping Technology*, 13 – 16 June 2011, Cracow, Poland
- El-Sheimy, N. (2005). An Overview of Mobile Mapping Systems. In *Proceedings of the FIG Working Week 2005 and GSDI-8*, Cairo, Egypt, 2005; pp. 16-21.
- Fernandez D. (2015). National Building Information Model Standard Project Committee, USA) https://www.nationalbimstandard.org/files/NBIMS-US_FactSheet_2015.pdf, (accessed on 17 January 2019)
- Gandolfi, S., Barbarella, M., Ronci, E., Burchi, A. (2008). Close photogrammetry and laser scanning using a mobile mapping system for the high detailed survey of a high density urban area, *The International Archives of the Photogrammetry, Remote Sensing and Spatial Information Sciences* (ISSN: 1682-1750). Part B5, Beijing 3-11 July 2008, Vol. XXXVII, pp. 909-914:
- Heikkilä, R., and Marttinen, M. (2013). Development of BIM based rehabilitation and maintenance process for roads. 10.22260/ISARC2013/0136. <https://doi.org/10.1007/s12518-018-0222-6>
- Kennedy, S.; Hamilton, J.; Martell, H. (2006). Architecture and system performance of SPAN NovAtel's GNSS/INS solution. In *Proceedings of the ION PLANS 2006*, San Diego, CA, USA, 25–27 April 2006; pp. 23–25
- Klaus, P., Schwarz, N., El-Sheimy, N. (2012). Mobile mapping systems-State of the art and future trends. *Int. Arch. Photogramm. Remote Sens. Spat. Inf. Sci.* 2012, 35: 759–768
- Marttinen, M., and Heikkilä, R. (2015). Relative Information Modelling Based Optimization for Asphalt Pavement Renovation. 10.22260/ISARC2015/0048.
- Orbitgt (2018). Generic-Mobile-Mapping, <https://orbitgt.com/wp-content/uploads/2018/10/2018-Generic-Mobile-Mapping-1.pdf> [Accessed 11 November 2018].
- Qian, C.; Liu, H.; Tang, J.; Chen, Y.; Kaartinen, H.; Kukko, A.; Zhu, L.; Liang, X.; Chen, L.; Hyypä, J. (2017). An Integrated GNSS/INS/LiDAR-SLAM Positioning Method for Highly Accurate Forest Stem Mapping. *Remote Sens.* 9(3): 3-16.
- Sairam, N., Nagarajan, S., Ornitz, S. (2016) Development of Mobile Mapping System for 3D Road Asset Inventory, *Sensors (Basel)* 2016 Mar; 16(3): 367. Published online 2016 Mar 12. doi:10.3390/s16030367
- Schwarzbach, F. (2014). Road Maintenance with an MMS - Accurate and Detailed 3D Models Using Mobile Laser Scanning, *GIM International*, Vol. 28(7), July 2014
- Soininen, A. (2012) Mobile Accuracy & Control https://www.terrasolid.com/download/presentations/2012/mobile_accuracy_and_control.pdf; (accessed on 20 Dec. 2018).
- Soininen, A. (2018) Terrasolid software, Available online: <http://www.terrasolid.com/download/tscan.pdf>, (accessed on 20 Dec. 2018), <http://www.terrasolid.com/download/tmatc.pdf> (accessed on 20 Dec. 2018).
- Teledyne Optech, (2017). Maverick Mobile Mapping System. http://info.teledyneoptech.com/acton/attachment/19958/f-02bf/1/-/-/2017-09-19_Optech_Maverick-Spec-Sheet_Eng_web.pdf, [Accessed 15 December 2018].
- TopoDOT (2018). TopoDOT Workflow. https://new.certainty3d.com/workflow/extract/process_section, [Accessed 10 December 2018].
- Waypoint Products Group. (2018). ANovAtel Precise Positioning Product: Inertial Explorer 8.70 User Manual v4, March 2018. <https://www.novatel.com/assets/Documents/Waypoint/Downloads/Inertial-Explorer-User-Manual-870.pdf>
- Yang, B., Liu, Y., Liang, F., Dong, Z. (2016). Using Mobile Laser Scanning Data for Features Extraction of High Accuracy Driving Maps. *Int. Arch. Photogramm. Remote Sens. Spat. Inf. Sci.* 2016; XLI-B3:433–439. doi: 10.5194/isprsarchives-XLI-B3-433-2016.

Development of Irrigation Water Quality Index for Wadi Araba Basin, Southern Jordan

Ali El-Naqa¹ and Amani Abu Al Adas²

¹ Hashemite University, Department of Water Management Environment, Faculty of Natural Resources and Environment, Zarqa, Jordan

² Hashemite University, Department of Earth and Environmental Sciences, Faculty of Natural Resources and Environment, Zarqa, Jordan

Received 17 January 2019; Accepted 4 April, 2019

Abstract

This paper attempts to evaluate the quality of irrigation water regards to potential soil, crop problems and irrigation types for specific use. For this purpose, the Water Quality Index for irrigation (IWQI) was introduced which is a technique that can be used to classify irrigation waters with respect to three suitability classes and three degrees of restriction on use. The objective of this index is to transform complicated water quality data into information that can be utilized by the public. The IWQI was used to identify the irrigation water along Wadi Araba area in southern Jordan. Irrigation water quality was assessed based on salinity hazard, sodium hazard (soluble sodium percentage and sodium adsorption ratio, bicarbonate hazards (residual sodium carbonate), magnesium hazard, permeability index, Kelly's ratio, chloride hazard and boron hazard. The spatial distribution of water quality index (WQI) map has been prepared using ArcGIS 10.2 in which 59.5% of groundwater used for drinking purposes was classified as poor water category, where 75.7% of the water has a medium suitability based on irrigation water quality index. Moreover, the Wilcox's diagram was used for classifying the irrigation water based on the salinity and sodium hazard, where 67.6% of the groundwater have permissible to doubtful irrigation water quality due to the presence of high salinity and low sodium hazard (Class C3S1).

© 2019 Jordan Journal of Earth and Environmental Sciences. All rights reserved

Keywords: Keywords: IWQI, FAO, Hazard maps, Suitability, Alluvial Aquifer, Groundwater.

1. Introduction

In recent decades groundwater became one of the most important natural resources as a result of increasing water demand, decreasing rainfall amount and surface water supplies. It became very essential to find groundwater that has high quantity and good quality to be used for multi-purposes. It is sometimes necessary to analyze all related parameters as a combination rather than focusing on a single isolated parameter. With this objective in mind, the paper focused on the implementation and validation of water quality index based on FAO's criteria in order to assess the water suitability for irrigation purposes.

A water quality index in a simplified concept is a management technique for linking the water quality data into a single value or single status to provide the composite influence of individual water quality parameters on the overall water quality. This study involved the development of a new index called the 'Irrigation Water Quality Index (IWQI)'. The Water Quality Index has been applied to assess the quality of groundwater in the recent years due to its serves the understanding of water quality issues by integrating complex data and generating a score that describes water quality status (khalid, 2011; Rizwan and Singh, 2010). The water quality index (WQI) was calculated for evaluating influence of natural and anthropogenic activities based on several key parameters of groundwater chemistry (Krishna et al., 2014). World Health Organization (2011) standards for drinking water quality have been used to calculate the WQI. To calculate the WQI, the weight has been assigned for the

physico-chemical parameters according to the parameters relative importance in the overall quality of water for drinking water purposes.

The WQI technique was applied to assess the irrigation water quality of based on water quality data in Wadi Araba area. The hydrochemical data representing two periods of sampling (pre- and post-rainfall seasons). This WQI aims to help decision makers in reporting the spatial state of the water quality variations.

The spatial distribution of IWQI index was constructed using the GIS to categorize the irrigation water quality based on the spatial variations of physicochemical quality parameters during pre- and post-rainfall seasons.

2. Description of study area

The study area includes Wadi Araba Basins (North and South) which is considered part of Jordan Rift Valley, and it occupies approximately 5835 km². The northern Wadi Araba catchment extends for about 100 km from the Dead Sea shore southward, with a width of 25 to 30 km and a total area of 3080 km² while southern Wadi Araba catchment extends around 75 km north of the Gulf of Aqaba, with a maximum E-W width of 30 km and total catchment area measures 2756 km², the Alluvial deposits which is the main target aquifer in this study represent approximately 1700 km² which is extend along the western side of the tow sub-basins (Figure 1A). The Wadi Araba catchment area includes the eastern escarpment and highlands where the elevation ranges from 1735 m above sea level at Jabal Al Hisha) to 425 m below sea level in the floor of Wadi Araba south Ghor Es-Safi. (Fig. 1-A). The

* Corresponding author e-mail: elnaqa@hu.edu.jo

wadi floor of the Wadi Araba basin is comprised of alluvial sediments which forms the fresh and brackish groundwater in the uppermost parts of the aquifer (Dames and Moore, 1979).

The recharge to alluvium aquifer comes from precipitation falling on the surrounding mountains in the east and infiltrates in the barren rocks and flows laterally into the fluvial and

alluvial deposits of Quaternary age that covers the wadi floor (El-Naqa and Kuisi 2012). The groundwater flow direction map of Wadi Araba aquifer system is from the foot of the eastern escarpment towards the Wadi Araba floor and from the south to the north, towards the Dead Sea as shown in Fig. 1-B.

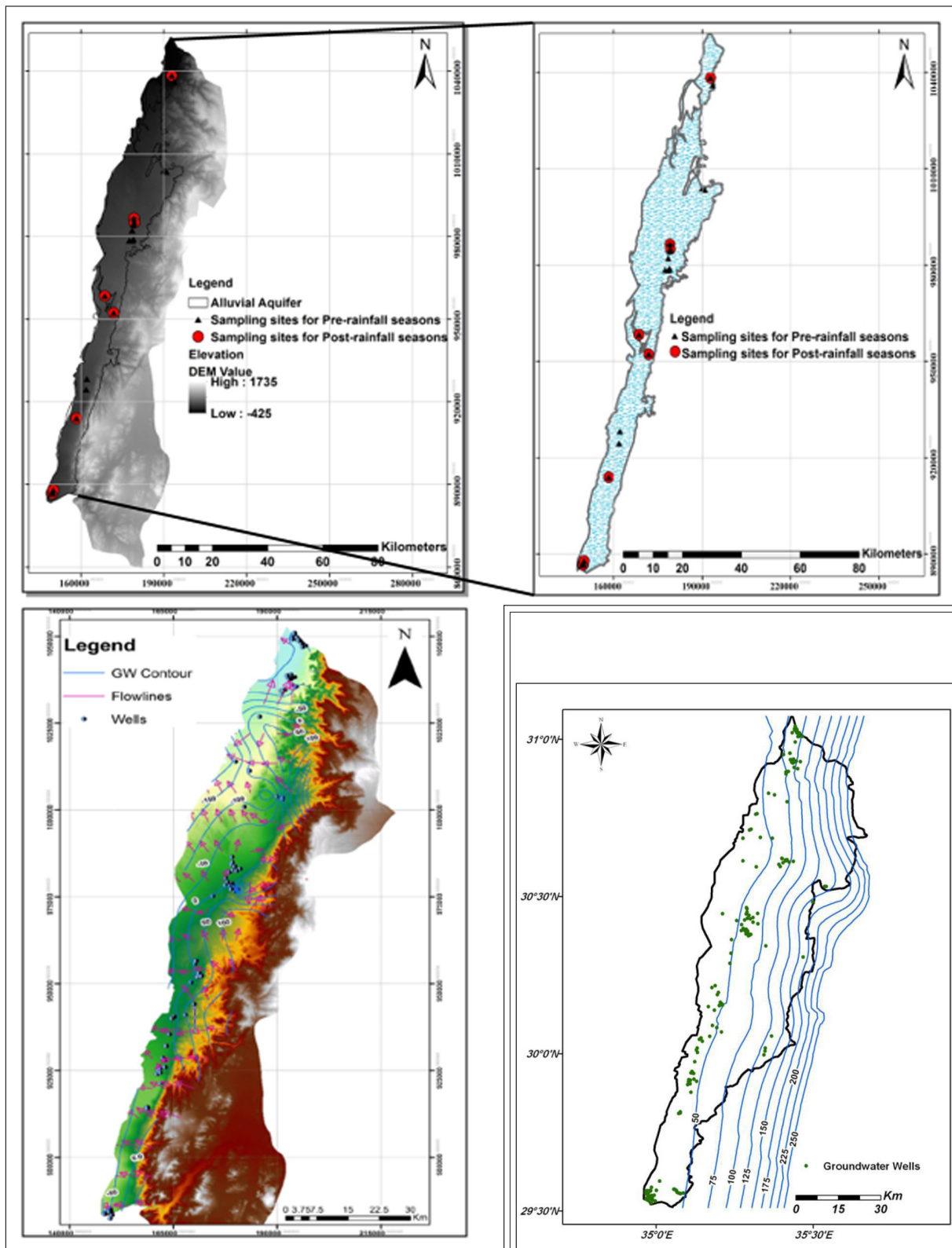


Figure 1. (A): Digital Elevation Model of Wadi Araba Groundwater Basins and focusing on the locations of samples both in two periods. (B): Groundwater flow direction map of Alluvial Aquifer System (El-Naqa and Al Kuisi, 2012).

Figure 2. Isohyet map of Wadi Araba Basin (El-Naqa et al. 2009).

The area of Wadi Araba has in general a very arid-hot climate; the rainfall over Wadi Araba basin is orographic and seasonal. The average monthly temperature in the south of Jordan ranges from 20°C to 31°C. The average relative humidity ranges from 41% to 63%. The prevailing winds are from the west. Rainfall generally occurs between September and May with most of the rainfall occurring between December and March (El-Naqa and Al Kuisi, 2012). The mean annual rainfall is very low, ranges between 50 to 100 mm along the floor of Wadi Araba and upward from 300 to 400 mm along the escarpment and highlands (Fig. 2) (El-Naqa et al., 2009).

2. Materials and methods

2.1. Sample collection

Twenty-three (23) water samples were collected during pre-rainfall seasons (August-September 2014) and 14 water samples were collected during post-rainfall seasons (April-May 2014). These water samples were collected from 21 boreholes (4 private wells and 17 governmental wells). The water samples were collected polyethylene bottles of one liter size after washing them twice by samples water in order to avoid the contamination and then stored and transported to the Laboratory of Ministry of Water and Irrigation to analyze the major cations & anions and some trace elements. The sampling plan was to collect site-specific

information relating to the agricultural activities near the water sampling sites. The physical parameters including pH, electrical conductivity (EC), and temperature carried out directly in the field using the portable instruments.

Spatial Analyst tool in ArcGIS 10.2 was used to generate the final irrigation water quality index maps which constructed based on the calculated quality value multiplied by the recommended weight of each parameter then constructed by overlying of the thematic maps of above mentioned parameters and reclassified it according to the water quality classes of IWQI. The inverse distance weight (IDW) technique was used in the spatial modeling of the distribution of groundwater quality parameters. This technique is proved to be the ideal interpolation method which covers all samples along the narrow strip of alluvial aquifer. The average cannot be greater than the highest or lesser than the lowest input.

2.2. Analytical method

Samples were analyzed in the Laboratory for the major ions chemistry and trace elements. The analytical methods used for the analyses of the different parameters are listed in Table 1. These analytical techniques were performed according to the procedures mentioned in the Standard Methods for Examination of Water and Wastewater (1998).

Table 1. Methods of analysis used to determine Physical and Chemical properties for Alluvial Aquifer along Wadi Araba groundwater samples.

Parameter	Unit	Analytical Methods
Electrical Conductivity at 25 C°	µs/cm	Field EC-meter
pH-Value	–	Field pH-meter
Total Dissolved Solid (TDS)	mg/l	By calculation Eq.(5)
Total Harness (TH)	mg/l	By calculation Eq.(6)
Sodium, Potassium, Calcium, Magnesium	mg/l	ICP-MS
Chloride	mg/l	Titration with 0.01 AgNO ₃ using Potassium Chromate(K ₂ CrO ₄) indicator
Sulfate	mg/l	Ultra violet visible spectrophotometer wave length 492 nm
Nitrate	mg/l	Ultra violet visible spectrophotometer– wave length 206 nm
Phosphate	mg/l	Ultra violet visible spectrophotometer– wave length 690 nm
Bicarbonate	mg/l	Titration with 0.02N H ₂ SO ₄ using Diphenyl carbazone indicator.
Ammonium	mg/l	Ultra violet visible spectrophotometer– wave length 425 nm
As, Zn, Se, Ni, Fe, Mn, Cu, Cd, Cr, B	mg/l	ICP-MS

The analytical precision for ions was determined by the ionic balances calculated as $100 \times (\text{cations} - \text{anions}) / (\text{cations} + \text{anions})$, which is generally within $\pm 5\%$ (Srinivasamoorthy et al. 2010). The descriptive statistics of chemical analyses and trace elements of groundwater samples collected from pre- and post-rainfall seasons are presented in Table 2.

2.3. Mapping Irrigation Water Quality Index (IWQI)

Water quality index (WQI) is an important parameter for identifying the water quality and its sustainability for drinking purposes (Subba, 2006) and Magesh et al., 2013). WQI is defined as a technique of rating that provides the composite influence of individual water quality parameters on the overall water quality (Mitra, 1998).

It is commonly accepted that the problems originating from irrigation water quality vary in type and severity as a function of numerous factors including the type of the soil and the crop, the climate of the area as well as the farmer who utilizes the water. Nevertheless, there is now a common understanding that these problems can be categorized into the following major groups: (a) salinity hazard, (b) infiltration and permeability problems, (c) toxicity hazards; and, (d) miscellaneous problems (Ayers and Westcot, 1985). The toxicity hazards can further be grouped into problems associated with specific ions as well as hazards related to the presence of trace elements and heavy metals. The criteria classification of irrigation water quality is presented in Table 3 and Table 4.

Table 2. Basic statistics of field parameters and analytical data for groundwater samples both in two periods.

Parameter	Unit	Descriptive statistics pre-rainfall seasons				Descriptive statistics post-rainfall seasons			
		Minimum	Maximum	Mean	Std. Deviation	Minimum	Maximum	Mean	Std. Deviation
pH	- -	6.48	7.99	7.52	0.38	6.84	7.94	7.52	0.31
EC	$\mu\text{S}/\text{cm}$	882.00	4800.00	1851.30	1000.09	772.00	5860.00	1909.79	1217.55
TDS	mg/l	519.50	2828.80	1101.08	589.72	439.40	3554.20	1105.70	764.20
Ca^{2+}	mg/l	21.64	261.92	118.04	59.18	71.14	428.25	135.02	91.25
Mg^{2+}	mg/l	14.11	163.55	57.77	32.16	4.01	206.80	53.54	54.22
Na^{+}	mg/l	50.83	538.20	190.62	122.51	37.26	556.60	186.97	124.06
K^{+}	mg/l	3.13	15.25	7.01	3.05	1.96	16.81	6.02	3.37
Cl^{-}	mg/l	85.20	1322.73	408.04	293.71	94.08	1873.70	438.45	438.24
HCO_3^{-}	mg/l	18.30	251.32	155.19	62.84	75.64	281.82	173.18	66.70
SO_4^{2-}	mg/l	21.12	488.16	238.37	119.51	33.12	422.88	193.20	121.98
NO_3^{-}	mg/l	0.22	19.31	7.47	4.24	0.23	46.54	11.93	12.16
SAR	---	1.18	7.06	3.54	1.59	0.92	5.53	3.39	1.13
Trace Elements									
As	Ppm	0.002	0.01	0.006	0.004	0.002	0.01	0.008	0.004
Se	Ppm	0.01	0.01	0.010	3.55E-18	0.01	0.01	0.010	1.80E-18
Cu	Ppm	0.01	0.12	0.030	0.035	0.01	0.12	0.033	0.034
Cr	Ppm	0.01	0.07	0.013	0.013	0.01	0.07	0.014	0.016
Ni	Ppm	0.01	0.02	0.015	0.005	0.02	0.01	0.012	0.004
Mn	Ppm	0.01	0.096	0.022	0.021	0.01	0.096	0.034	0.024
Fe	Ppm	0.03	0.22	0.085	0.058	0.02	0.22	0.068	0.054
Zn	Ppm	0.008	0.25	0.062	0.068	0.01	0.25	0.102	0.087
B	Ppm	0.23	0.55	0.409	0.097	0.23	0.54	0.023	0.085
Cd	Ppm	0.003	0.02	0.005	0.005	0.003	0.02	0.005	0.005

Table 3. Food and Agriculture Organization (FAO) guidelines for interpretation of water quality for irrigation (Ayers and Westcot, 1985).

Potential irrigation problems	Units	Degree of restriction on use		
		None	Slight to moderate	Severe
(1) Salinity (affects crop water availability)				
EC	$\mu\text{S}/\text{cm}$	< 700	700 – 3000	> 3000
TDS	mg/l	< 450	450 – 2000	> 2000
(2) Permeability (effects infiltration rate of water into soil)				
SAR = 0 – 3	and EC= ($\mu\text{S}/\text{cm}$)	> 700	700 – 200	< 200
SAR = 3 – 6		> 1200	1200 – 300	< 300
SAR = 6 – 12		> 1900	1900 – 500	< 500
SAR = 12 – 20		> 2900	2900 – 1300	< 1300
SAR = 20 – 40		> 5000	5000 – 2900	< 2900
(3) Specific ion toxicity (effects sensitive crops)				
Sodium (Na)	SAR	< 3	3 – 9	> 9
Surface irrigation		< 3	> 3	–
Sprinkler irrigation		< 3	> 3	–
Chloride (Cl^{-})				
Surface irrigation	mg/l	< 140	140 – 350	> 350
Sprinkler irrigation	mg/l	< 3	> 3	–
Boron (B)	mg/l	< 0.7	0.7 – 3.0	> 3.0
(4) Trace elements toxicity (Table 7)	ppm	–	–	–
(5) Miscellaneous effects (effects susceptible crops)				
Nitrate–nitrogen ($\text{NO}_3 - \text{N}$)	mg/l	< 5	5 – 30	> 30
Bicarbonate (HCO_3^{-}) effects only on sensitive plants and sprinkler irrigation	mg/l	< 90	90 – 500	> 500
pH	–		Normal range 6.5 – 8.4	

Table 4. Recommended maximum concentrations of trace elements in irrigation water (Ayers and Westcot, 1985).

Element	Recommended Maximum Concentration (mg/l)	Remarks
Zn (Zinc)	2.00	Toxic to many plants at widely varying concentrations; reduced toxicity at pH>6.0 and in fine textured organic soils.
As (Arsenic)	0.10	Toxicity to plants varies widely, ranging from 12 mg/l for Sudan grass to less than 0.05 mg/l for rice.
Cd (Cadmium)	0.01	Toxic to beans, beets and turnips at concentrations as low as 0.1 mg/l in nutrient solutions. Conservative limits recommended due to its potential for accumulation in plants and soils to concentrations that may be harmful to humans.
Cr (Chromium)	0.10	Not generally recognized as an essential growth element. Conservative limits recommended due to lack of knowledge on its toxicity to plants.
Cu (Copper)	0.20	Toxic to a number of plants at 0.1 to 1.0 mg/l in nutrient solutions.
Fe (Iron)	5.00	Not toxic to plants in aerated soils, but can contribute to soil acidification and loss of availability of essential phosphorus and molybdenum. Overhead sprinkling may result in unsightly deposits on plants, equipment and buildings.
Mn (Manganese)	0.20	Toxic to a number of crops at a few-tenths to a few mg/l, but usually only in acid soils.
Ni (Nickel)	0.20	Toxic to a number of plants at 0.5 mg/l to 1.0 mg/l; reduced toxicity at neutral or alkaline pH.
Se (Selenium)	0.02	Toxic to plants at concentrations as low as 0.025 mg/l and toxic to livestock if forage is grown in soils with relatively high levels of added selenium. An essential element to animals but in very low concentrations.

In the proposed technique, each one of these parameters is given a weighing coefficient from 1 to 5 such that the most and the least important intensity groups in irrigation water quality are given the highest (5) and lowest (1) points. As the salinity hazard is considered to be the most intensity important factor in irrigation water quality assessment, it is given the highest significance. On the other hand, the miscellaneous effects to sensitive crops are generally considered as the least important factor influencing the irrigation water quality. Between these two extremes, the infiltration and permeability hazard, specific ion toxicity and trace element toxicity are rated in decreasing order of significance for irrigation water quality. The technique assigns rating factors for each parameter as shown in Tables 5, 6, and 7. In the present study, Irrigation Water Quality Index (IWQI) is developed based on the method given by Ayers and Westcot (1985) and Simsek and Orhan (2007) with regards the guidelines presented by Ayers and Westcot (1985). The proposed IWQ index is then calculated as:

$$IWQ \text{ Index} = \sum_{i=1}^5 G_i \dots\dots\dots (1)$$

Where i is an incremental index and G represents the contribution of each one of the five hazard categories that are important to assess the quality of an irrigation water resource.

The first category is the salinity hazard that is represented by the EC value of the water and is formulated as:

$$G1 = w1r1 \dots\dots\dots (2)$$

Where w is the weight value of this hazard group and r is the rating value of the parameter as given in Table 5.

The second category is the infiltration and permeability hazard that is represented by EC-SAR combination and is

formulated as:

$$G2 = w2r2 \dots\dots\dots (3)$$

where w is the weight value of this hazard group and r is the rating value of the parameter as given in Table 6.

The third category is the specific ion toxicity that is represented by SAR, chloride and boron ions in the water and is formulated as a weighted average of the three ions:

$$G3 = \frac{w3}{3} \sum_{j=1}^3 r_j \dots\dots\dots (4)$$

Where j is an incremental index, w is the weight value of this group as given in Table 3 and r is the rating value of each parameter as given in Table 5. The fourth category is the trace element toxicity that is represented by the elements given in Table 4 and is formulated as a weighted average of all the ions available for analysis:

$$G4 = \frac{w4}{N} \sum_{k=1}^N r_k \dots\dots\dots (5)$$

Where k is an incremental index, N is the total number of trace element available for the analysis, w is the weight value of this group and r is the rating value of each parameter as given in Table 7.

The fifth and the final category is the miscellaneous effects to sensitive crops that are represented by nitrate-nitrogen, bicarbonate ions and the pH of the water, and is formulated as a weighted average:

$$G5 = \frac{w5}{N} \sum_{m=1}^3 r_m \dots\dots\dots (6)$$

Where m is an incremental index, w is the weight value of this group and r is the rating value of each parameter as given in Table 5.

Table 5. Classification for IWQ index parameters.

Hazard	Weight	Parameter	Range	Rating	Suitability
Salinity hazard	5	Electrical conductivity ($\mu\text{S}/\text{cm}$)	$\text{EC} < 700$	3	High
			$700 \leq \text{EC} \leq 3000$	2	Medium
			$\text{EC} > 3000$	1	Low
Infiltration and permeability hazard	4	Table 6 for details			
Specific ion toxicity	3	Sodium adsorption ratio (–)	$\text{SAR} < 3.0$	3	High
			$3.0 \leq \text{SAR} \leq 9.0$	2	Medium
			$\text{SAR} > 9.0$	1	Low
		Boron (mg/l)	$\text{B} < 0.7$	3	High
			$0.7 \leq \text{B} \leq 3.0$	2	Medium
			$\text{B} > 3.0$	1	Low
		Chloride (mg/l)	$\text{Cl} < 140$	3	High
			$140 \leq \text{Cl} \leq 350$	2	Medium
			$\text{Cl} > 350$	1	Low
Trace element toxicity	2	Table 7 for details			
Miscellaneous effects to sensitive crops	1	Nitrate Nitrogen (mg/l)	$\text{NO}_3\text{--N} < 5.0$	3	High
			$5.0 \leq \text{NO}_3\text{--N} \leq 30.0$	2	Medium
			$\text{NO}_3\text{--N} > 30.0$	1	Low
		Bicarbonate (mg/l)	$\text{HCO}_3 < 90$	3	High
			$90 \leq \text{HCO}_3 \leq 500$	2	Medium
			$\text{HCO}_3 > 500$	1	Low
		pH	$7.0 \leq \text{pH} \leq 8.0$	3	High
			$6.5 \leq \text{pH} < 7.0$ and $8.0 < \text{pH} \leq 8.5$	2	Medium
			$\text{pH} < 6.5$ or $\text{pH} > 8.5$	1	Low

Table 6. Classification for infiltration and permeability hazard.

SAR					Rating	Suitability
3>	6–3	12–6	20–12	20<		
700<	1200 <	1900<	2900<	5000<	3	High
200–700	300–1200	500–1900	1300–2900	2900–5000	2	Medium
200>	300>	500>	1300>	2900>	1	Low

Table 7. Classification for trace element toxicity.

Factor	Range	Rating	Suitability
Arsenic (mg/l)	$\text{As} < 0.1$	3	High
	$0.1 \leq \text{As} \leq 2.0$	2	Medium
	$\text{As} > 2.0$	1	Low
Cadmium (mg/l)	$\text{Cd} < 0.01$	3	High
	$0.01 \leq \text{Cd} \leq 0.05$	2	Medium
	$\text{Cd} > 0.05$	1	Low
Chromium (mg/l)	$\text{Cr} < 0.1$	3	High
	$0.1 \leq \text{Cr} \leq 1.0$	2	Medium
	$\text{Cr} > 1.0$	1	Low
Copper (mg/l)	$\text{Cu} < 0.2$	3	High
	$0.2 \leq \text{Cu} \leq 5.0$	2	Medium
	$\text{Cu} > 5.0$	1	Low
Iron (mg/l)	$\text{Fe} < 5.0$	3	High
	$5.0 \leq \text{Fe} \leq 20.0$	2	Medium
	$\text{Fe} > 20.0$	1	Low
Manganese (mg/l)	$\text{Mn} < 0.2$	3	High
	$0.2 \leq \text{Mn} \leq 10.0$	2	Medium
	$\text{Mn} > 10.0$	1	Low
Nickel (mg/l)	$\text{Ni} < 0.2$	3	High
	$0.2 \leq \text{Ni} \leq 2.0$	2	Medium
	$\text{Ni} > 2.0$	1	Low
Selenium (mg/l)	$\text{Se} < 0.01$	3	High
	$0.01 \leq \text{Se} \leq 0.02$	2	Medium
	$\text{Se} > 0.02$	1	Low
Zinc (mg/l)	$\text{Zn} < 2$	3	High
	$2 \leq \text{Zn} \leq 10$	2	Medium
	$\text{Zn} > 10.0$	1	Low

3. Results and discussion

The assessment of chemical characteristics of the groundwater samples that were analyzed compared with World Health Organization (WHO) and Jordanian water quality standards. Groundwater quality for drinking purposes was evaluated by calculation the Water Quality Index (WQI) for each sample that indicates the influence of individual water quality parameters on the overall water quality. The Water Quality Index (WQI) was calculated for evaluating influence of natural and anthropogenic activities based on several key parameters of groundwater chemistry. The weight has been assigned for the physico-chemical parameters according to the parameters relative importance in the overall quality of water for drinking water purposes. The IWQI has advantages by reflecting the suitability of water for specific use. The proposed index method utilizes five limitation groups that have been mentioned by Ayers and Westcot (1985) with few modification in their classification categories for irrigation water quality assessment. These limitation groups are: (a) salinity limitation, (b) infiltration and permeability limitation, (c) specific ion toxicity, (d) trace element toxicity; and, (e) miscellaneous impacts on sensitive crops. These parameters are given a weighing coefficient from 1 to 5 such that the most and the least important groups in irrigation water quality are given the highest (5) and lowest (1) points. As the salinity hazard is considered to be the most intensity important factor in irrigation water quality assessment, it is given the highest priority.

After the total value of the index is computed, a suitability analysis is determined based on the three different categories given in Table 8. The values given in Table (8) is obtained by assigning different rating factors (i.e., 1, 2 and 3) to each parameter without changing its weighing coefficient, thus yielding two different index values (i.e., 30 and 39). The suitability map can be constructed based on the computed index value which is evaluated according to three categories given in Table 8. When the IWQI value is greater than 37, the quality of irrigation water is high and no problems with irrigation water quality. However when the IWQI ranges between 22 and 37, the quality of irrigation water is of moderate suitability for irrigation purposes. Finally if the IWQ index is less than 22, the quality of irrigation water is considered poor and not suitable for irrigation.

Table 8. Irrigation water quality (IWQ) index.

IWQ index	Suitability of water for irrigation
< 22	Low
22 – 37	Medium
> 37	High

The irrigation water quality index (IWQI) maps was prepared using ArcGIS to represent the suitability of irrigation water quality in Wadi Araba area. The IWQI classify the quality of irrigation water into two categories as moderate and high suitability water for irrigation. Accordingly, 75.7 % of the irrigation water has a medium suitability for irrigation in both periods pre and after wet season, whereas only 24.3 % has exhibit high suitability for irrigation for both investigating periods (Fig.3). The northern regions of Wadi Araba basin appear to have high water suitability for irrigation purposes

as in wadi Feifa, Umruq, Wadi Musa, Feedan, and some wells in Um Methla and Risha areas. It can be noticed that the suitability of irrigation water quality can be deteriorated towards the southern part of the study area.

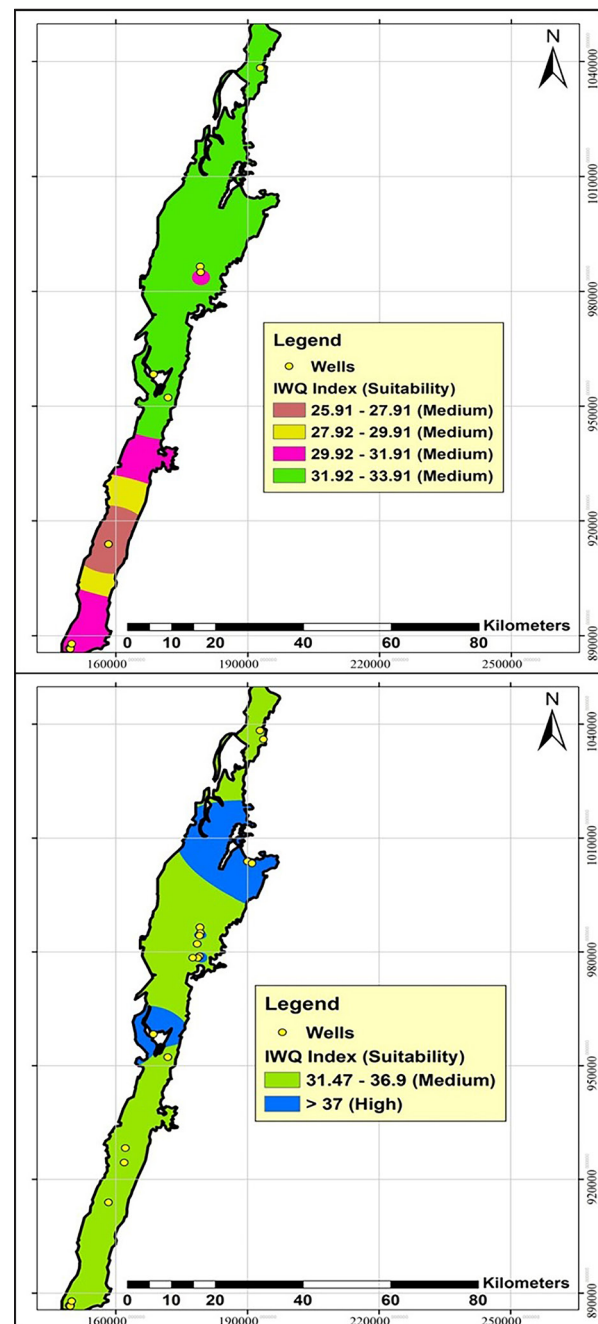


Figure 3. Spatial distribution of IWQI values in the study area during two periods and their suitability: pre-rainfall period and post-rainfall periods, respectively.

The suitability map obtained from the computed index value is evaluated according to three categories given in Table 9. When the computed index value is bigger than 37, the corresponding area is considered to have minimum problems with respect to irrigation quality. When the computed index value is between 22 and 37, the corresponding waters demonstrates moderate suitability for irrigation purposes. Within this range, values higher than 30 are considered to represent waters that could be easily used on resistant crops. However, the IWQ index values of less than 22 are considered to be poor quality irrigation waters and are not suitable for

irrigating agricultural fields; this range of index value does not represent all samples.

Table 9. The contribution of each one of the five hazard categories that are important to assess the quality of an irrigation in the pre and post-rainfall periods.

Pre-rainfall period									
Station ID	Station Name	Sampling Date	G ₁	G ₂	G ₃	G ₄	G ₅	IWQI	Suitability
DA1008	WADI MUSA No.7	10–Aug	5	12	6	5.2	2.67	30.87	Medium
DA1010	FEIFA No.2	06-Sep	10	8	6	5.2	2.67	31.87	Medium
DA1010	FEIFA No.2	10–Aug	10	12	9	5.2	2.67	38.87	High
DA1020	UMRUQ No.2	10–Aug	10	12	6	5.2	2.67	35.87	Medium
DA1027	WADI MUSA No.10	10–Aug	10	12	8	5.2	2.67	37.87	High
DA1029	WADI MUSA No.12	10–Aug	10	12	8	5.2	2.67	37.87	High
DA1102	WADI MUSA No.1	10–Aug	5	12	6	5.2	2.67	30.87	Medium
DE1001	FEEDAN No.1	14–Sep	10	12	9	5.2	3	39.2	High
DE1003	FEEDAN No.6	14–Sep	10	12	9	5.2	2.67	38.87	High
DF1003	UM MITHLA No.1B	10–Aug	5	12	6	5.2	2.67	30.87	Medium
DF1005	UM MITHLA No.5	10–Aug	10	12	8	5.2	2.67	37.87	High
DA3039	UM MITHLA No.8	10–Aug	10	12	8	5.2	3	38.2	High
EA1005	RAHMA No.6	10–Aug	10	12	6	5.2	3	36.2	Medium
EA1013	RAHMA No.7	10–Aug	10	12	6	5.2	2.67	35.87	Medium
EA3013	QATAR No.2	10–Aug	10	8	7	5.2	3	33.2	Medium
EA3018	Q'A ASSAIDIYIN No.2A	10–Aug	10	12	6	5.2	2.67	35.87	Medium
DA3046	WADI ARABA No.3 (WA3)/ RISHA	10–Aug	10	12	8	5.2	2.67	37.87	High
EA3033	PILOT PROJECT OBSERVATION WELL No.1	06–Sep	10	12	6	5.2	2.67	35.87	Medium
EA3034	PILOT PROJECT OBSERVATION WELL No.2	06–Sep	10	12	6	5.2	2.67	35.87	Medium
EA3034	PILOT PROJECT OBSERVATION WELL No.2	14–Sep	10	8	7	5.2	2	32.2	Medium
EA3035	PILOT PROJECT OBSERVATION WELL No.3	06–Sep	10	12	6	5.2	2.67	35.87	Medium
EA3035	PILOT PROJECT OBSERVATION WELL No.3	14–Sep	10	12	7	5.2	2.67	36.87	High
EA3036	PILOT PROJECT OBSERVATION WELL No.4	06–Sep	10	12	6	5.2	2.67	35.87	Medium
Post-rainfall period									
Station ID	Station Name	Sampling Date	G ₁	G ₂	G ₃	G ₄	G ₅	IWQI	Suitability
DA1010	FEIFA No.2	02–Apr	10	12	9	0.5	2.33	33.85	Medium
DF1002	UM MITHLA No.1A	13–Apr	10	12	8	0.5	2.67	33.19	Medium
DF1005	UM MITHLA No.5	13–Apr	10	12	6	0.5	2.67	31.19	Medium
DF1005	UM MITHLA No.5	14–May	10	12	8	0.5	2.67	33.19	Medium
DF1005	UM MITHLA No.5	28–May	10	12	6	0.5	2.67	31.19	Medium
EA3013	QATAR No.2	13–Apr	5	12	6	0.5	2.33	25.85	Medium
EA3018	Q'A ASSAIDIYIN No. 2A	13–Apr	10	12	7	0.5	2.67	32.19	Medium
DA3046	WADI ARABA No.3 (WA3)/ RISHA	13–Apr	10	12	8	0.5	2.67	33.19	Medium
EA3033	PILOT PROJECT OBSERVATION WELL No.1	28–May	10	12	6	0.5	2.67	31.19	Medium
EA3033	PILOT PROJECT OBSERVATION WELL No.1	13–Apr	10	12	6	0.5	2.67	31.19	Medium
EA3033	PILOT PROJECT OBSERVATION WELL No.1	02–Apr	10	12	6	0.5	2.33	30.85	Medium
EA3034	PILOT PROJECT OBSERVATION WELL No.2	14–May	10	8	7	0.5	2.67	28.19	Medium
EA3035	PILOT PROJECT OBSERVATION WELL No.3	14–May	10	12	7	0.5	3	32.52	Medium
EA3036	PILOT PROJECT OBSERVATION WELL No.4	14–May	10	12	7	0.5	2.67	32.19	Medium

4. Conclusions

The IWQ index is a numerical index which can be used for the assessment of the suitability of water quality for irrigation. The irrigation water quality index map was constructed using ArcGIS to identify the suitability of irrigation water in the investigated area.

The suitability map obtained from the computed index value which is evaluated according to specific categories. Accordingly, the IWQI maps showed that 75.7% of the water

quality in pre and post rainfall seasons has medium suitability and 24.3% has high suitability for irrigation use. The IWQI values in pre-rainfall seasons quite decrease of IWQI values in post-rainfall seasons as a result of water dilution or aquifer recharge from rainfall and decreasing the water discharge from wells. As the aquifer was being recharged, the concentration of the major ions decreased which led to reduction in the IWQI values.

The water quality for irrigation showed signs of water

deterioration towards the southern part of the investigated area. While in the northern part, the water quality for irrigation is highly suitable during the pre-rainfall period as in Feifa, Umruq, Wadi Musa and Feedan areas. Accordingly, the water quality from in Wadi Araba is currently suitable for use in irrigation. It is believed that the proposed IWQI can be used as a tool in future agricultural management plans that serve decision-makers and farmers in Wadi Araba area.

Acknowledgments

The Ministry of Water and Irrigation (MWI) is acknowledged for their support in carrying out the chemical and physical analyses that achieved at their laboratories.

References

- American Public Health Association (APHA), (1998). A standard methods for examination of water and wastewater, 20th edition, Washington, NW.
- Ayers, R.S., and Westcot, D.W. (1985). Water quality for agriculture. FAO Irrigation and Drainage Paper No. 29, Food and Agriculture Organization, Rome.
- Dames and Moore. (1979). Preliminary Evaluation of the Hydrology of Wadi Araba and Southern Ghor, Water Resources Study. Amman-Jordan.
- El-Naqa, A., and Al Kuisi, M. (2012). Groundwater resources assessment for irrigable agricultural lands in the Wadi Araba area, southern Jordan. *Journal of Arab J Geosci*, doi: 10.1007/s12517-012-0579-5.
- El-Naqa, A., Hammouri, N., Ibrahim, K., and El-Taj, M. (2009). Integrated Approach for Groundwater Exploration in Wadi Araba Using Remote Sensing and GIS. *Jordan Journal of Civil Engineering*, Volume 3, No.3.
- Khalid, H.L. (2011). Evaluation of Groundwater Quality for Drinking Purpose for Tikrit and Samarra Cities using Water Quality Index. *European journal of scientific research* 58(4): 472–481.
- Krishna, K., S., Logeshkumaran, A., Magesh, N., Prince, S., Godson, N. (2014). Hydro-geochemistry and application of water quality index (WQI) for groundwater quality assessment, Anna Nagar, part of Chennai City, Tamil Nadu, India. *Appl. Water Sci.*, DOI 10.1007/s13201-014-0196-4.
- Magesh, N., Krishna, K., Subbiah, K., Chandra, S. (2013). Groundwater quality assessment using WQI and GIS techniques, Dindigul district, Tamil Nadu, India. *Arabian Journal of Geosciences*, 6(11): 4179–4189.
- Mitra, B.K. (1998). Spatial and temporal variation of ground water quality in sand dune area of Aomori Prefecture in Japan. *ASABE*.
- Rizwan, R., and Gurdeep, S. (2010). Assessment of Ground Water Quality Status by Using Water Quality Index Method in Orissa, India. *World Applied Sciences Journal*, 9(12): 1392-1397.
- Simsek, C. and Orhan, O. (2007). IWQ Index: A GIS-Integrated Technique to Assess Irrigation Water Quality. *Environ. Monit.*, 128: 277–300.
- Srinivasamoorthy, K., Vijayaraghavan, K., Vasanthavigar, M., Sarma, V.S., Rajivgandhi, R., Chidambaram, S., Anandhan, P., Manivannan, R. (2010). Assessment of groundwater vulnerability in Mettur region, Tamilnadu, India using drastic and GIS techniques. *Arab J. Geosci.*, doi:10.1007/s12517-010-0138-x.
- Subba, R.N. (2006). Seasonal variation of groundwater quality in a part of Guntur district, Andhra Pradesh, India. *Environmental Geology*, 49: 413–429.



الجامعة الهاشمية



صندوق دعم البحث العلمي



المملكة الأردنية الهاشمية

المجلة الأردنية لعلوم الأرض والبيئة

JJEES

مجلة علمية عالمية محكمة

المجلد (١٠) العدد (٢)

<http://jjees.hu.edu.jo/>

ISSN 1995-6681

المجلة الأردنية لعلوم الأرض والبيئة

مجلة علمية عالمية محكمة

المجلة الأردنية لعلوم الأرض والبيئة : مجلة علمية عالمية محكمة ومفهرسة ومصنفة، تصدر عن عمادة البحث العلمي في الجامعة الهاشمية وبدعم من صندوق البحث العلمي - وزارة التعليم العالي والبحث العلمي، الأردن.

هيئة التحرير :

رئيس التحرير :

- الأستاذ الدكتور فايز أحمد
الجامعة الهاشمية، الزرقاء، الأردن.

مساعد رئيس التحرير

- الدكتور محمد القنة
الجامعة الهاشمية، الزرقاء، الأردن.

أعضاء هيئة التحرير :

- الأستاذ الدكتور نجيب أبو كركي
الجامعة الأردنية

- الأستاذ الدكتور نزار أبو جابر
الجامعة الأردنية الألمانية

- الأستاذ الدكتور أنور جريس
جامعة مؤتة

- الأستاذ الدكتور خالد الطراونة
جامعة الحسين بن طلال

- الأستاذ الدكتور عاطف خرابشة
جامعة البلقاء التطبيقية

- الأستاذ الدكتور عبد الله ذيابات
جامعة آل البيت

- الأستاذ الدكتور نزار الحموري
الجامعة الهاشمية

- الأستاذ الدكتور مهيب عواودة
جامعة اليرموك

فريق الدعم :

المحرر اللغوي

- الدكتورة هاله شريتح

تنفيذ وإخراج

- عبادة الصمادي

ترسل البحوث إلكترونياً إلى البريد الإلكتروني التالي :

رئيس تحرير المجلة الأردنية لعلوم الأرض والبيئة

jjees@hu.edu.jo

لمزيد من المعلومات والأعداد السابقة يرجى زيارة موقع المجلة على شبكة الانترنت على الرابط التالي :

www.jjees.hu.edu.jo



المملكة الأردنية الهاشمية صندوق دعم البحث العلمي الجامعة الهاشمية

JJEES

المجلة الأردنية
لعلوم الأرض والبيئة

المجلد (١٠) العدد (٢)



مجلة علمية عالمية مدعمة تصدر بدعم من صندوق دعم البحث العلمي

ISSN 1995-6681

jjees.hu.edu.jo

حزيران ٢٠١٩